Technische Universität München

Klinik und Poliklinik für Innere Medizin II des Klinikum rechts der Isar

Bcl-3 deficiency regulates cancer stem cell-ness and metastatic properties in pancreatic ductal adenocarcinoma

Jiaoyu Ai

Vollständiger Abdruck der von der Fakultät für Medizin der Technischen Universität München zur Erlangung des akademischen Grades eines

Doktors der Medizin (Dr. med.)

genehmigten Dissertation.

Vorsitzende(r): Prof. Dr. Ernst J. Rummeny

Prüfer der Dissertation:

1. Prof. Dr. Hana Algül

2. Prof. Dr. Roland M. Schmid

Die Dissertation wurde am 14.09.2017 bei der Technischen Universität München eingereicht und durch die Fakultät für Medizin am 21.02.2018 angenommen.

To cure sometimes,

To relieve often,

To comfort always.

--------Edward Livingston Trudeau

Zusammenfassung

Ziel der vorliegen Arbeit war es die Rolle von B-cell CLL/lymphoma 3 (Bcl-3) in der pankreatischen Karzinogene zu untersuchen. Das duktale Pankreaskarzinom (PDAC) gehört nach wie vor zu den Tumorentitäten mit der höchsten Letalität. Prognostischen Berechnungen zufolge wird die Krebs-assoziierte Letalität zum Jahr 2030 an zweiter Stelle rangieren. Trotz der Fortschritte in den letzten Jahren bleibt die Prognose des Pankreaskarzinoms extrem schlecht. Hierfür ist neben der verspäteten Diagnose die frühe Metastasierung verantwortlich.

Bcl-3 gehört zur atypischen Subklasse von IκB Proteinen. Im Gegensatz zu den klassischen IκB Proteinen wird Bcl-3 in den Zellkern transloziert, wo es mit DNA bindenden NF-κB1/p50 oder NF-κB2/P52 Homodimeren die Transkription von Genen beeinflusst. Die Funktion von Bcl-3 wird nicht nur über die Expression, sondern auch über eine Vielzahl von post-translationalen Modifikationen, die unter anderem die nukleäre Translokation, die Stabilität von Bcl-3 und/oder die transkriptionelle Aktivität beeinflussen, reguliert. Die Aktivierung von Bcl-3 konnte in hämatologischen malignen Systemerkrankungen nachgewiesen werden. Die Bedeutung von Bcl-3 in soliden Tumoren hingegen ist weniger erforscht. Mehrere Studien weisen jedoch darauf hin, dass Bcl-3 auch in einigen soliden Tumoren eine Rolle spielt. Um die Bedeutung von Bcl-3 für die pankreatische Karzinogenese aufzuklären, wurden *in vivo* und *in vitro* Untersuchungen durchgeführt.

Eine Bcl-3 Überexpression konnte erstmalig sowie in humanen als auch in murinen PDAC Gewebe und Tumorzelllinien dokumentiert werden. Deletion von Bcl-3 in $Kras^{G12D}$ Mausmodell mit pankreasspezifischer Inaktivierung von p53 resultierte in eine akzelerierte Tumorentstehung und eine verstärkte Metastasierung. Weiterhin führte die Inaktivierung von Bcl-3 in primären Pankreaskarzinomzellen in *in vitro* Experimenten zu einer verstärkten Migration und Invasion. Bemerkenswerterweise konnte eine hohe Inzidenz von undifferenzierten/anaplastischen/ sarkomatodien Pankreastumoren in Bcl-3-defizienten Mäusen beobachtet werden, was auf einen Einfluss von Bcl-3 auf die epithelial-mesenchymale Transition (EMT) in der Pankreaskarzinogenese hindeutet. Des Weiteren zeigten Analysen des Transkriptoms und Metaboloms, dass die Deletion von Bcl-3 in Tumorzellen zu metabolischen Veränderungen führte, die den oxidativen Metabolismus und einen Krebsstammzell-ähnlichen Phänotyp fördern.

Demnach wird hier die Bedeutung von Bcl-3 für die pankreatische Karzinogene und Metastasierung erstmalig belegt.

Part of this thesis was submitted for publication and was under revision at the time of thesis submission.

Additional publications not related to this thesis include:

1) Wörmann SM, Song L, **Ai J**, Diakopoulos KN, Kurkowski MU, Görgülü K, Ruess D, Campbell A, Doglioni C, Jodrell D, Neesse A, Demir IE, Karpathaki AP, Barenboim M, Hagemann T, Rose-John S, Sansom O, Schmid RM, Protti MP, Lesina M, Algül H. Loss of P53 Function Activates JAK2-STAT3 Signaling to Promote Pancreatic Tumor Growth, Stroma Modification, and Gemcitabine Resistance in Mice and Is Associated With Patient Survival. Gastroenterology. 2016 Jul;151(1):180-193.e12. doi: 10.1053/j.gastro.2016.03.010. Epub 2016 Mar 19. PMID: 27003603.

2) Song L, Wörmann S, **Ai J**, Neuhöfer P, Lesina M, Diakopoulos KN, Ruess D, Treiber M, Witt H, Bassermann F, Halangk W, Steiner JM, Esposito I, Rosendahl J, Schmid RM, Riemann M, Algül H. BCL3 Reduces the Sterile Inflammatory Response in Pancreatic and Biliary Tissues. Gastroenterology. 2016 Feb;150(2):499-512.e20. doi: 10.1053/j.gastro.2015.10.017. Epub 2015 Oct 23. PMID:26526716.

3) Fu L, Qin YR, Ming XY, Zuo XB, Diao YW, Zhang LY, **Ai J**, Liu BL, Huang TX, Cao TT, Tan BB, Xiang D, Zeng CM, Gong J, Zhang Q, Dong SS, Chen J, Liu H, Wu JL, Qi RZ, Xie D, Wang LD, Guan XY. RNA editing of SLC22A3 drives early tumor invasion and metastasis in familial esophageal cancer. Proc Natl Acad Sci U S A. 2017 May 22. pii: 201703178. doi: 10.1073/ pnas.1703178114. Epub 2017 May 22. PMID:28533408.

4) Li J, Yang H, Chen L, Li Y, Zhu Y, Dai Y, Chen K, **Ai J**, Zeng T, Mao X, Liu L, Li X, Guan XY. Establishment and characterization of human non-small cell lung cancer cell lines. Mol Med Rep. 2012 Jan;5(1):114-7. doi: 10.3892/mmr.2011.613. Epub 2011 Oct 3. PMID:21971914.

5) Qin YR, Tang H, Xie F, Liu H, Zhu Y, **Ai J**, Chen L, Li Y, Kwong DL, Fu L, Guan XY. Characterization of tumor-suppressive function of SOX6 in human esophageal squamous cell carcinoma. Clin Cancer Res. 2011 Jan 1;17(1):46-55. doi: 10.1158/1078-0432.CCR-10-1155. Epub 2010 Nov 17. PMID:21084391.

Parts of this thesis were presented at the following scientific meeting:

1) Bcl-3 acts as a proto-oncogene in pancreatic cancer in humans and mice.
   Scientific presentation.
   Jiaoyu Ai, Sonja Wörmann, Nina Diakopoulos, Kivanc Görgülü, Dietrich Rueß, Derya Kabacaoglu, Angelika Karpathaki, Alexandra Berninger, Marlena Kowalska, Matthias Treiber, Marina Lesina, Roland M.Schmid, Hana Algül.

24th United European Gastroenterology(UEG) week October 15-19, 2016, ACV, Vienna, Austria.

2) Bcl-3 acts as a proto-oncogene in pancreatic cancer in humans and mice.
Scientific poster presentation.
Jiaoyu Ai, Sonja Wörmann, L Song, Nina Diakopoulos, Marina Lesina, Angelika Karpathaki, Kivanc Görgülü, Dietrich Rueß, Roland M.Schmid, Hana Algül.
36. Deutscher Pankreasclub 18.02-20.02.2016 Freising/München.

3) Bcl-3 acts as a proto-oncogene in pancreatic cancer in humans and mice.
Scientific poster presentation.
Jiaoyu Ai, Sonja Wörmann, L Song, Nina Diakopoulos, Marina Lesina, Angelika Karpathaki, Kivanc Görgülü, Dietrich Rueß, Roland M.Schmid, Hana Algül.
<interact Munich> 2016 9th Munich life science symposium, Munich, 3-4 November 2016.

Table of Contents

1 Introduction

1.1 Pancreatic cancer

1.1.1 Epidemiology

Pancreatic ductal adenocarcinoma (PDAC), the most common form of pancreatic cancer, is a fourth cause of mortality worldwide [1] with an estimated 367,000 new cases diagnosed in 2015 and an associated 359,000 deaths in the same year [2]. Owing partially to its resistance to chemo- and radiotherapy, PDAC is expected to become the second most common cause of cancer-related deaths, overtaking deaths from breast and prostate as well as surpassing all other gastrointestinal cancers such as colorectal cancer, following only lung cancer by 2030 [3]. The overall median survival is less than 6 months after diagnosis [4] and a disease recurrence in up to 80% of resected tumors within 2 years [5]. Surgical resection, which is able to cure disease, is performed in only 15-20% of all pancreatic cancer patients and most of them including early-stage will develop local and/or metastatic recurrence at the end [6]. Because of the anatomically inaccessible location of the pancreas, which blocks normal examination and absence of clinically informative early diagnostic symptoms and biomarkers, the consequence is that the patients are often unaware of their disease until very late in its course [7] [8]. Lack of early detection and the efficient diagnosis and therapeutic options, including some targeted therapies which can minimize harmful side effects while treating the patients, have not made a real impact on the disease with poor prognosis and dismal survival rates in pancreatic cancer [8] [9].

1.1.2 Genetics of pancreatic cancer

PDAC is a complex genetic disease, and its progression from normal glandular epithelial cells into invasive adenocarcinomas requires the consecutive accumulation of several genetic and epigenetic alterations including activated *KRAS*, Telomere shortening, and inactivated *CDKN2A, TP53,* and *SMAD4* [9] [10] (Figure 1-1).

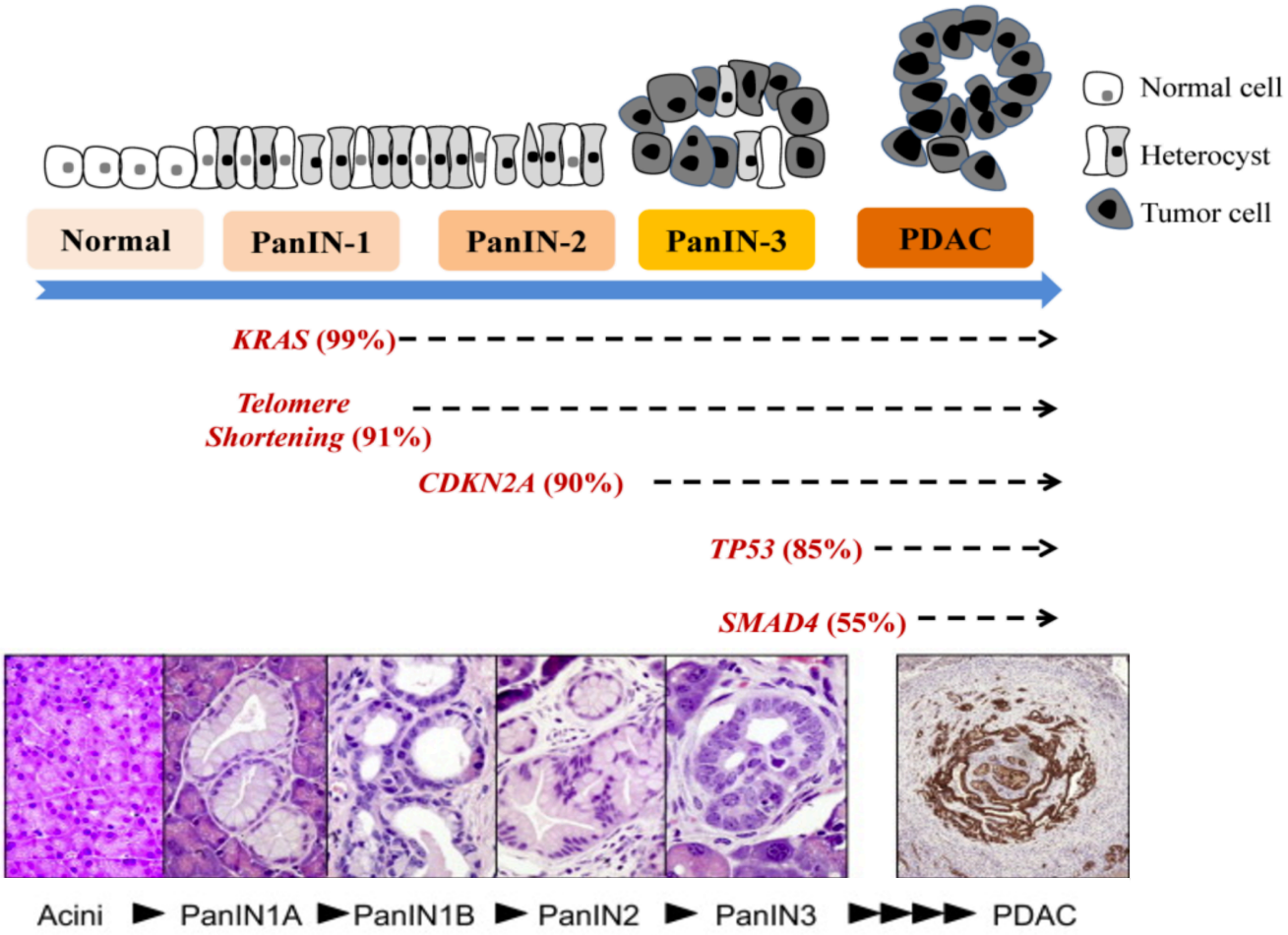

Figure 1-1: the model of genetic progression of pancreatic carcinogenesis. The molecular changes during pancreatic carcinogenesis can be classified as different stage such as the early panIN (telomere shortening and activating KRAS mutations), mediate panIN (inactivating mutations of *CDKN2A*), and late panIN (inactivating mutations of *TP53* and *SMAD4*) genetic alterations. Adapted from [9] [10].

One prominent feature of PDAC is an activation of the KRAS oncogene which follows point mutations. These mutations can be found in up to 90% of pancreatic carcinoma tissues. They maintain the protein in its active form independent of external signals resulting in activation of downstream effector pathways. In addition to involvement of KRAS in cell proliferation and survival of transformed cells, increasing evidence indicates that sustained KRAS signaling leads to the activation of inflammatory signaling pathways that play critical roles in regulating the initiation of pancreatic intraepithelial neoplasia (PanIN) and the progression of PDAC [11] [12] [13] [14]. Therefore, it requires to be based on a better understanding of the biology of *KRAS* mutations and the progression from PanIN to PDAC which is critical to find the biomarkers for early detection and diagnosis and new therapeutic approaches [9]. The genetically engineered mouse models of PDAC played a crucial role in understanding tumor initiation and tumorigenesis, which other experiments cannot address [15].

1.1.3 Genetically engineered mouse models of PDAC

In order to understand the biology of PDAC and to design therapeutic approaches several genetically engineered mouse models (GEMM) recapitulating key aspects of the disease have been developed. These models reproduce not only the histological changes, but also a desmoplastic stroma reaction and inflammatory response that are characteristic for human pancreatic tumors [10].

Most of the relevant GEMMs currently utilized are conditional Cre/loxP-based models. To activate or inactivate gene of interest bacterial Cre recombinase were used to delete a DNA sequence flanked by specific shot repeats (loxP sites) [16]. Since the best characterized initiating event during PDAC development is the single point mutation in codon 12 of the *KRAS* proto-oncogene, the model involved activation of an endogenous mutant *KRAS* allele in pancreatic progenitor cells was generated by the Tuveson group [17]. The *Lox-STOP-Lox* (*LSL*) construct that inhibit transcription and translation flanked by functional *LoxP* sites was inserted into the mouse genomic *KRAS* locus upstream of a modified exon 1 engineered to contain a G → A transition in codon 12. The mutated allele was activated by interbreeding *LSL-KRAS*^{G12D} mice with transgenic strains that expressed the bacterial Cre recombinase under the control of either the Pdx1 or the Ptf1a/P48 pancreatic-specific promoters. Although mutant *KRAS*^{G12D} is activated during early embryonic development, which probably does not reflect the occurrence of sporadic mutations in adult cells in humans, this model displays ADM and PanIN lesions histologically indistinguishable from those present in human patients, which progress to invasive and metastatic PDAC.

Other relevant prenatal mouse models of pancreatic cancer which have an impact in understanding of PDAC have been developed by inserting additional genetic changes during PanIN progression include mutation or inactivation of the tumor suppressor genes *TP53*, *INK4a/ARF*, and *SMAD4*.

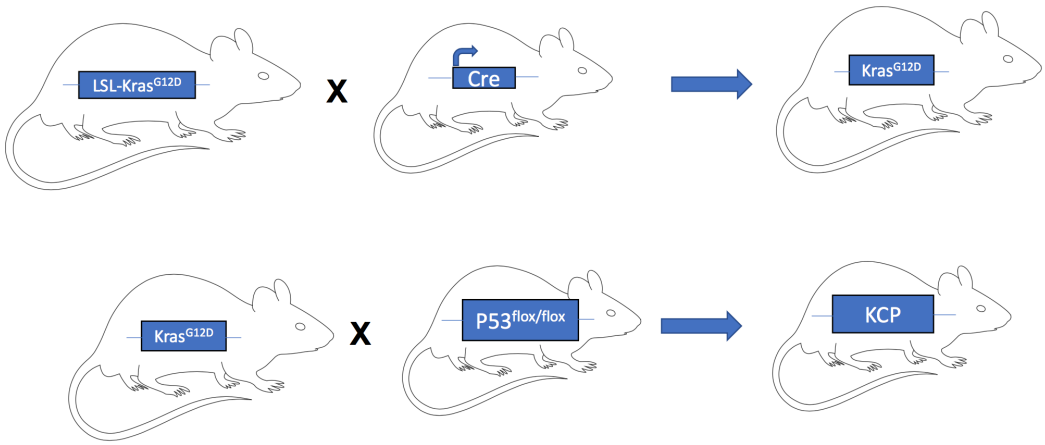

Figure 1-2: Schematic shows mutant *KRAS*-driven mouse models of pancreatic cancer. Cre/loxP mediated conditional activation of an endogenous mutant KRAS allele with additional inactivation of P53 in *KRAS*^{G12D} mouse model. KCP: Kras^{G12D}; Ptf1a/P48-Cre; P53$^{flox/flox}$.

1.2 Metastasis

Tumor cell metastasis - the spread of cancer cells from the primary tumor to distant sites - is responsible for approximately 90% of the deaths related to cancer, representing a toll of around 8.2 million patients worldwide in 2012 [18] [19] [20]. Metastasis is the fatal stage of tumor progression and remains the most poorly understood constituent of cancer pathogenesis [21]. The invasive and migratory capabilities of carcinoma cells require a loss of cell adhesion and increase cell mobility, collectively described as epithelial to mesenchymal transition (EMT) [19] [22].

1.2.1 Metastatic progression

In order to metastasize, cancer cells must go across several discrete steps. The first step is a loss of cellular adhesion and increased motility and invasiveness to access to the blood or lymphatic circulation. They must be able to overcome several stresses, including physical damage and immune-mediated removal. Once malignant cells have survived the circulation, they become trapped in the capillary beds of distant organs [18]. The next step is the entry into new environment and finally colonization of a secondary site (Figure 1-3) [23] [18] [24].

1.2.2 Metastasis in Pancreatic cancer

The poor prognosis of pancreatic cancer is related to several factors, one of them is metastatic dissemination [25]. The better understanding the biology of metastatic progression is useful to develop therapeutic strategies in pancreatic cancer. Giovannetti et al. summarize some factors, which are implicated in the formation of PDAC metastasis: epigenetic factors, such as microRNAs (miRNAs) played a major role in invasion and migration [26], the subpopulation of CD133 and CXCR4 double positive cancer stem cells (CSCs) that may directly or indirectly contribute to the generation of metastasis [27], tumor microenvironment (stellate cells, fibroblasts, endothelial and immune cells, an extracellular matrix, and a liquid milieu of cytokines/growth factors) [28]. Costa-Silva and collaborators demonstrated that PDAC-derived exosomes induced pre-metastatic niche formation and consequently increased liver metastatic burden [29]. Exosome-mediated TGFβ secretion and up-regulation of fibronectin by hepatic stellate cells support the survival of disseminated PDAC cells and their colonization in the liver. Furthermore, exosomes mediate the transfer of integrins, that favor PDAC metastasis to the lungs [28]. The genetic alterations that underlie PDAC metastasis have also been investigated. Yachida et al. use whole exome sequencing data of seven pancreatic cancer samples to analyze the clonal relationships between primary and metastatic cancers [30]. Notable, primary pancreatic cancers contain a mix of distinct subclones that are present within the primary carcinoma years before the metastases become clinically evident. Furthermore, Yachida et al. showed that clonal populations that give rise to distant metastases are genetically evolved from the original parental, non-metastatic clone, suggesting that genetic heterogeneity of metastases reflects the heterogeneity within the primary tumor [30]. But no metastasis-specific genetic alterations have been found in PDAC [30]. Increasing evidence indicates that activation of the embryonic programme ‘epithelial–mesenchymal transition' (EMT) promotes cancer cell invasion and metastasis in PDAC.

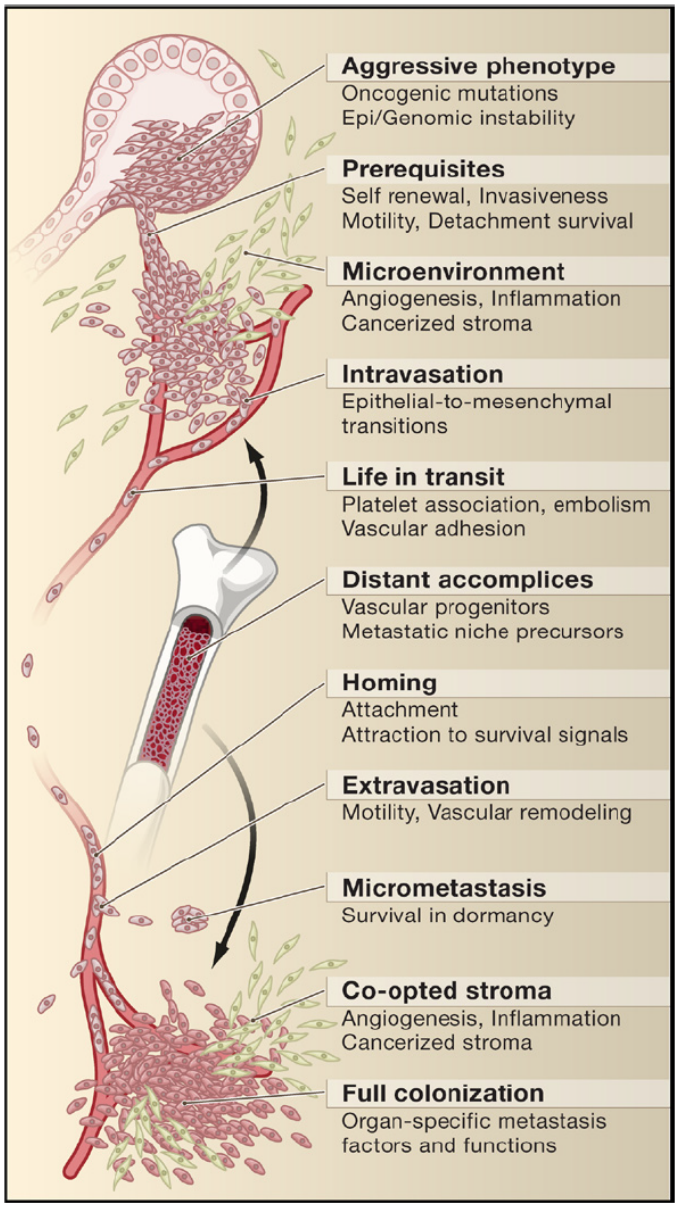

Figure 1-3: Stages of Metastatic Progression. adapted from Gaorav P. Gupta, Joan Massagué. Metastasis proceeds acquire some steps to spread distant organs. Loss of cellular adhesion, EMT, move to circulation, colonization in faraway organs [24].

1.3 Epithelial-to-mesenchymal transition (EMT)

An epithelial-mesenchymal transition (EMT) is a dynamic process that allows a polarized epithelial cell to undergo multiple biochemical changes that enable it to receive a mesenchymal cell phenotype [31]. While EMT is well studied during implantation, embryogenesis, and organ development, it also plays a role in tissue regeneration and organ fibrosis as well as in metastatic dissemination.

1.3.1 EMT associated with tumor progression

The activation of an EMT program, which is triggered by environmental factors such as inflammation and hypoxia, is a central driver of tumor malignancy and enhances the migratory and metastatic properties of cancer cells [32]. It is now accepted that EMT process not only increases the motility and invasiveness of cancer cells but also helps cells to escape apoptosis, anoikis, cellular senescence and immune defense [33]. This is associated with the activation of genes, the products of which enhance the competency for metastasis at all levels of the metastasis cascade [34].

Some studies report that EMT progress requires the phenotype of loss of epithelial markers such as E-cadherin, β-catenin and acquisition of mesenchymal markers N-cadherin, fibronectin, or vimentin [35] [36] [37].

Cadherins are cell surface glycoproteins with critical roles in cell-cell adhesion and cancer [38]. E-cadherin is a crucial component of apical zonula adherens in epithelial monolayers and considered as the key regulator of the epithelial phenotype [39]. Loss of E-cadherin expression was also associated with poorer prognosis and increased cancer progression in gastrointestinal cancers such as esophageal and gastric cancers, hepatocellular carcinomas and pancreatic cancers [40] [41] [42] [43].

β-catenin is part of a protein complex that forms adherens junctions. It plays dual functions which are associated with human malignancies. One role is activating the transcription of target genes responsible for proliferation and differentiation by Wnt signalling pathway. Another role is that it binds to E-cadherin to mediate the cell-cell adhesion [44]. Tomizawa et al. reported the E-cadherin promoter can be inhibited by mesenchymal marker such as Snail, Slug, ZEB-1, ZEB-2 and Twist [45].

Twist, as the basic helix-loop-helix transcription factor, induces metastasis in tumor cells by promoting epithelial-mesenchymal transition (EMT) as well as induces cellular de-differentiation program [46] [47]. Yang et al. reported that Twist played an important role in metastasis. Increased Twist results in decreasing cell-cell adhesion by loss of E-cadherin, activation of mesenchymal marker and induction of cell motility. Inhibition of Twist expression in metastatic mammary carcinoma cells suppresses their capacity to metastasize from mammary gland to lung [48]. Some other studies reported that Twist overexpression was associated with decreased expression of E-cadherin by binding to the promoter part and repressing transcription of E-cadherin [46] [49]. Inversely, increased Twist expression is associated with overexpression of N-cadherin which is important in the regulation of cell migration, invasion [46] [50].

1.3.2 EMT in pancreatic cancer

In human pancreatic tumor samples, mesenchymal marker fibronectin and vimentin are increased in high-grade tumors and within poorly differentiated areas of low-grade tumors, with a corresponding

decrease in epithelial marker E-cadherin expression [51]. In resected PDAC specimens nearly 80% have moderated to strong Snail expression while only 50% show similar Slug expression, with very few having strong Twist expression [52]. E-cadherin expression in tumor samples is inversely correlated with advanced tumor grade and worse outcomes. Arumugam et al. showed in pancreatic cancer tissue an inverse relationship between Zeb1, a crucial inducer of EMT in various human tumors, and E-cadherin expression. Similar results were published in pancreatic cell lines, in which silencing of mesenchymal marker Zeb1 leads to the up-regulation of E-cadherin and restoration of an epithelial phenotype [53] . Burk et al. report that ZEB1 triggers a miRNA-mediated feedforward loop that stabilizes EMT and promotes invasion of pancreatic cancer cells. Von Burstin et al. provided *in vivo* evidence that histone deacetylase 1 (HDAC1) and HDAC2 and Snail play an essential role in silencing E-cadherin during the metastatic process of pancreatic cancer cells [54].

TGF-β pathway is one of the central modulator of EMT. TGF-β can induce Snail, Slug and Zeb1 expression resulting in repressing of E-cadherin and causing the loss of cellular adhesion [55] [56]. One study by Hiraga et al. reported that Nox4-derived ROS transmit TGF-β□triggered EMT phenotype including morphological changes, increased migration and altered expression of E-cadherin and Snail in pancreatic cancer [57]. Similarly, Wu.et al. showed that TGF-β increased DEC1 as a basic-helix-loop-helix (bHLH) transcription factor by elevating EMT-related factor including SMAD3, Snail and N-cadherin, enhanced migration and invasion of Panc-1 cells [58].

Yang et al. found that vascular endothelial growth factor receptor-1 (VEGFR-1) promoted EMT, including increased expression of Vimentin and N-cadherin and decreased expression of E-cadherin, and tumor cell invasion and migration in pancreatic carcinoma cells [59]. Hamada et al. revealed that the treatment of Panc-1 cells with bone morphogenetic protein 4 (BMP4) increased expression of Vimentin and decreased expression of E-cadherin. BMP4 treatment also induced homeobox gene MSX2 expression, which was previously showed to be associated with EMT in pancreatic carcinoma cells [60]. LIV-1 as a downstream target of STAT3 is frequently expressed in PDAC tissues, and its expression is associated with tumor size and lymphatic filtration. LIV-1 induces EMT to promote cellular migration and metastasis [61].

1.4 Cancer stem cells (CSCs)

Cancer stem cells (CSCs), also known as tumor-initiating cells or tumor-propagating cells, are thought to be responsible for tumor initiation, drug and radiation resistance, invasive growth and metastasis, which are the main causes of cancer-related deaths [62]. CSCs are a subpopulation of tumor cells with unlimited self-renewal, multipotency and intrinsic stem-like properties for example expression of CSC markers [63] [64] [65] as well as resistance to treatment of gemcitabine [66].

1.4.1 Concept of CSCs

Nguyen et al. summary the concept of CSCs which demand more complex models to describe properties. The concept may open new insights into the biology of tumors and how to progress the anticancer treatment strategies (Figure 1-4) [67].

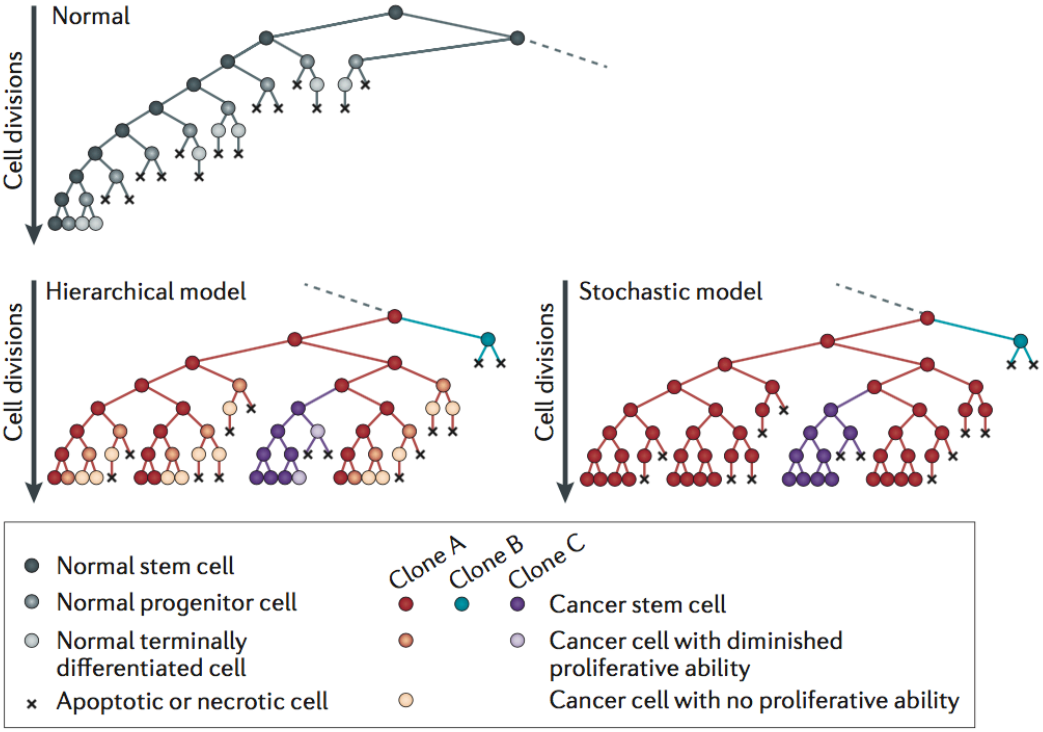

Figure 1-4: Hierarchical versus stochastic models of tumor cell heterogeneity. Adapted from L.V. Nguyen et al. nature reviews cancer 2012. The hierarchical model assumes that cancer stem cells (CSCs) represent a biologically distinct subset within the total malignant cell population. By contrast, the stochastic model assumes that every cell within a tumor has the same potential to act as a CSC [67].

Cancer stem cells are thought to be derived from stem cells in normal adult tissue, their progenitors, and/or dedifferentiated mature cells [68]. For this reason, the signal transduction pathways in CSCs, which play important roles in self-renewal, are similar with those involved in normal embryonic stem cell development. Signal pathways such as Wnt, Hedgehog, and Notch and downstream effectors, including the transcription factors β-catenin (β-cat), signal transducer and activator of transcription 3 (STAT3), and Nanog play key roles in CSC properties [62].

1.4.2 CSCs and Metastasis

Recent studies suggest that CSCs may directly or indirectly contribute to the generation of metastasis [69]. Malanchi et al. used the MMTV-PyMT mouse breast cancer model, which spontaneously metastasizes to the lungs to isolate the population of CSCs from primary MMTV-PyMT tumors and their pulmonary metastases. It was reported that the cell population positive for the stem cell markers CD90 and CD24 is responsible for metastases to the lung [70]. In publication by Shipitsin et al., the correlation between the proportion of $CD44^{+}CD24^{low}$ cancer stem cells in the primary breast cancer and increased risk of distant metastasis has been shown [71]. CD133 Protein as a CSC marker is associated with the cell polarity, which constitutes a crucial role for tumor growth, invasion and metastasis [72]. Moriyama et al. also show the behaviour of CD133+ cells including enhanced cell proliferation, migration and invasion [73]. The correlation between CD133 expression and clinical

outcome has been shown in gastric adenocarcinoma [74], rectal cancer [75] and non-small cell lung cancer [76].

Some reports have shown that EMT is a crucial mechanism in generating properties of stemness in cancer cells [77] [78] [79]. Some transcription factors induced by EMT including Snail, ZEB1 and Twist1 enhance CSC properties [80] [81] [82]. Puisieux et al. also reported the oncogenic role of Twist, Snail and ZEB to induce malignant transformation as well as acquirement of stemness properties from EMT-inducing transcription factors [83]. The similar studies also show that EMT is not only promoting migration of cancer cells but also maintaining the phenotype of cancer stem cells to form metastasis [84] [85] and to carry the ability to initiate new tumors [33]. Other factors, for example TGF-β1, are also thought to enhance both EMT markers and CSC markers such as Oct4, Sox2, Nanog, Klf4 in breast and lung cancer cells [86] [87].

1.4.3 CSCs in pancreatic cancer

CSC-like population were identified in different cancer types, including PDAC [88]. In the publication by Hermann et al., to identify pancreatic CSC in tissue samples derived from patients with pancreatic cancer, the surface marker CD133, which is expressed by normal and malignant stem cells, was used [27]. Histological analysis revealed the presence of rare CD133+ cells in the invasive front in serial pancreatic cancer sections. Furthermore, freshly isolated patient-derived CD133+ pancreatic cancer cells were capable of inducing tumor formation after transplantation into the pancreas of athymic mice. Interestingly, tumor formation following injection of CD133+ cells was faster and more efficient than tumor formation obtained with the total pancreatic cancer cell population. Histological analysis showed that tumor xenografts derived from CD133+ cells reproduced the original tumor. The ability of CD133+ pancreatic cancer cells to generate tumors after serial transplantations was evaluated. Second- and third- generation tumor cells from transplanted mice increased their aggressiveness, as indicated by rapid tumor formation. Moreover, a subpopulation of migrating CD133+ CSCs expressing the CXCR4 receptor was isolated. This specific CD133+ CXCR4+ CSC subpopulation has been shown to be responsible for tumor metastasis [27].

Other cell surface markers have been identified as markers for pancreatic CSCs, including CD24, CD44, CD166, epithelial cell adhesion molecule (EpCAM) [89]. The HGF receptor c-Met was shown as a marker of pancreatic CSCs associated with PDAC aggressiveness, metastatic behavior and intrinsic chemoresistance [90] [28].

The key signaling pathways, which regulate the function of pancreatic CSC population include Wnt/β-catenin, Hedgehog, Notch, NF-κB, PI3K/Akt and PTEN. Inhibition of the Notch pathway, which was found to be upregulated in pancreatic CSCs, using either a gamma secretase inhibitor or Hes1 shRNA in pancreatic cancer cells reduced the percentage of CSCs and tumorsphere formation [91]. Another crucial signaling pathway in maintenance of pancreatic CSC is Hedgehog signaling pathway. Inhibition of Hh signaling was demonstrated to reduce the self-renewal of pancreatic CSCs and reverse chemoresistance [92].

Another marker for pancreatic CSCs is doublecortin like kinase 1 (DCLK1), that may regulate Snail, Snug, Twist, ZEB1 and ZEB2 through a miR-200a-dependent mechanism, contributing to invasive and

metastatic potentials of pancreatic CSCs [93]. However, specific universal markers for pancreatic CSCs have not been found [62].

1.5 B-cell CLL/lymphoma 3 (Bcl-3)

1.5.1 Molecular functions of Bcl-3

B-cell CLL/lymphoma 3 (Bcl-3) is a proto-oncogene, identified as a translocation t(14;19) (q32;q13.1) in several patients of chronic lymphocytic leukemia [94], which is an atypical member of the IκB (inhibitor of NF-κB) family with seven Ankyrin repeat motifs. Unlike other members of IκB family, which inhibit activation of NF-κB signalling in the cytoplasm, Bcl-3 can locate in the nucleus, where it binds NF-κB1/p50 or NF-κB2/p52 homodimers on DNA and promotes gene transcription [95] [96]. Bcl3 contains a transactivation domain (TAD) and is found primarily in the nucleus[95]. The potential of Bcl-3 to either promote or suppress transcription has been shown to depend partly on different post translational modifications, such as phosphorylation of Bcl-3. Bcl-3 can be regulated by NF-κB1 and by itself. Cylindromatosis (Cyld) gene product inhibits nuclear translocation of Bcl-3 by its deubiquitinating [97] [98] [99].

Some studies reported that Bcl-3 induced cell proliferation and oncogenesis through activating of cyclin D1 promoter by acting as a coactivator with NF-κB p50 and p52 subunits [100] [101]. However, Bcl-3 has also been described as a gene suppression stabilizing p50 complex that inhibits transactivation of gene [102] [103] [104]. Although Bcl-3 formally belongs to the IκB family due to the presence of ankyrin repeats in its structure, the functional outcome of interaction between Bcl-3 and NF-κB has been controversial: depending on phosphorylation and concentration of Bcl-3 it results in either NF-κB target gene expression as a coactivator or gene suppression as an IκB in various conditions [95] [105] [106].

1.5.2 Role of Bcl-3 in tumorigenesis

Bcl-3 plays important roles as oncogene in hematological malignancies such as Hodgkin lymphomas [107]; anaplastic large cell lymphoma [108] [109] [110] and non-Hodgkin's lymphomas [111] [112] [113]. To the contrary, Bassetti et al. reported that overexpression of Bcl-3 slowed T cell activation in T cell responses to antigen [114]. Another study from Brocke-Heidrich et al. showed that overexpression of Bcl-3 increased apoptosis and repressed transcription in multiple myeloma [115].

In addition, Bcl-3 has been found to increase in a variety of solid cancers, including colorectal cancer [116] [117], breast cancer [118], hepatocellular carcinoma [119] [120], endometrial carcinoma [121], and nasopharyngeal carcinoma [122], to regulate tumorigenesis. The study from Liu et al. reported that Bcl-3 stabilizes c-MYC protein and promotes tumorigenesis in colorectal cancer [116]. Recently the study from Urban et al. showed Bcl-3/NF-κB complexes play the activated role in anti-apoptotic AKT signalling pathway to promote colorectal tumorigenesis [117]. To the contrary, a protective role of Bcl-3 was shown in the inflammatory DSS-model of colon cancer [123] as well as in the DEN/PB-

induced hepatocarcinogenesis model [124]. These opposite functions reveal that Bcl-3 is a transcriptional activator or repressor in tumor-initiation and -progression.

Some studies show that the post-translational modifications of Bcl-3 such as phosphorylation and ubiquitination activate or repress the downstream signalling pathways (Figure 1-5) [98] [125] [126] [127] [128] [99]. However, how Bcl-3 regulates transcription of genes remains to be elucidated.

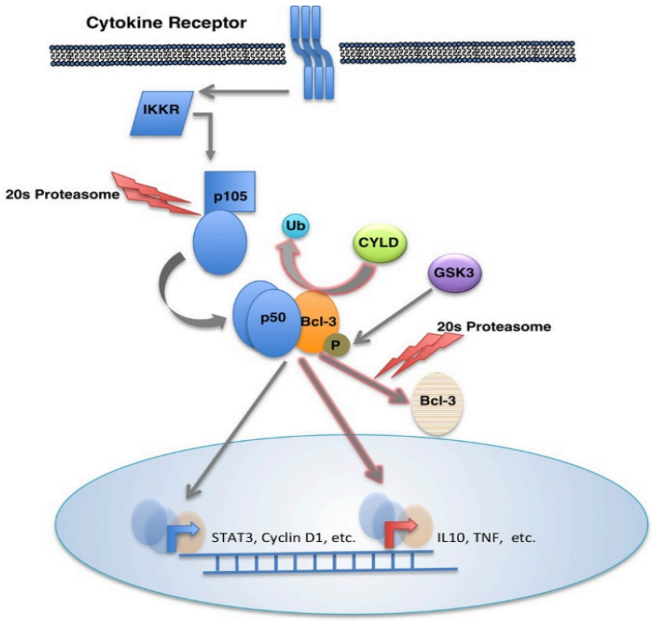

Figure 1-5: Bcl-3 signaling cascade (adapted from Maldonado et al. Molecular Cancer. 2011). Post-translational modifications such as phosphorylation by GSK3 and deubiquitination by CYLD regulate Bcl-3. Phosphorylated Bcl-3 delays its degradation. Ubiquitinated Bcl-3 promotes its nuclear translocation [99].

1.5.3 Bcl-3 and metastasis

Puvvada et al. showed that the nuclear Bcl-3 expression is negatively associated with survival and is prognostic in metastatic colorectal cancer [38]. Bcl-3 has been shown to be able to promote metastasis in mouse models of HER2-positive breast cancer [129]. Recently, overexpression of Bcl-3 was significantly associated with metastatic progression and metastasis-free survival in breast cancer patients. Bcl-3 was shown to regulate the process of breast cancer pulmonary metastasis by stabilization of Smad3 protein during TGF-β signalling [130].

However, the function of Bcl-3 in pancreatic cancer and metastasis has not been addressed so far.

1.6 Aim of study

In this study, we aimed to elucidate the role of Bcl-3 in pancreatic carcinogenesis by using *in vivo* and *in vitro* models. Bcl-3 deficient $Kras^{G12D}$ mouse model with additional pancreas-specific deletion of p53 (KCPB) was generated and analyzed. To characterize the functional role of Bcl-3 expression *in vitro*, tumor cell lines were isolated from pancreatic tumors developed in KCP and KCPB mice. The role of Bcl-3 in the process of pancreatic cancer metastasis was analyzed by experimental metastatic assay.

The correlation between expression of Bcl-3 and metastasis was analyzed in human data. Moreover, transcriptomics and metabolomics were performed to assess the changes in pancreatic cancer cells caused by Bcl-3 deficiency.

2 Materials and methods

2.1 Mouse models

$Kras^{G12D}$ ($Kras^{tm4Tyj}$) [131]: By homologous recombination in ES cells, the Kras locus was targeted with a cassette containing an oncogenic form of the KRAS protein in which the glycine at position 12 had been substituted with an aspartic acid. A loxP flanked stop codon was included upstream of the inserted Kras sequence, such that the mutant transcript would be expressed only after cre-mediated recombination.
Ptf1a-cre^{ex1} ($Ptf1a^{tm1(cre)Hnak}$) [132]: Part of exon 1 (ex1) in the Ptf1a locus was replaced with the Cre recombinase.
$p53^{flox/flox}$ ($Trp53^{tm1Brn}$) [133]: exons 2 through 10 were flanked by two loxP sites.
Bcl-$3^{-/-}$ (C57BL/6 background) ($Bcl3^{tm1Rie}$) [134]: A neomycin selection cassette replaced sequence encompassing all of exons 3 through 5 and a portion of exon 6.
LSL-$Kras^{G12D}$, Ptf1a-cre^{ex1}, $p53^{flox/flox}$ and Bcl-$3^{-/-}$ strains were interbred to obtain compound mutant LSL-$Kras^{G12D}$; Ptf1a-cre^{ex1} (termed KC), mutant LSL-$Kras^{G12D}$; $p53^{flox/flox}$; Ptf1a-cre^{ex1} (termed KCP), mutant LSL-$Kras^{G12D}$; Bcl-$3^{-/-}$; Ptf1a-cre^{ex1} (termed KCB), mutant LSL-$Kras^{G12D}$; $p53^{flox/flox}$; Bcl-$3^{-/-}$; Ptf1a-cre^{ex1} (termed KCPB) mice. LSL-$Kras^{G12D}$ mice were used as control animals. C57BL/6 and NSG™ (NOD *scid* gamma) mice (6-8 weeks of age) were purchased from Jackson laboratory. AthymicNude-Foxn1nu (6-8 weeks of age) were purchased from Envigo.
For all the experiments, mice were housed under specific pathogen-free conditions. All animal procedures were reviewed and approved by the Zentrum für Präklinische Forschung of the Technical University of Munich, which follows the federal German guidelines for ethical animal treatment.

2.2 DNA/RNA analyses

2.2.1 DNA isolation from biopsies

Tail tips or clipped ear parts of mice were lysed in 200 µl DIRECTPCR-TAIL Lysis Buffer (VIAG102-T, PEQlab) with 10 µl proteinase K (20 mg/ml, Roche) at 56 °C for 2-12 hours. After the incubation, samples were mixed and incubated at 85 °C for 45 minutes to inactivate the proteinase K. Samples were centrifuged at 4°C for 10 minutes.

Table 2-1: Genotyping PCR protocol

Type of mice	Step		Temperature	Time	
Bcl-3$^{-/-}$	Pre-incubation		94 °C	10 min	
	Amplification	Denaturation	94 °C	0.5 min	32 cycles
		Annealing	60 °C	0.5 min	
		Extension	72 °C	1.5 min	
	Final extension		72 °C	10 min	
	Cooling		4 °C	∞	
Kras	Pre-incubation		94°C	4 min	
	Amplification	Denaturation	94°C	0.5 min	40 cycles
		Annealing	58°C	0.5 min	
		Extension	72 °C	1.5 min	
	Final extension		72 °C	10 min	
	Cooling		4 °C	∞	
Cre	Pre-incubation		95 °C	5 min	
	Amplification	Denaturation	94 °C	45 sec	40cycles
		Annealing	58°C	30 sec	
		Extension	72 °C	1 min	
	Final extension		72 °C	10 min	
	Cooling		4 °C	∞	
P53$^{lox/lox}$	Pre-incubation		95 °C	5 min	
	Amplification	Denaturation	94 °C	45 sec	38 cycles
		Annealing	58 °C	30 sec	
		Extension	72 °C	1.5 min	
	Final extension		72 °C	10 min	
	Cooling		4 °C	∞	

2.2.2 Genotyping PCR

All genotyping PCRs were performed using the RedTaq Ready Mix (Sigma) or GreenTaq Mix (Kapa Biosystems) with 1-2 µl DNA (supernatant) templates with a standard genotyping polymerase chain reaction (PCR) protocol (Table 2-1). All primers (Table 2-2) were used at a final concentration of 10 pM. Mice were genotyped with the assistance of Chantal Geisert, Viktoria Mayr, Marlena Kowalska and Alexandra Berninger.

Table 2-2: Genotyping primer

Type of mice		Primer sequence (5'-3')	Product size (bp)
***Bcl-3*$^{-/-}$**	MRINT3 as	CCA CAG AGC AAC CTG GAA GCA	1250 bp (KO) 1500 bp (WT)
	EX32 as	GGC TCC CAA GCT TGA AAA GGC	
	MRNEO as	GCA TCG CCT TCT ATC GCC TTC	
Cre	Cre 01	ACCAGCCAGCTATCAACTCG	~ 200 bp (mut/+) ~ 350 bp (WT)
	Cre 02	TTACATTGGTCCAGCCACC	
	Cre 03	CTAGGCCACAGAATTGAAAGATCT	
	Cre 04	GTAGGTGGAAATTCTAGCATCATCC	
Kras	Kras ^{G12D} mut-UP	CCATGGCTTGAGTAAGTCTGC	~ 200 bp (mut/+) ~ 300 bp (WT)
	Kras-wt-UP1	CACCAGCTTCGGCTTCCTATT	
	Kras-URP-Lp1	AGCTAATGGCTCTCAAAGGAATGTA	
***P53*$^{lox/lox}$**	Loxp-1	CACAAAAACAGGTTAAACCCAG	~ 350 bp (flox) ~ 280 bp (WT)
	Loxp-2	AGCACATAGGAGGCAGAGAC	

2.2.3 RNA isolation

After sacrificing mice, small tissue pieces were taken from pancreas and immediately transferred into RLT lysis buffer containing 1 % β-mercaptoethanol, homogenized and frozen in liquid nitrogen. Cells were washed twice with ice-PBS and collected by scratched with cell scraper (Sarstedt). Cell pellets were transferred into RLT buffer as described for tissue. The RNeasy Mini Kit (Qiagen) was used to isolate RNA according to the manufacturer's instruction. RNA concentration was measured in a NanoDrop 2000 spectrophotometer (Peqlab). To judge the integrity and overall quality of a total RNA preparation, native agarose gel electrophoresis was performed by inspection of the 28s and 18s rRNA bands.

2.2.4 cDNA synthesis

Complementary DNA (cDNA) synthesis was performed using the Superscript™ II Reverse Transcriptase Kit (Invitrogen) and Oligo(dt) primer (500 µg/ml, Invitrogen) according to the manufacturer's instruction. The concentration of cDNA was adjusted to 20 ng/µl.

Table 2-3: Quantitative RT-PCR program

Step		Temperature	Time	
Pre-incubation		95 °C	10 min	
Amplification	Denaturation	95 °C	10 sec	45 cycles
	Annealing	60 °C	20 sec	
	Extension	72 °C	10 sec	
Melting		95 °C	1 min	
		55 °C	1 sec	
		98 °C	continuous 0.11 °C / sec	5 acquisitions / sec
Cooling		37 °C	5 min	

2.2.5 Quantitative real-time PCR (RT-PCR) analysis

Quantitative RT-PCR was performed on a LightCycler 480 (Roche) using the LightCycler 480 SYBR Green Master Mix I (Roche) according to the protocol as described previously [12].

Table 2-4: Primers used for RT-PCR

Gene	Forward primer	Reverse primer
Cyclophilin	ATG GTC AAC CCC ACC GTG	TTC TGC TGT CTT TGG AAC TTT TGC
BCL3	GGA GCC GCG AAG TAG ACG T	TGT GGT GAT GAC AGC CAG GT
HES1	TGC CAG CTG ATA TAA TGG AGA A	CCA TGA TAG GCT TTG ATG ACT TT
OCT3/4	TCT TTC CAC CAG GCC CCC GGC TC	TCT TTC CAC CAG GCC CCC GGC TC
SOX2	TAG AGA TAG ACT CCG GGC GAT GA	TTG CCT TAA ACA AGA CCA CGA AA
Snail	CCG GAA GCC CAA CTA TAG CGA	ACA GCG AGG TCA GCT CTA CG
ZEB1	CCA CTG TGG AGG ACC AGA AT	CTC GTG AGG CCT CTT ACC TG
PGC-1a	AAC CAG TAC AAC AAT GAG CCT G	AAT GAG GGC AAT CCG TCT TCA
BNIP3	CTG GGT AGA ACT GCA CTT CAG	GGA GCT ACT TCG TCC AGA TTC AT
TFAM	GAG CAG CTA ACT CCA AGT CAG	GAG CCG AAT CAT CCT TTG CCT
Nrf1	TCT CAC CCT CCA AAC CCA AC	CCC GAC CTG TGG AAT ACT TG
Nrf2	TTC TTT CAG CAG CAT CCT CTC CAC	ACA GCC TTC AAT AGT CCC GTC CAG
Nix	CCT CGT CTT CCA TCC ACA AT	TTC TTG TGG TGA AGG GCT GT
HPRT	TCC TCC TCA GAC CGC TTT T	CCT GGT TCA TCA TCG CTA ATC
huBCL3	CGC CAA CGT GAA CGC GCA AA	ATG TCG ATG ACC CTG CGG CTG

huHPRT	CCT GGC GTC GTG ATT AGT GA	AGA CGT TCA GTC CTG TCC ATA A
huβ-actin	GCG AGC ACA GAG CCT CGC CTT	CAT CAT CCA TGG TGA GCT GGC GG

50ng - 100ng cDNA were used as a template. Melting Curve analysis was performed to check primer-dimer artifacts and to ensure reaction specificity (Table 2-3). Different primers were used for real-time PCR assay. Cyclophilin was used as a housekeeping gene for normalization (Table 2-4). Values were calculated using the following equation: Fold difference = $2^{\Delta Ct} = 2^{(Ct\ gene\ of\ interest\ -\ Ct\ cyclophilin)}$. *P* values were calculated using the statistical software Prism 5 (GraphPad Software, Inc).

2.2.6 Microarray Data Analysis

RNA isolation from either KCP cells or KCPB tumor cells and Affymetrix GeneChip (*Mus musculus*) Mouse Gene 1.0 ST Array was conducted by the service facility KFB Center of Excellence for Fluorescent Bioanalytics (Regensburg, Germany, www.kfb-regensburg.de). Microarray data were analyzed by using the Gene set enrichment analysis software (GSEA) provided by the Broad Institute. CGP (chemical and genetic perturbations) analysis was performed for the genotypes mentioned. A FDR <0.25, NES >1, and p-value <0.05 were considered statistically significant. Gene array hybridization raw data have been deposited in the ArrayExpress database under accession number: E-MTAB-5624.

2.2.7 Significance Analysis of Microarrays (SAM)

Statistically significant changes in gene expression were determined performing SAM analysis. To quantify the intensity of the relationship between gene expression and response, gene specific t-tests were carried out. The SAM analysis software package was provided by Stanford University. Genes at least two-fold up-regulated were considered as statistically significant.

2.3 Histology

2.3.1 Hematoxylin and eosin (H&E) staining

For H&E staining, paraffin-embedded sections (1.5-3 μm) were de-paraffinized in xylene (X-TRA Solv, Medite GmbH) twice for 5 min. The sections were rehydrated in ethanol (100%, 96% and 70%; 2 x 3 minutes) and water (2 x 3 minutes). The slides were stained in hematoxylin solution (Merck Millipore) for 6 min and washed with flowed tap water for 10 min. Afterwards, the slides were stained in eosin solution (Waldeck GmbH) for 3.5 minutes, and dehydrated in 96% ethanol and isopropanol for 25 seconds of each and xylene (twice for 3 minutes). Finally, the slides were covered with mounting medium (Pertex, Medite GmbH) and coverslips.

2.3.2 Immunohistochemistry

Slides were de-paraffinized and rehydrated as described under 2.3.1. For antigen retrieval, slides were boiled in either 10 mM citrate acid buffer (pH 6.0) or 1 mM EDTA (pH 8.0) (depending on the

primary antibody) shortly and sub-boiled for 10 minutes. Slides were cooled down at room temperature for 20-30 minutes and washed with water twice for 5 minutes. To quench endogenous peroxidase activity, sections were incubated with 3% H_2O_2 in the dark for 15 minutes. Subsequently, slides were washed twice with wash buffer (TBS-T or PBS-T, depending on the primary antibody) for 5 minutes. To block unspecific antibody binding, slides were incubated in blocking solution (5 % goat or rabbit serum, depending on the secondary antibody with or without avidin, depending on the primary antibody, in wash buffer) for 1 hour at room temperature. After washing with wash buffer twice for 5 minutes, slides were incubated with primary antibody in blocking solution (with or without biotin, depending on the primary antibody) overnight at 4°C or at room temperature, depending on the primary antibody (Table 2-5).

After incubation with the primary antibody, slides were washed with wash buffer twice for 5 minutes and incubated with the secondary antibody (Vector laboratories) in blocking solution for 1 hour at room temperature. Signal detection was performed with avidin-biotin peroxidase complex for biotinylated secondary antibodies (Table 2-7). ABC kit (Vector laboratories) and DAB reagent (Vector laboratories) were used according to the manufacturer's instruction.

Subsequently, slides were counterstained with hematoxylin solution (Merck Millipore) for 2-3 seconds and washed with flowed tap water for 10 minutes. The slides were rehydrated in ethanol (70%, 96%, 100%; 2x20 seconds) and xylene (twice for 3 minutes). Finally, the slides were done as 2.3.1.

Table 2-5: Primary antibodies for immunohistochemistry

Antibody	Dilution	Source	Company	Product no.
BCL3	1:100	Rabbit	Santa Cruz	sc-185
Vimentin	1:200	mouse	Abcam	ab8978
Twist	1:100	Rabbit	Abcam	ab49254
E-cadherin	1:500	Rabbit	Cell Signaling	#4065
β-catenin	1:200	Rabbit	Cell Signaling	#9562
CD44	1:100	Rat	Santa Cruz	sc-18849

2.3.3 Immunofluorescence

Immunofluorescence staining was performed according to a previously published protocol [12] [135]. $2x10^4$ cells were seeded on an 8 well chamber slide (Corning Life Sciences**)** 24 hours prior to staining. Adherent cells were washed twice with ice cold phosphate-buffered saline and treated with 3 % bovine serum albumSigma) and 0.1 % Triton X-100 Sigma) in phosphate-buffered saline for 15 minutes at room temperature. After blocking with 10 % goat serum (Sigma) and 1 % bovine serum albumin in phosphate-buffered saline for 1 hour at 4°C, cells were stained with primary antibodies (Table 2-6) in blocking solution overnight at 4°C. After washing steps, secondary antibodies (goat anti-rabbit, Alexa Fluor 568 nm; Invitrogen; or goat anti-mouse, Alexa Fluor 488 Invitrogen) were applied for 1 hour at room temperature. For paraffin-embedded slides antigen retrieval was performed according to the immunohistochemistry protocol. After blocking with 5 % goat serum (Sigma) or donkey serum (D9663; Sigma) (depending on the secondary antibody) in wash buffer for 2 hours at room temperature, slides were incubated overnight with primary antibodies in blocking solution at 4°C. Subsequently, secondary

antibodies (Table 2-7) were applied for 1 hour at room temperature. Slides were covered with DAPI containing mounting medium (H-1200; Vectashield). Fluorescence microscopy (Zeiss Axiovert 200M) was used for evaluating stained sections.

Table 2-6: Primary antibodies for Immunofluorescence

Antibody	Dilution	Source	Company	Product no.
Vimentin	1:200	mouse	Abcam	ab8978
E-cadherin	1:500	Rabbit	Cell Signaling	#4065
CD133	1:50	Rat	eBioscience	#17-01331-81

Table 2-7: Secondary antibodies list for IHC and IF

Antibody name	Catalog number	Application	Producer
Biotinylated Anti-Rat IgG(H+L) in Rabbit	BA-4000	IHC	VECTOR, USA
Biotinylated Anti-Rabit IgG(H+L) in goat	BA-1000	IHC	VECTOR, USA
Biotinylated Anti-Mouse IgG(H+L) in goat	BA-9200	IHC	VECTOR, USA
Biotinylated Anti-Goat IgG(H+L) in Rabbit	BA-5000	IHC	VECTOR, USA
Polyclonal Goat Anti-Rabbit Immunoglobulins/HRP	P0448	IF	Dako Deutschland GmbH (Hamburg, Germany)
Polyclonal Goat Anti-Mouse Immunoglobulins/HRP	P0447	IF	Dako Deutschland GmbH (Hamburg, Germany)

IHC = Immunohistochemistry; IF = Immunofluorescence.

2.3.4 Histological analyses

Histological analyses were performed with the Axiovert Imager (Carl Zeiss, Göttingen, Germany). Murine pancreatic tissue alterations were analyzed and graded according to the most recent consensus report on pathology of genetically engineered mouse models of pancreatic exocrine cancer [136] with respect to the WHO classification of tumors of the exocrine pancreas [158]. Undifferentiated/anaplastic or sarcomatoid carcinoma were graded as “G4”.

2.4 Protein biochemistry

2.4.1 Protein isolation from tissue or cells

The following solutions and buffers were prepared in advance:

IP-buffer (1x): 50 mM Hepes, pH 7.9 (Sigma-Aldrich); 150 mM NaCl (Sigma-Aldrich); 1 mM EDTA, pH 8.0 (Sigma-Aldrich); 0.5 % NP-40 (Sigma-Aldrich); 10 % Glycerol (Sigma-Aldrich).
IP-buffer working solution (1x): 1 % Protease inhibitor (Serva) and 1 % Phosphatase inhibitor (Serva) were added before using.
Laemmli-buffer (5x): 300 mM Tris-HCl, pH 6.8 (Sigma-Aldrich); 10 % SDS (Sigma-Aldrich); 50 % Glycerol (Sigma-Aldrich); 0.05 % Bromphenol blue (Sigma-Aldrich); 5 % β-Mercaptoethanol (Sigma-Aldrich).

For protein isolation, the tissues/cells were homogenized with suitable volume of IP-buffer working solution or MLB (1x) buffer as previously described [137] according to the amounts of tissues/cells, and put on ice until foam is gone. Afterwards, the samples were centrifuged at 4°C for 10 minutes full speed, and the supernatants were kept on ice. Protein concentration was measured with the Bio Rad Protein Assay Kit (Bio Rad) and the samples were adjusted to 3 µg/µl with 5x Laemmli buffer.

2.4.2 Immunoblotting Analysis

Protein lysates were denatured at 95 °C for 5 minutes and kept on ice. Protein separation was performed with a SDS-PAGE gel (Gel percentage was depended on the protein size ranging from 7.5 % to 15 %) in running buffer at 120 V in a Bio Rad Mini Protein Gel System chamber. Discontinuous Gels were consisted of two fractions, which are a Stacking Gel (upper part of the gel, Table 2-8) and a Resolving Gel (lower part of the gel, Table 2-9). Loaded gels were run in running buffer. Separated protein was transferred to a PVDF membrane (Merck Millipore) or Nitrocellulose Blotting membrane (GE Healthcare Life Science) in a blotting chamber with 1× transfer buffer (Wet Transfer). The pore size of PVDF and Nitrocellulose membranes (0.2 µm or 0.45 µm), the voltage (300 mA - 400 mA) and duration time (1-3 hours) of membrane transfer were decided according to the size of target protein.

Table 2-8: Formulations of stacking gel

Stacking gel	**4%**
ddH_2O	3.0 ml
0.5 M Tris-HCl (pH 6.8) (Sigma-Aldrich)	1.3 ml
30% Acrylamide/Bis (Roche)	750 µl
10% SDS (Sigma-Aldrich)	50 µl
10% APS (Sigma-Aldrich)	25 µl
TEMED (Sigma-Aldrich)	10 µl
Total volume	5 ml

Table 2-9: Formulations of resolving gel

Resolving gel	**7.5%**	**10%**	**15%**
ddH_2O	4.9 ml	4.1 ml	2.5 ml
1.5 M Tris-HCl (pH 8.8) (Sigma-Aldrich)	2.6 ml	2.6 ml	2.6 ml
30% Acrylamide/Bis (Roche)	2.5 ml	3.3 ml	5.0 ml
10% SDS (Sigma-Aldrich)	100 µl	100 µl	100 µl

10% APS (Sigma-Aldrich)	50 µl	50 µl	50 µl
TEMED (Sigma-Aldrich)	15 µl	15 µl	15 µl
Total volume	10 ml	10 ml	10 ml

After member transfer, PVDF and Nitrocellulose membranes was incubated with 5% skim milk (or 5% BSA) in TBS-T for 1 hour to block any unspecific antibody binding. Afterwards, the membrane was incubated with primary antibody in 5% skim milk (or 5 % BSA) in TBS-T overnight at 4°C (Table 2-10). On the second day, the membrane was washed 3-5 times with TBS-T and incubated with the species-specific HRP-coupled secondary antibody in 5 % skim milk (or 5 % BSA) in TBS-T for 1 hour at room temperature (Table 2-11). After washing 3-5 times with TBS-T, the protein band was visualized using the ECL Western Blotting Detection Reagents (RPN2106, GE Healthcare) and Biorad Chemi Doc analyzer (XRS; Image lab software 5.21) and Amersham Hyperfilms (GE Healthcare).

Table 2-10: Primary antibodies for immunoblot list

Antibody	Dilution	Source	Company	Product no.
BCL-3	1:1000	Rabbit	Santa Cruz	sc-185
Vimentin	1:1000	mouse	Abcam	ab8978
Twist	1:200	mouse	Abcam	ab50887
E-cadherin	1:1000	mouse	BD	#610181
β-Catenin	1:1000	Rabbit	Cell Signaling	#9562
Phospho-ERK1/2	1:1000	Rabbit	Cell Signaling	#9101
ERK2	1:1000	Rabbit	Santa Cruz	sc-154
Phospho-AKT	1:1000	Rabbit	Cell Signaling	#9271
AKT	1:1000	Rabbit	Cell Signaling	#9272
Phospho-JNK	1:1000	mouse	Cell Signaling	#925
JNK	1:1000	Rabbit	Cell Signaling	#9258
Phospho-p38	1:1000	Rabbit	Cell Signaling	#4631
P38	1:1000	Rabbit	Cell Signaling	#9212
P50	1:1000	Rabbit	Abcam	ab32360
P105	1:1000	Rabbit	Abcam	Ab32360
P52	1:1000	Rabbit	Cell Signaling	#4882
P100	1:1000	Rabbit	Cell Signaling	#4882

RelA	1:1000	Rabbit	Santa Cruz	sc-372
RelB	1:1000	Rabbit	Santa Cruz	sc-226
c-Rel	1:1000	Rabbit	Santa Cruz	sc-71
IκB-α	1:1000	Rabbit	Santa Cruz	sc-371
IκB-β	1:1000	Rabbit	Santa Cruz	sc-945
Slug	1:1000	Rabbit	Cell Signaling	sc-9585
Snail	1:1000	Rabbit	Abcam	ab-180714
ZEB-1	1:1000	Rabbit	Novus	NBP1-05987
c-Myc	1:1000	Rabbit	Abcam	ab32072
PGC-1α	1:1000	Mouse	Millipore	ST1202
LaminA/C	1:1000	Rabbit	Santa Cruz	H-110
HSP90	1:1000	Rabbit	Santa Cruz	sc-7947
P53	1:500	Rabbit	Novocastra	CM5p
β-actin	1:2000	Mouse	Sigma	A5441

Table 2-11: Secondary antibodies list

Antibody name	Catalog number	Application	Producer
Anti-Rabbit IgG, HRP linked whole antibody (from donkey), 1ml	NA934V	WB	GE Healthcare (Little Chalfont, UK)
Anti-Mouse IgG, HRP linked whole antibody (from sheep), 1ml	NA931V	WB	GE Healthcare (Little Chalfont, UK)
Anti-Rat IgG, HRP linked whole antibody (from goat), 1ml	NA935V	WB	GE Healthcare (Little Chalfont, UK)

Application key: WB = western-blot.

Stock solutions and buffers:

1.5 M Tris-HCl (pH 8.8): 18.17 g Tris base (Sigma-Aldrich); 60 ml ddH_2O, adjust to pH 8.8 with HCl, bring total volume to 100 ml with ddH_2O, store at 4°C.

0.5 M Tris-HCl (pH 6.8): 6 g Tris base (Sigma-Aldrich); 60 ml ddH_2O, adjust to pH 6.8 with HCl, bring total volume to 100 ml with ddH_2O, store at 4°C.

10% (w/v) SDS: 10 g SDS (Sigma-Aldrich) was dissolved in 90 ml ddH_2O with gentle stirring and bring to 100 ml with ddH_2O, store at room temperature.
10% (w/v) APS (fresh daily): 100 mg ammonium persulfate (APS, Sigma-Aldrich) was dissolved in 1 ml ddH_2O, aliquoted and store at -20°C.
10x Running Buffer: 30.3 g Tris base (Sigma-Aldrich); 144.0 g Glycin (Sigma-Aldrich); 10.0 g SDS (Sigma-Aldrich), dissolve and bring total volume to 1 liter with ddH_2O, do not adjust pH with acid or base, store at 4°C.
10x Transfer Buffer: 30.3 g Tris base (Sigma-Aldrich); 144.0 g Glycin (Sigma-Aldrich), dissolve and bring total volume to 1 liter with ddH_2O, store at 4 °C.
1x Transfer Buffer: Dilute 100 ml 10x Transfer buffer with 200 ml Methanol and 700 ml ddH_2O, prechill the buffer before use.
10x TBS (pH 7.6): 24.2 g Tris base (Sigma-Aldrich), 80 g NaCl (Sigma-Aldrich), adjust to pH 7.6 with HCl and bring total volume to 1 liter with ddH_2O.
TBS-T: Dilute 100 ml 10x TBS with 900 ml ddH_2O, add 1 ml Tween 20 (0.1 %, Sigma-Aldrich).

2.4.3 Phosphatase assay

Protein lysates from human cell samples were prepared in IP-buffer at a final protein concentration of 3 μg/μl. Protein lysates were incubated either with phosphatase-inhibitor (1.56 mg/ml) (SERVA) or phosphatase (200U/ml) (10,000U/ml; Biolabs) for 30 minutes at 37°C. Samples in Laemmli-buffer were denatured by heating at 95°C for 5 minutes, cooled down, centrifuged shortly and used for immunoblot analysis.

2.4.4 Ras Assay

Pancreatic tissue of 13 week old KC and KCB mice was lysed with MLB (1x) buffer as previously described [137]. The Ras activation assay (Millipore) was performed according to the manufacturer's protocol. Briefly, 500 μl of protein lysate (protein concentration of 1 μg/μL) was incubated with 10 μL of Ras assay reagent (Raf-1 RBD, Agarose) for 45 minutes at 4°C under agitation. Following incubation steps, tubes were centrifuged at 14,000xg at 4°C to pellet the beads. The supernatant was discarded and the beads were washed 3 times with 400 μL MLB (1x) buffer. After washing, the beads were re-suspended with 40 μL laemmli buffer (2x) and boiled for 5 minutes at 95°C. Immunoblot analysis was performed.

2.4.5 Subcellular Fractions

Hypotonic buffer comprising of 100 mM HEPES (Gibco), 15 mM $MgCl_2$, 100 mM KCl, 5 mM DTT (Invitrogen), 1% NP40 (Roche), protease inhibitor Roche complete mini (Roche) and 100 μM Na3VO4 (Sigma) and 25 mM beta-glycerophosphate (Sigma) and nucleus buffer comprising of 200 mM HEPES (Gibco), 1 M KCl, 1 M NaCl, 1 % NP40, 5 mM DTT, 20 % Glycerol (Carl Roth), protease inhibitor Roche complete mini (1 tablet) and 100 μM Na3VO4 and 25 mM beta-glycerophosphate were prepared. Cells, sub-confluent (80%) grown on a 15cm cell culture plate were washed twice with ice cold phosphate buffered saline before 200 μl hypotonic buffer per plate was added. Cells were scratched and collected with buffer into an Eppendorf tube and centrifuged at 1200 rpm for 5 minutes.

After centrifuging, cells were kept for 20 minutes on ice for digestion. Following a centrifugation step at 13,200 rpm at 4°C for 20 minutes, the supernatant containing the cytoplasmic fraction was frozen until usage. After washing the pellet twice with hypotonic buffer, the nuclear buffer was added to the pellet in the same amount as the hypotonic buffer before. The pellet was pressed through a small syringe and the mix together with 0.5 µl Benzonase (Sigma) per 200 µl nuclear buffer was kept on ice for 20 minutes. After centrifugation at 13,200 rpm at 4°C for 15 minutes, the supernatant containing the nuclear fraction was obtained, and immunoblot analysis was performed.

2.5 Cell Culture

2.5.1 Pancreatic tumor cell lines

Primary murine pancreatic tumor cell lines were established from isolated murine pancreatic tumors. Cell lines were routinely cultured under standard conditions (5 % CO_2, 37°C) in culture media (Dulbecco's modified Eagle medium (DMEM) supplemented with 10% fetal bovine serum (FBS) (Gibco), 1 % PenStrep (Gibco), 1 % non-essential amino acid (NEAA) (Gibco). An overview of pancreatic tumor cell lines isolated from KCP and KCPB pancreatic tumors including mouse numbers, genotype and histology is provided in Table 2-12.

Table 2-12: List of mouse cell lines

Mouse number	Genotype	Histology
3039	KCP	PDAC
3042	KCP	PDAC
K2101	KCP	PDAC
M3346	KCP	PDAC
M3715	KCP	PDAC
K1654	KCP	PDAC
K1733	KCP	PDAC
M3568	KCPB	PDAC
M3525	KCPB	PDAC
K1907	KCPB	PDAC
M2954	KCPB	PDAC
M4016	KCPB	PDAC
M3581	KCPB	PDAC
M3580	KCPB	PDAC
M3529	KCPB	PDAC

Human pancreatic cancer cell lines Aspc-1, Bxpc-3, Capan-1, Colo-357, MiaPaCa-2, Su86.86, Panc-1 and T3M4 were obtained from Leibniz Institute DSMZ-German Collection of Microorganisms and Cell

Cultures GmbH. Human pancreatic cell lines and human PDAC patient-derived xenograft primary low passage cultures (patient tumors kindly provided by Dr. Mert Erkan, Koc University Hospital, Istanbul, Turkey) were cultured with DMEM or RPMI 1640 medium (Gibco) with 10 % FBS and 1 % PenStrep.

2.5.2 Proliferation Assay

Cells were seeded in a 6-well plate in a quantity of 5 x 10^4 per well in 1 ml DMEM supplemented with 10 % fetal bovine serum. The culture media were changed every other day. Cells were counted under microscopy after trypsinization every 24 hours after seeding, up to 144 hours using the neubauer counting chamber.

2.5.3 Colony formation assay

Six different cell lines from each group of KCP and KCPB were used for colony formation. Cells were counted under microscopy and seeded in the 6-well plates (300 cells/well). The plates were incubated at 37°C for 8 days with media exchanges every 2-3 days. At the end of incubation period, the media were removed and the cells were fixed with 4 % PFA and stained with 0.1 % crystal violet (C3886; Sigma), washed with water, and their area was quantified using imageJ.

2.5.4 Wound healing assay

1.5x10^5 cells were seeded in 6-well plates till confluence. Cell monolayer was artificially scratched with 10µl pipette tips. After scratching, the media was replaced by 2 ml culture media. The same locations were marked and take pictures under microscope with AxioCam camera. The time points were chosen in 0, 4 hours, 8 hours,12 hours and 16 hours for taking pictures to compare the wound healing behavior. The wound-closure percentages were calculated using ImageJ.

2.5.5 Migration Assay

1.5x10^5 cells were seeded in 6-well plates till confluence. Cell monolayer was artificially scratched with 10 µl pipette tips. After scratching the media was replaced by 2 ml culture media supplemented with 1 µM cytarabine (PHR1787 Sigma) to inhibit the proliferation of cells. The migratory behavior was recorded via digital time-lapse microscopy (Observer D1; Carl Zeiss Imaging), equipped with a CO2 incubation chamber, an AxioCam camera and a plan objective over a total observation time of 16 hours per movement front. Single pictures were taken at 30 min intervals, compiled as a video and subsequently used to quantify the migratory behavior. The wound-closure percentages were calculated using ImageJ.

2.5.6 Invasion Assay

6.5mm Transwell (Sigma, Corning Costar, USA) with 8.0 µm Pore polyester membrane insert was used in 24-well culture plates. The upper surface of the membrane was coated with 100 µl mixed matrigel (corning Life Sciences) per well. The matrigel was incubated at 37°C for gelling. 5x10^4 cells with 200 µl serum-free DMEM were placed in the upper chamber. The lower chamber was filled with 750 µl of culture media. After 48 hours, the cells were fixed by formaldehyde 3.7 % in phosphate buffered saline, permeabilized by 100 % methanol and stained with crystal violet. Cells that invaded to

the lower surface area of the membrane were calculated using ImageJ. Experiments were repeated at least in triplicates.

2.5.7 Anoikis assay

For the anoikis assay, 6-well plates were coated with poly-HEMA (20mg/ml) (Sigma) dissolved in 96 % ethanol under the cell culture hood. $5x10^5$ cells were seed and cultured for 48 hours in culture media. Under microscopy, the suspended sphere cells were checked. Surviving cells in the media were calculated using the neubauer counting chamber after trypsin and pipetted to obtain the single cell. The cells amount was analyzed by Prism software.

2.5.8 Luciferase Assay and Bioluminescence Imaging

Cultured in 6-well plates till 70 % confluence, KCP and KCPB tumor cells were transfected with the luciferase reporter plasmid 357 (10,149bp, 2500ng/well, kindly provided by Mathias Heikenwalder lab) by using Lipofectamine 2000 (11668-027, Invitrogen) according to the manufacturer's protocol. After 48 hours of transfection, the culture media was replaced with a media supplemented with G-418 (700 µg/ml) (Roche) for clonal selection. Colonies from single cell cloning were detected with luciferase reporter assay Kit (K801-200, Biovision) to verify positive clonal selection. Bioluminescence imaging was performed every 7 days starting 14 days after tail vein injection, to monitor for metastasis development. A cooled charge-coupled device camera attached to a light intensifier unit (Hamamatsu) was used. Mice were intraperitoneally injected with 300 µL of D-luciferin (15 mg/ml) (SYNCHEM) and 180 µL of anesthetic (82 % saline, 10 % ketamine (Ketavet; Pharmacia & Upjohn), and 8 % xylazine (Rompun; Bayer). After 10 minutes time delay, mice were positioned dorsally on a gel cushion in a dark box, and images were processed using Simple PCI software (Hamamatsu). Photographic images were obtained under dimmed light. The bioluminescence images were recorded with an exposure time of 240 seconds and merged with corresponding dimmed-light images. The light emissions were transformed into pseudocolors. Mean gray-level intensities were measured in regions of interest (ROIs) over the urogenital region of the mice to quantify the light emissions, and corrected for background.

2.5.9 Nontargeted Metabolomics Profiling

LC MS/MS–based nontargeted metabolomics analysis was conducted at the Genome Analysis Centre, Helmholtz Zentrum München as previously described [138]. In total $1x10^6$ primary pancreatic cells were essential for nontargeted metabolomics profiling. $3.75x10^5$ cells were seeded in 6-well plate with 2 ml culture medium and grown for 48 hours until 80-90 % confluent and an approximate number of $0.5x10^6$ was reached. When seeding the cells to the 6-well plate, 3 wells is for each cell line (one well for counting and 2 wells for metabolomics). The medium were collected into the Eppendorf tube (precooled by dry ice) and snap-freeze on dry ice and then store at -80°C. Cells were washed two times with PBS (37°C). Dry ice cold 80 % v/v methanol (400 µl) containing 4 recovery standard compounds to monitor extraction efficiency was added to the cells to cover the cells immediately. Cells were scraped and the cell suspension was transfered into a precooled (dry ice) 2ml screw cap micro tube filled with 160 mg glass sand 0.5mm diameter (Sarstedt Micro tube 2 ml, PP). Another 100 ul of dry ice cold methanol extraction solvent to wash the well was added and transferred to the micro tube.

The obtained cell suspensions were pooled into one tube in order to receive samples with 1 ml cell suspension and a total number of $1x10^6$ cells, representing 2 wells per tube. The samples were stored immediately at -80°C until metabolomic analysis was performed. The metabolites were assigned to cellular pathways based on PubChem, KEGG, and the Human Metabolome Database. Metabolic pathways were described as significantly up- or down-regulated, when metabolites assigned to those specific pathways were increased or decreased, respectively.

2.5.10 Seahorse Experiments

Two-step seeding process was done when seeding in Seahorse 24-well XF cell culture microplates. KCP and KCPB cells were collected and re-suspended to desired final cells $0.1x10^6$ in 100 µl of cell culture medium (DMEM (4.5 g/L glucose, +L-Glutamine, -Pyruvate, pH 7.6 at RT) supplemented with 10 % heat inactivated FBS (Gibco) and 1 % Pen/Strep) per well. Each cell line was triplicate. The background correction wells (A1, D6) are only medium (without cells). The pipette tip should be hold at an angle when seeding the cells and it is helpful to keep homogeneous cell layer. The cell culture microplate with KCP and KCPB cells were placed into the 37°C incubator for 2 hours to wait the cells to adhere. 150 µl of cell culture medium was slowly added once more. The cells were growing overnight in the cell culture incubator and were measured 48 hours after seeding. On the day of assay, the XF24 plate was transferred to a temperature-controlled (37°C) XF24 Extracellular Flux analyzer (Seahorse Bioscience) and equilibrated for 10 minutes. To determine the basal respiration four assay cycles (1-min mix, 2-min wait and 3-min measuring period) were used. Oligomycin (4 µM; inhibiting ATP synthase) was then added by automatic pneumatic injection (three assay cycles), followed by an injection of FCCP (carbonyl cyanide p-trifluoromethoxyphenylhydrazone) (0.5 µM) to completely uncouple mitochondria. A final injection of a cocktail of rotenone (4 µM) and antimycin A (2 µM) was used to end each experimental trace and to correct for the non-mitochondrial respiratory rate. Raw data were normalized to protein content.

2.5.11 Spheres Cultures

$6x10^4$ cells of either KCP or KCPB cell line were cultured in ultralow cell culture flasks (75 cm^2, Corning) in 30 ml serum-free DMEM/F12 medium (1:1; Gibco), supplemented with Pen/Strep (1:100; # Gibco), Fungizone (1:250; Gibco), L-Glutamine (1:100; Gibco), B-27 (1:50; Gibco), FGFβ (1:5000; Gibco). All cell culture was carried out at 37°C in a 5 % CO2 humidified incubator. After 7 days, spheres containing media was diluted 1:10 with complete media and the number of spheres/ml was calculated manually using a 4X objective. A total of 4 replicate measurements were calculated.

2.5.12 siRNA

KCP tumor cells were transfected with siRNAs targeting the Bcl-3 mRNA (mouse Bcl-3, EMU019281-20UG, SIGMA) by using Lipofectamine 2000 reagent (#11668-027; Invitrogen) according to the manufacturer's protocol. After either 48 hours or 72 hours, cells were collected for RNA and protein analysis. The siRNA targeting EGFP mRNA (esirna1, EHUEGFP-20UG, SIGMA) was used as a negative control.

2.5.13 Lentiviral ShRNA

To generate Bcl-3 knock-down mouse cell lines, cells were transduced with lentiviral vectors (Sigma-Aldrich no. SHCLNV-NM_033601 Bcl-3 MISSION® shRNA lentiviral transduction particles (TRCN00000 42556); expressing shRNA targeted to the coding strand sequence 5'-CCGGCCTTTACTACCAGGGA CCTTTCTCGAGAAAGGTCCCTGGTAGTAAAGGTTTTTG-3` located in the bcl-3 mouse gene. Transduced cells were selected and maintained in medium containing puromycin (1 µg/ml).

2.5.14 Human Bcl-3 Overexpression

The FLAG tagged Bcl-3 wild type construct was a gift from Dr. Alain Chariot (Laboratory of Medical Chemistry, Unit of Molecular Biology of Diseases, University of Liege, Belgium) [139]. To generate Bcl-3 over-expressing human PDAC cells, Panc-3 cells were transfected with either the pcDNA3.1-FLAG BCL-3 wild type plasmid or an empty pcDNA3.1 plasmid as a negative control using Lipofectamine 2000 (11668-027, Invitrogen) according to the manufacturer's protocol. Transfected cells were selected and maintained in culture media containing Geneticin (G-418) (700 µg/ml).

2.5.15 Flow Cytometry

FACS buffer and digestion solution were prepared before sacrificing mice.

FACS buffer: 1 % FCS (#10082147; Gibco) in phosphate buffered saline (PBS) (#14190-094; Gibco).

Digestion solution: 10 ml DMEM (#41965-039, Gibco), 12 mg collagenase (#C2139, Sigma), 2 mg Trypsin inhibitor (#T6522, Sigma). The ready digestion solution should be stored on ice until usage.

KCP and KCPB mice were sacrificed and the pancreata were harvested and washed three times in ice cold phosphate buffered saline and put with 10ml digestion solution in a culture dish under hood. Pancreata were injected with digestion solution, minced, and placed into the 37°C incubator for digestion for 15 minutes. After passing through a 70µm cell strainer, the single-cell suspensions of pancreatic cells were immunolabeled with fluorochrome-conjugated antibodies (Table 2-13) in FACS buffer. At first, cell suspensions were pre-incubated with purified anti-mouse CD16/CD32 (0.5-1 µl per 100 µl cell suspension) for 20 minutes on ice prior to staining for blocking non-specific Fc-mediated interactions. Fluorochrome-conjugated antibodies were added into the cell suspensions (1 µl per 100 µl cell suspension) and incubated for at least 30 minutes in the dark on ice or at 4 °C. Cell suspensions were washed with FACS buffer and centrifuged at 300-400 × g for 5 minutes at 4°C twice. Stained cells were resuspended in FACS buffer, and stained with propidium iodide (#556463; BD Biosciences) to assess viability or DAPI to exclude dead cells. Flow cytometry analysis was performed on a Gallios flow cytometer (Beckman Coulter; Brea, CA) after gating and excluding dead cells or an Attune Nxt Acoustic Cytmeter (ThermoFisher Scientific). For mitochondrial mass and membrane potential assays, cells were trypsinized and single-cell suspensions were incubated for 20 minutes at room temperature with 1 nM MitotrackerTM Deep Red FM or 5 nM MitoTracker® Red CMXRos (all from Life Technologies, Carlsbad, CA) prior to FACS analysis, as previously described [140]. Data were analyzed using FlowJo software (Ashland, OR).

Table 2-13: The antibodies used for FACS analysis

Antibody	Dilution	Source	Company	Product no.
muEpCAM-FITC	1:100	Rat	eBioscience	11-5791-80
muCD133-APC	1:100	Rat	eBioscience	17-01331-81
muCD44-eFluor450	1:100	Rat	eBioscience	48-0441-80
huEpCAM-FITC	1:10	Mouse	Biolegend	324204
huCD133-APC	1:10	Mouse	Miltenyi	130-090-826
huCXCR4-PE	1:20	Mouse	Biolegend	306510

2.5.16 In vivo Tumorigenicity Assay

KCP and KCPB Cells were trypsinized, resuspended in 50 µl of Matrigel, and then subcutaneously injected into female 6- to 8-week-old NU-Foxn1nu nude mice (Envigo). Tumor growth was monitored weekly for up to 6 weeks.

2.5.17 Metastasis Assay

NSG™, NOD *scid* gamma mice purchased from Jackson laboratory or Littermates of KCP mice 8 weeks of age were injected intravenously through the tail vein with 3×10^6 of either KCP or KCPB tumor cells. The mice were sacrificed 25 days after injection. The lungs were collected, embedded in paraffin and stained with hematoxylin and eosin (H&E). The area of metastasis was calculated on 1x magnification images using Zeiss axiovision microscopy program (Axiovision Rel.4.8).

2.6 Patient Data

2.6.1 Human PDAC samples

PDAC tissues and clinical data were collected from patients at the Klinikum rechts der Isar, Technical University of Munich. Fresh frozen tissue specimens (n=66) and Formalin fixed and paraffin embedded tissue specimen (n=66) were provided from the Institute of Pathology of the Technical University of Munich (Table 2-14). For immunoblot analysis tumor cell content of fresh frozen pancreatic cancer samples was set at least 20%. All human samples were histologically confirmed as PDACs by a pathologist. Informed consent was obtained from all patients. The study was approved by the institutional review board Ethikkommission der Fakultät für Medizin der Technischen Universität München.

2.6.2 TCGA Data Analysis

The RNA-seq dataset were retrieved from the Cancer Genome Atlas (TCGA) and the UCSC database. RSEM normalized counts log2(x+1) were applied to downstream analysis. Bivariate scatterplots with a fitted line were generated with R and Pearson correlation was computed. The heat map was

generated using Morpheus provided by the Broad Institute. Data were subjected to unsupervised hierarchical clustering and euclidean distance measurement, average linkage clustering was applied. In addition, human PDACs were sorted for their gradient BCL-3 expression level.

2.7 Statistical Analysis

Data are displayed as mean ± standard deviation. Mann-Whitney test or 2-sided Student t tests was performed to compare the parameters for the groups. An appropriate and statistical significance was set at *P < 0.05, **P < 0.01, and ***P < 0.001. Survival rates were calculated and displayed by the Kaplan–Meier method. Survival curves were compared by log-rank test.

Table 2-14: Clinical human data

ID	Histology	T	N	M	G
1018	PDAC	3	1	0	1
M606	PDAC	3	1	x	3
1017	PDAC	1	1	0	3
M607	PDAC	3	1	x	3
1021	PDAC	3	1	1	3
1003	PDAC	3	1	0	2
M711	PDAC	3	0	0	3
M680	PDAC	3	1	0	2
1014	PDAC	3	1	0	3
M272	PDAC	2	1	x	2
M060	PDAC	4	1	x	2
M584	PDAC	3	1	0	1
M312	PDAC	3	1	x	3
1010	PDAC	3	1	0	2
1024	PDAC	3	0	0	2
M704	PDAC	3	1	0	3
1020	PDAC	3	1	1	2
1016	PDAC	3	1	0	3
M214	PDAC	3	1	0	2
M596	PDAC	3	0	x	3
1011	PDAC	3	1	0	2
M190	PDAC	3	1	0	3
M758	PDAC	3	1	1	3
M109	PDAC	3	0	x	3
M247	PDAC	4	1	0	3

M539	PDAC	3	0	x	3
M603	PDAC	4	1	0	3
M279	PDAC	3	0	0	3
M669	PDAC	2	0	0	2
M713	PDAC	3	1	0	3
1026	PDAC	3	1	0	3
M270	PDAC	3	0	x	2
1012	PDAC	3	1	0	2
M604	PDAC	3	1	1	3
1004	PDAC	3	1	0	2
1034	PDAC	3	1	0	3
1028	PDAC	3	0	0	2
M119	PDAC	3	0	x	2
M111	PDAC	3	1	0	2
M323	PDAC	3	1	x	2
1022	PDAC	3	1	0	3
1023	PDAC	3	0	0	3
M440	PDAC	3	1	0	3
M592	PDAC	3	1	x	3
1032	PDAC	3	1	x	x
M185	PDAC	3	1	0	2
M762	PDAC	4	1	x	2
M287	PDAC	2	1	0	1
1031	PDAC	2	0	0	3
1029	PDAC	3	0	0	2
1007	PDAC	3	1	0	3
1033	PDAC	3	1	0	2
M724	PDAC	3	1	x	2
1030	PDAC	3	0	0	3
1001	PDAC	3	1	0	3
1008	PDAC	3	1	0	3
1002	PDAC	3	1	0	2
1025	PDAC	3	0	0	3
1006	PDAC	3	1	0	3
1015	PDAC	3	1	0	3
M510	PDAC	3	0	0	3
M234	PDAC	3	0	0	3
M732	PDAC	3	0	0	2

M130	PDAC	4	1	x	3
M211	PDAC	3	0	x	1
M324	PDAC	3	1	x	2

ID: human PDAC patients; T: Tumor size; N: Lymph node; M: Metastasis; G: Grade.

3 Results

3.1 Bcl-3 expression in human and murine PDAC considerably reduces tumor burden in mice.

While Bcl-3 overexpression has been reported in several solid tumor entities [99], its role in pancreatic cancer has not been studied to date. Hypothesizing that Bcl-3 [141] [142] is also critically involved in pancreatic tumorigenesis, various human PDAC cells lines and tissue samples were analyzed for Bcl-3 expression. Most human PDAC cell lines (Figure 3-1 A) and tumor lesions expressed Bcl-3 but to different levels, whereas in normal pancreatic tissues almost no Bcl-3 expression was found (Figure 3-1 B).

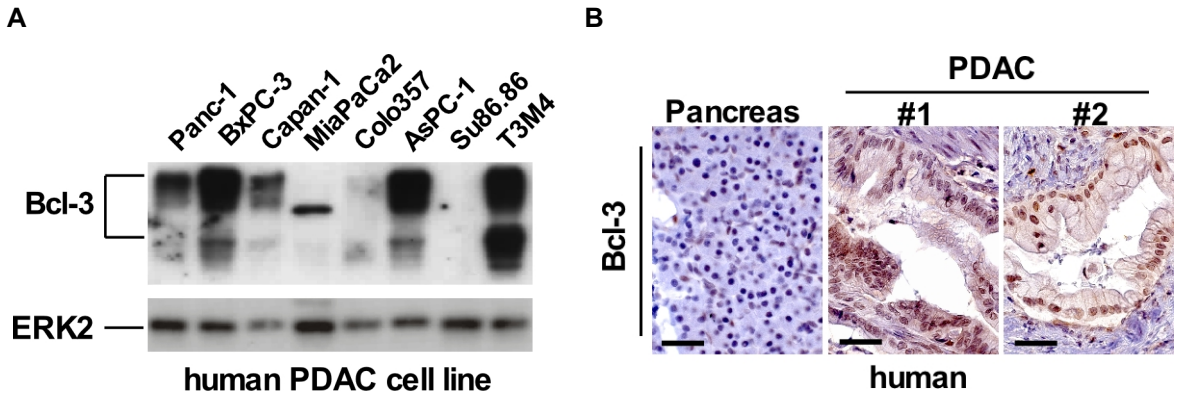

Figure 3-1: Bcl-3 is expressed in most human PDACs cells and tissues. (**A**) Immunoblot (IB) analysis of Bcl-3 expression in human PDAC cells. ERK2 served as a control. (**B**) Immunohistochemistry (IHC) for Bcl-3 in human PDAC tissue; representative images of sections of normal pancreas and human PDAC from two patients.

To understand the localization of Bcl-3 in pancreatic cancer, we performed the subcellular fractionation assay in human PDAC cell lines. Bcl-3 was highly expressed in the cytoplasm as well as in the nucleus (Figure 3-2 A). Since some studies show that the post-translational modification of Bcl-3 such as phosphorylation by GSK3 can modulate its nuclear entry and transcriptional activity [128], we analyzed a phosphorylation state of Bcl-3. Cells were analyzed in the presence or absence of the phosphatase or phosphatase inhibitor by western blotting. In the presence of the phosphatase, we observed de-phosphorylated Bcl-3. In contrast, the phosphatase inhibitor does delay the de-phosphorylation of Bcl-3 (Figure 3-2 B). These findings suggest that Bcl-3 is hyper-phosphorylated in human PDAC cell lines.

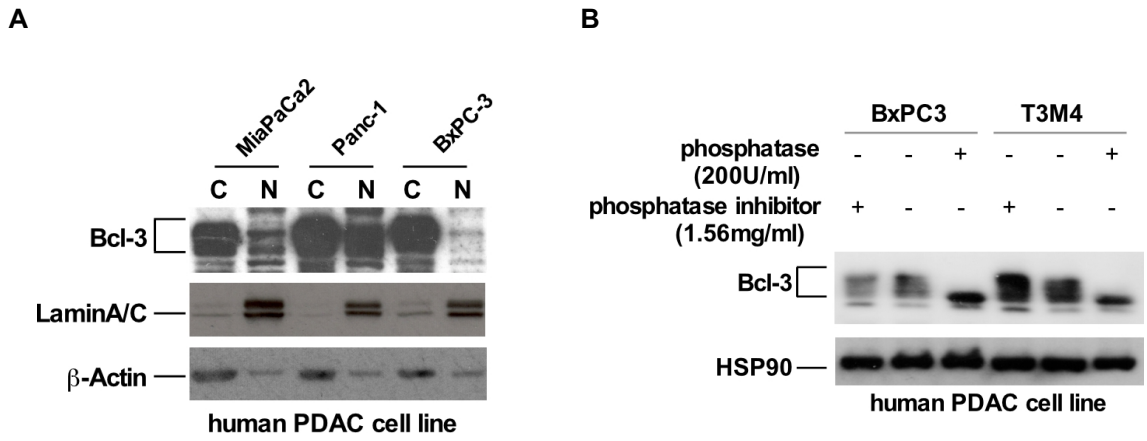

Figure 3-2: Expression and Phosphorylation state of Bcl-3 in human PDAC cells. (**A**) IB analysis of Bcl-3 in cytoplasmic and nuclear fractions of human PDAC cells lines. Lamin A/C and β-Actin served as controls. (**B**) IB analysis of Bcl-3 in human PDAC cells treated with phosphatase inhibitor (1.56mg/ml) prior to cell lysis and phosphatase (200U/ml) after cell lysis for 30 min at 37°C. HSP90 served as a control.

To further elaborate the functional role of Bcl-3 expression *in vivo*, we interbred the previously described *Kras*^{G12D} (KC) mouse model of PDAC [17] with Bcl-3 KO (termed Bcl-3$^{-/-}$) [134] and *p53*$^{flox/flox}$ (termed Trp53^{Fl}) [143] mice to obtain KCB, KCP and KCPB mice. While in the *Kras*^{G12D} driven mouse model (KC) Bcl-3 was highly expressed during all stages of pancreatic tumorigenesis, Bcl-3 expression was completely lost in Bcl-3 deficient (KCB) mice (Figure 3-3 A and B).

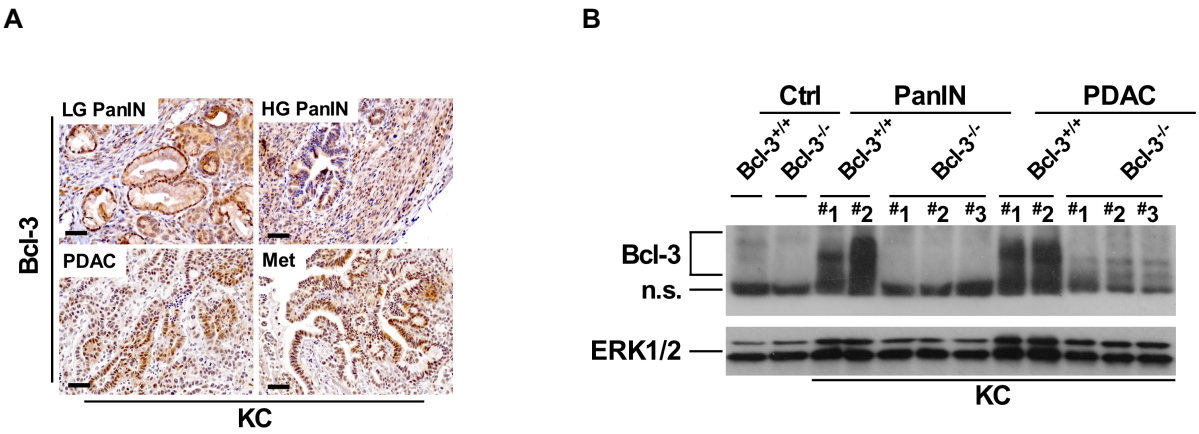

Figure 3-3: Bcl-3 is expressed in murine PDAC. (**A**) IHC for Bcl-3 in murine PDAC tissue including low grade PanIN (LG), high grade PanIN (HG), PDAC and Met (Metastasis). (**B**) IB analysis of Bcl-3 expression in representative pancreatic tissues: PanIN and PDAC stage from a non-Kras (Ctrl) and Kras driven mouse model harboring either wildtype or knockout Bcl-3. ERK1/2 served as a control.

In PDAC, the mutations of K-RAS oncogene are almost 90%. These mutations lead to an accumulation of GTP-bound proteins that maintains an active structure. Ras belongs to the super family of G proteins and plays important roles in signal transduction from membrane receptors in cells [144]. In order to elucidate if deletion of Bcl-3 has impacted on Ras activity, we performed Ras activity assay in murine pancreatic tissue from 13 week-old KC and KCB mice. Total Ras activity was not affected by Bcl-3 in spite of its considerable impact on tumor burden (Figure 3-4).

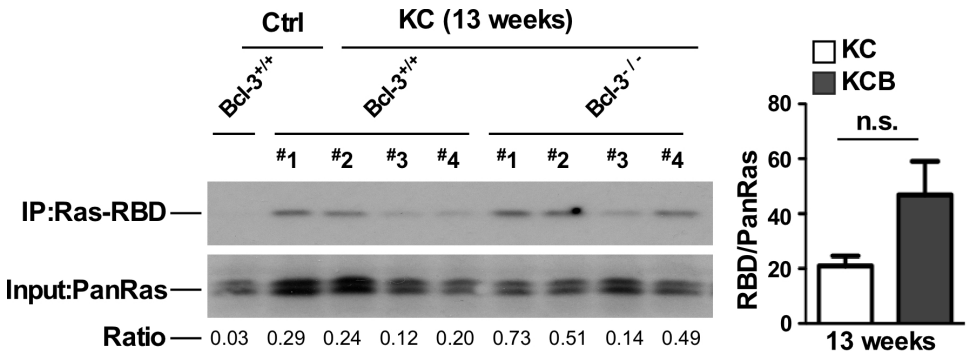

Figure 3-4: Ras activity assay. Ras activity assay in representative mouse pancreatic tissues from 13 weeks old non-Kras driven (Ctrl) and Kras driven mice harboring either wildtype (*KC*) or knockout Bcl-3 (*KCB*). Right: Immunoprecipitation and IB analysis of the RAS binding domain (RBD). panRAS served as input control. The density of bands was determined with ImageJ. Left: Summary of density ratios of RBD/panRAS. Means ± SD (*n*=4). n.s., not significant.

Bcl-3 deficiency in KCP mice (KCPB) was associated with a significantly reduced overall survival compared to KCP mice harboring wild type Bcl-3 (Figure 3-5 A), thus suggesting an unexpected but marked impact of Bcl-3 on the tumorigenesis of PDAC in mice. Although PDACs formed independently of Bcl-3 (KCP and KCPB show a tumor incidence rate of 100%; data not shown), the tumor volume was significantly enlarged in Bcl-3 deficient mice (Figure 3-5 B).

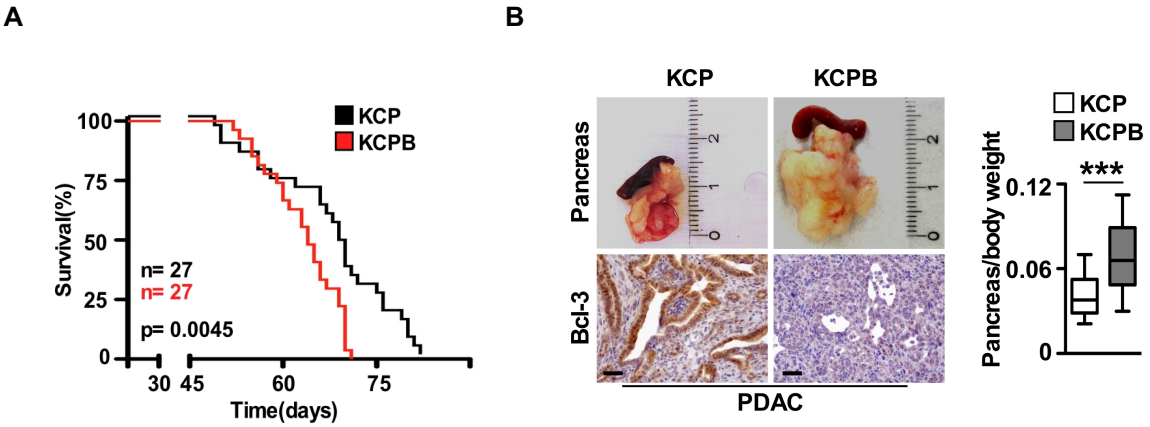

Figure 3-5: Bcl-3 considerably increases survival and reduces tumor burden in mice. (**A**) Kaplan-Meier survival curve of *KCP* (*n*=27) and *KCPB* (*n*=27) mice (Median survival *KCP*=69d, *KCPB*=64d; ***P*=0.0045). (**B**) IHC of Bcl-3 expression in representative pancreata from *KCP* and *KCPB* mice (left). Summary of relative pancreatic weight obtained from *KCP* vs. *KCPB* mice (right). Means ± SD (*n*=13); ****P*<0.001. Scale bars = 50µm.

To future characterize the functional role of Bcl-3 expression *in vitro*, tumor cell lines were isolated from KCP and KCPB PDAC tumors. Increased proliferation of KCPB cells was observed in proliferation and colony formation assay (Figure 3-6 A and B).

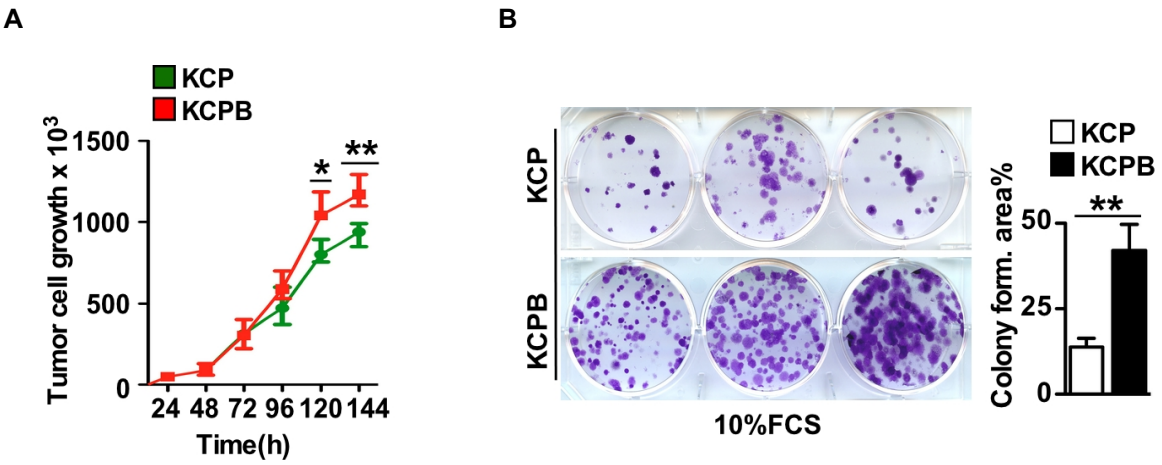

Figure 3-6: Proliferation assay and colony formation assay. (**A**) Growth curve of representative *KCP* and *KCPB* tumor cell lines over 144h. Means ± SD (*n*=4). **P*<0.05; ***P*<0.01. (**B**) Colony formation assay of representative *KCP* and *KCP* primary pancreatic tumor cells. Summary of the percentage area. Means ± SD (*n*=5-6). ***P*<0.01.

Bcl-3 was expressed in the cytoplasm as well as in the nucleus of murine PDAC cell lines isolated from KCP tumors, but not in KCPB tumor cell lines (Figure 3-7 A). More interestingly, the NF-κB signaling pathway could be excluded as directly being regulated by Bcl-3 in this context (Figure 3-7 A and B) as neither factors involved in the canonical nor in the non-canonical NF-κB signaling pathway were differently expressed upon Bcl-3 deletion.

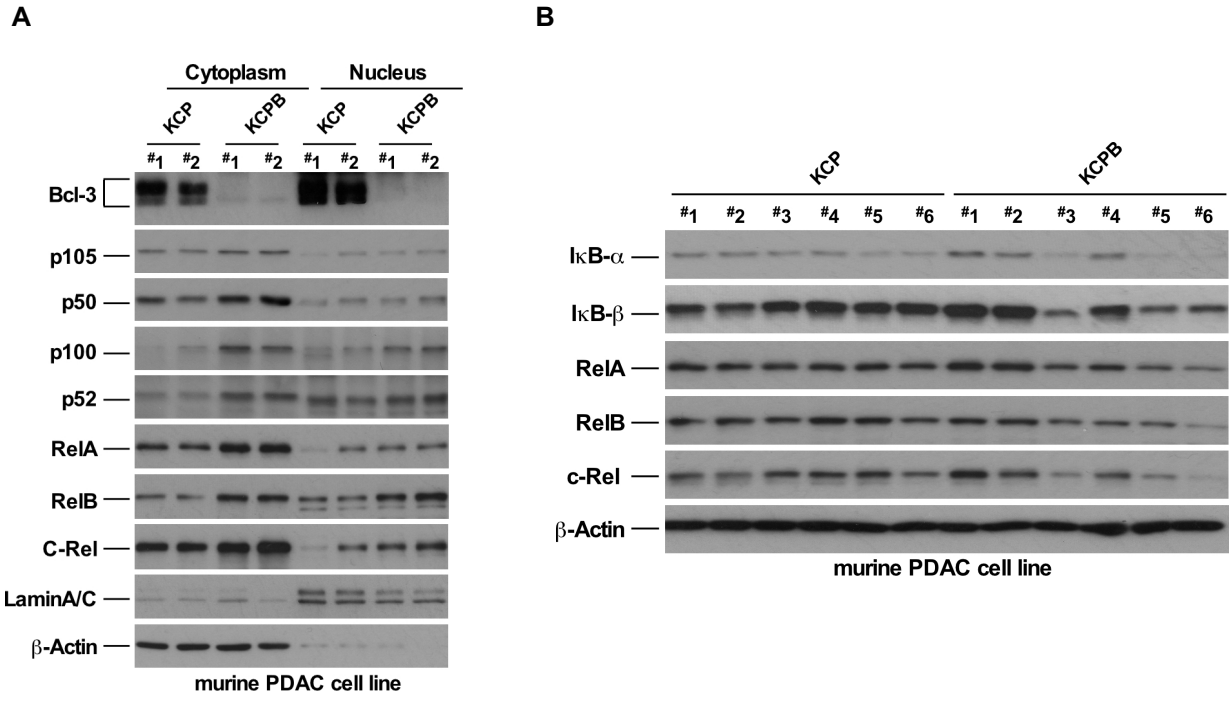

Figure 3-7: Characterization of KCP and KCPB tumor cell lines. (**A**) IB analysis of Bcl-3, p105, p50, p100, p52, RelA, RelB, C-Rel, and Lamin A/C in cytoplasmic and nuclear fractions of tumor cell lines obtained from Kras driven mice harboring either wild type or knockout Bcl-3. Lamin A/C and β-Actin served as controls. (**B**) IB analysis for IκBα, IκBβ, RelA, RelB, and C-Rel in tumor cell lines obtained from Kras driven mice harboring either wild type or knockout Bcl-3. β-Actin served as a control.

Thus, our data provide for the first time evidence that Bcl-3 is expressed in both human and murine PDAC. Loss of Bcl-3 significantly impacts tumor burden by accelerating tumorigenesis, proliferation and curtailing overall survival.

3.2 Bcl-3 expression influences tumor differentiation and averts an epithelial to mesenchymal transition.

Emerging evidence indicates that Bcl-3 is not only associated with the development of haematological neoplasias, but it is also of importance in solid tumor formation and growth [99]. To further elaborate the functional role of Bcl-3 in PDACs, 42 of the PDACs that developed in Bcl-3 competent (KCP) or deficient mice (KCPB) were reviewed. A remarkably high incidence of undifferentiated/anaplastic/ sarcomatoid PDACs was found in Bcl-3 deficient (KCPB) mice compared to KCP mice (83% vs. 22%) (Figures 3-8 A and B, Table 3-1).

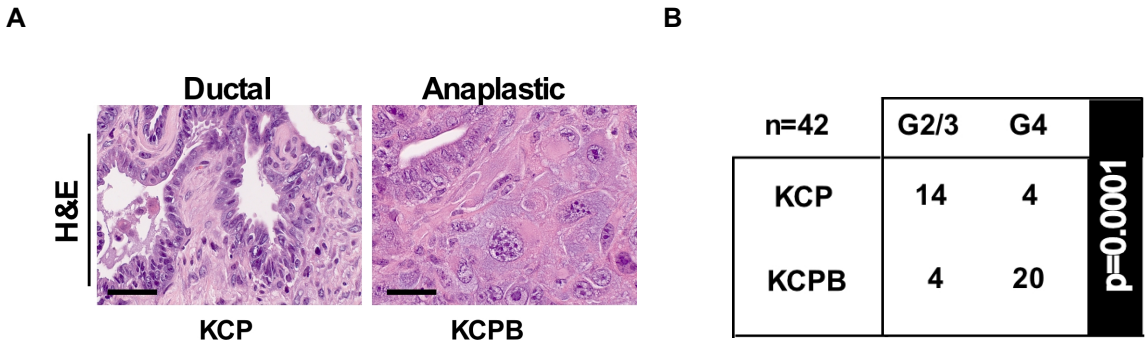

Figure 3-8: **Bcl-3 determines/favors tumor differentiation.** (**A**) H&E staining from representative *KCP* and *KCPB* tumors. (**B**) Pathologist based tumor grading of *KCP* and *KCPB* PDACs. Tumors were divided into two groups: G2/3 and G4 (*n*=42; ****P*=0.0001 using Fisher's exact test). Scale bars = 50μm.

Table 3-1 Histology of Mouse tissue samples

Mouse ID	Genotype	Grading	Metastasis
4335	KCP	4	no
M3346	KCP	3-4	no
656	KCP	3	no
4334	KCP	1-2	no
4384	KCP	2	no
4798	KCP	2	no
4621	KCP	2-3	no
4535	KCP	2-3	no
K1683	KCP	2-3	no
M3715	KCP	2	no
18418	KCP	3-4	no

K1653	KCP	2-3	no
K2101	KCP	2-3	no
3009	KCP	2	no
18528	KCP	1-2	no
K1733	KCP	3-4	no
18809	KCP	2-3	no
5533	KCP	2-3	no
[1]			
M4353	KCPB	4	LN, DIAPH
M4009	KCPB	4	no
M4349	KCPB	4	no
M4006	KCPB	3	no
K2680	KCPB	4	no
M4355	KCPB	2-3	no
K2673	KCPB	4	INTEST, PER
M3211	KCPB	3-4	no
K1721	KCPB	4	no
M2957	KCPB	3-4	no
M2954	KCPB	4	no
M2715	KCPB	2-3	no
M3206	KCPB	4	LIVER, LN
M3765	KCPB	4	no
K1907	KCPB	4	no
M4019	KCPB	4	no
M4446	KCPB	3-4	no
M4550	KCPB	4	no
M3525	KCPB	3-4	no
M3529	KCPB	4	LIVER
M3581	KCPB	4	LN
M3580	KCPB	3	LN
M4016	KCPB	4	LN, PER
M4549	KCPB	4	LIVER, PER, LN

LN: lymphnode metastasis; PER: peritoneal metastasis; DIAPH: diaphragm metastasis; INTEST: intestinal metastasis.

Moreover, the mesenchymal markers Vimentin and Twist were highly expressed over the epithelial markers E-cadherin and β-catenin in Bcl-3 deficient PDACs (KCPB), thus indicating a Bcl-3 deficiency-driven epithelial to mesenchymal transition (EMT) in murine PDAC tissue and cell line (Figures 3-9 and Figure 3-10 A and B). But the expression of mesenchymal markers Slug, Snail and ZEB1 were not different in KCP and KCPB PDAC tissue and cell lines (Figure 3-10 C and D). To ensure strict validity of this key finding, we performed additional analyses. First, we confirmed a cell autonomous Bcl-3 deficiency-driven effect on EMT by IB analysis (Figure 3-10 A-B) in KCP and KCPB PDAC

tissues and cells and by immunofluorescence (IF) staining for E-cadherin and Vimentin in primary pancreatic tumor cells obtained from KCP and KCPB mice (Figure 3-10 E).

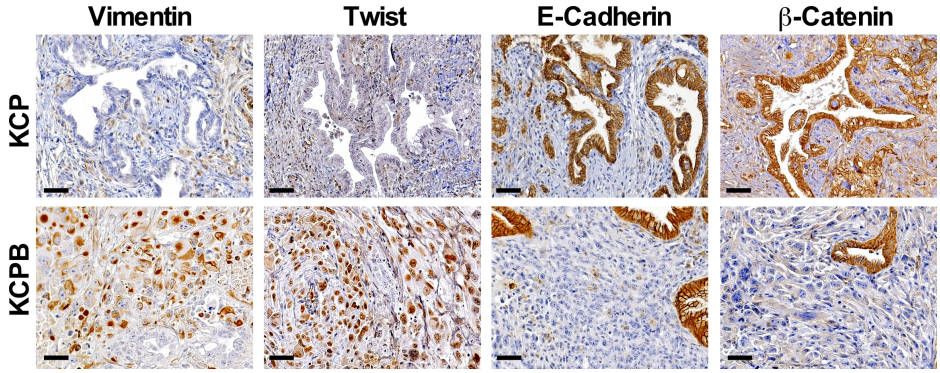

Figure 3-9: Bcl-3 averts an epithelial to mesenchymal transition. IHC for Vimentin, Twist, E-Cadherin and β-Catenin in *KCP* and *KCPB* PDACs. Scale bars = 50μm.

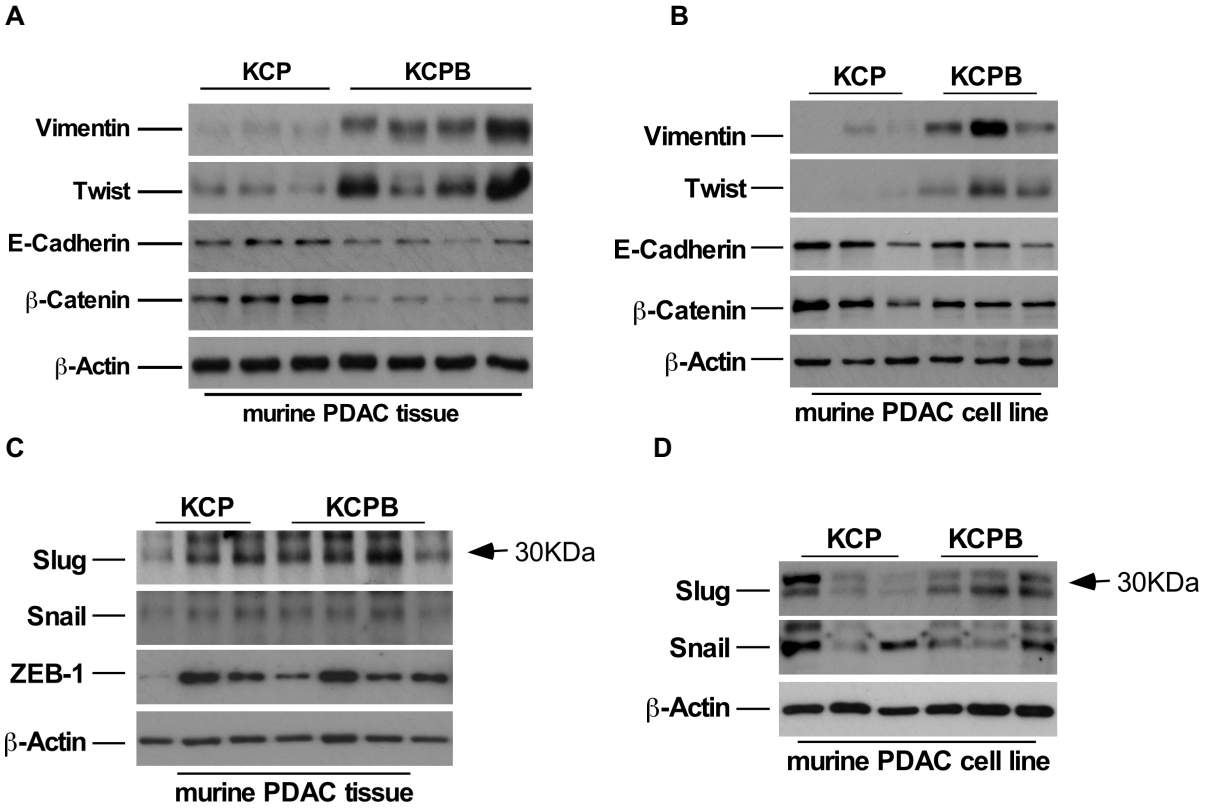

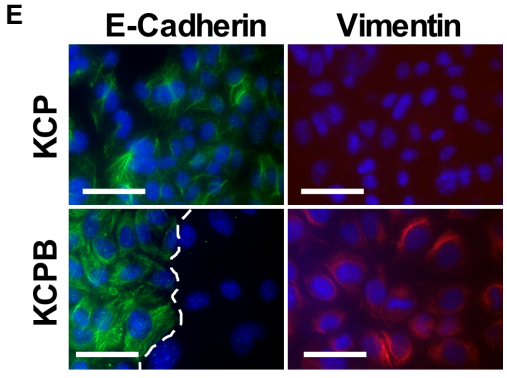

Figure 3-10: Expression of EMT markers in KCP and KCPB PDAC. (**A-B**) IB analysis of Vimentin, Twist, E-Cadherin and β-Catenin in representative *KCP* and *KCPB* PDAC in murine tissue and cell lines. β-Actin served as a control. (**C**) IB analysis of Slug, Snail, ZEB-1 in representative *KCP* and *KCPB* PDAC tissues. (**D**) Slug, Snail in representative *KCP* and *KCPB* cell lines. β-Actin served as a control. **(E)** Immunofluorescence (IF) staining of E-Cadherin and Vimentin in representative *KCP* and *KCPB* PDAC tissues. Scale bars = 50μm.

Second, we validated a Bcl-3 direct effect on EMT by performing a transient and stable knockdown of Bcl-3 mRNA, using Bcl-3 siRNA and shRNA, respectively, in primary pancreatic tumor cells isolated from Bcl-3 expressing KCP mice (Figure 3-11). The summary of these analyses confirmed a Bcl-3 deficiency-driven direct and cell autonomous effect on EMT in a *Kras*^{G12D} mouse model of PDAC.

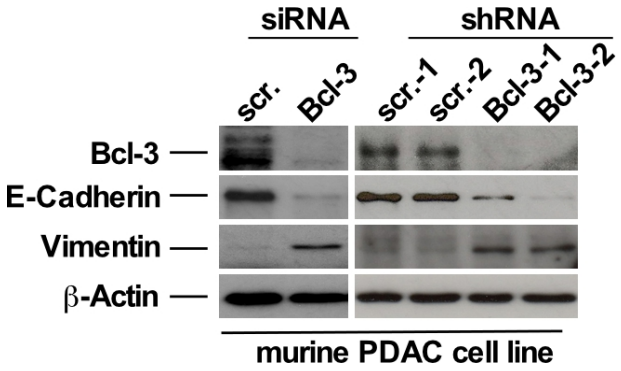

Figure 3-11: Transient and stable knockdown of Bcl-3 mRNA. IB analysis of Bcl-3, E-Cadherin and Vimentin in *KCP* primary pancreatic tumor cells with either a transient knock-down using Bcl-3 siRNA transfection or a stable knock-down using lentiviral transduction of Bcl3-shRNA. Scrambled siRNA and shRNA were used as controls. β-Actin served as a loading control.

Likewise, in humans, *BCL3* mRNA expression levels from 157 PDAC patients obtained from the UCSC RNAseq database were inversely correlated with EMT related genes (ECADHERIN, NCADHERIN, ZEB1, ZEB2, TWIST1, TWIST2, VIM, SNAIL, SLUG) [145] (Figure 3-12).

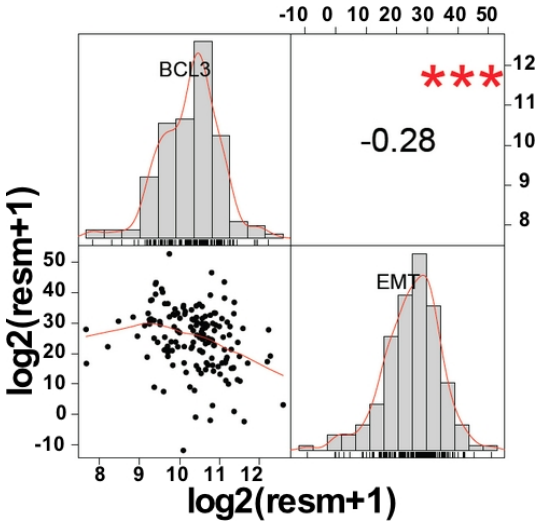

Figure 3-12: Bivariate scatterplots of mRNA expression levels of *BCL3* and EMT related genes from 157 PDAC patients. The EMT score was calculated from the sum of expression of well-known mesenchymal marker genes minus the total expression of known epithelial genes (# PMID: 24302555 Cancer Discovery. 2013 Dec 3) (*FN1* + *VIM* + *ZEB1* + *ZEB2* + *TWIST1* + *TWIST2* + *SNAI1* + *SNAI2* + *CDH2*) - (*CLDN4* + *CLDN7* + *TJP3* + *MUC1* + *CDH1*). ***P<0.001; Pearson's correlation; negative correlation of r=-0.28. Data were obtained from the UCSC RNAseq database.

In addition, a Pearson-correlation matrix of epithelial and mesenchymal genes in 182 human PDAC patients sorted for Bcl-3 mRNA levels and subjected to unsupervised hierarchical clustering (Euclidean distance measurement, average linkage clustering) confirmed an inverse correlation of Bcl-

3 mRNA expression levels with EMT genes, suggesting once more the same mechanism across species (Figure 3-13).

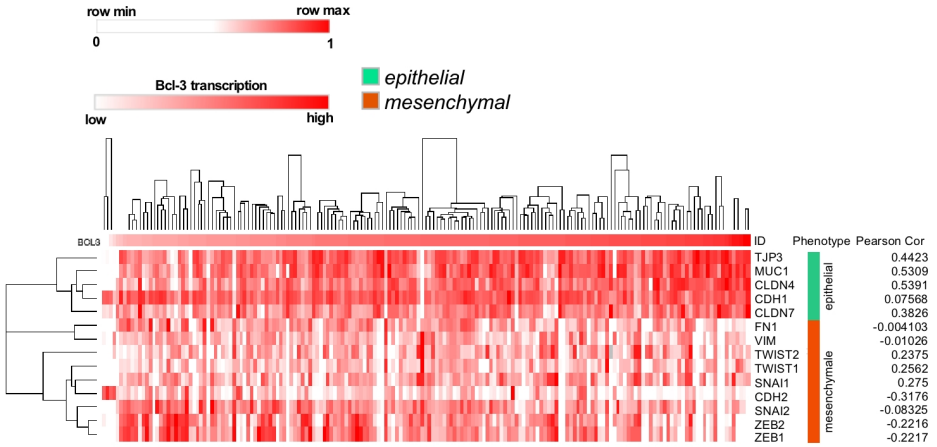

Figure 3-13: Pearson-correlation matrix of epithelial and mesenchymal genes in patients. Pearson-correlation matrix of epithelial and mesenchymal genes in 182 human PDAC patients sorted for Bcl-3 mRNA levels and nearest neighbor. The matrix was subjected to unsupervised hierarchical clustering (Euclidean distance measurement, average linkage clustering).

Taken together, our data conclusively demonstrate that Bcl-3 deficiency enhances tumor burden by pushing PDAC cells towards a more undifferentiated, EMT-like phenotype across species.

3.3 Bcl-3 deficiency significantly increases metastatic tumor burden in pancreatic cancer

Previously, a metastatic capacity has been proposed for Bcl-3 in a variety of solid tumor entities [130] [38] [129]. Herein we addressed the hypothesis of whether Bcl-3 deficiency drives metastatic tumor burden in PDAC. Specifically, to correlate Bcl-3 deficiency with metastasis, we compared 42 KCPB and KCP tumors. A significant increase in metastatic dissemination to different sites was obvious in Bcl-3 deficient mice (Figure 3-14).

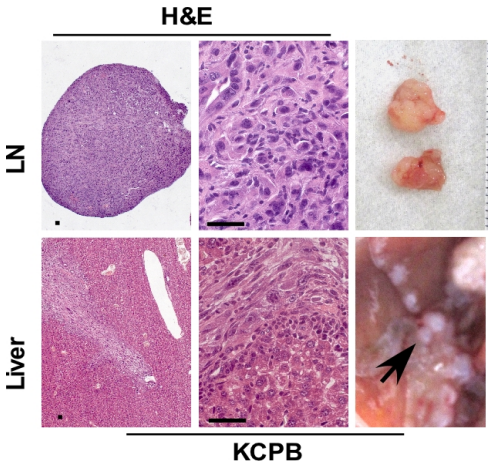

n=42	MET	No MET	
KCP	0	18	p=0.0066
KCPB	8	16	

Figure 3-14: Bcl-3 regulates metastatic properties in pancreatic cancer. H&E stainings and images of lymphnodes (LN) and liver metastasis (liver) in *KCPB* mice. *KCP* and *KCPB* mice were divided into two groups according to the presence of lymphnode and distance metastasis (MET) (*n*=42; ***P*=0.0066 by using Fisher's exact test).

In line with these data, a cell autonomous Bcl-3 deficiency driven effect in tumor cell invasion (Figure 3-15), migration (with Cytarabine 10μM) (Figure 3-16 A), wound healing (without Cytarabine) (Figure 3-16 B) and anoikis (Figure 3-17 A and B) capacity was found in *in vitro* assays.

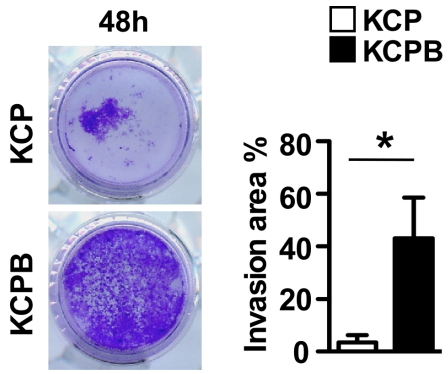

Figure 3-15: Loss of Bcl-3 promotes invasion *in vitro*. Cell invasion of *KCP* vs. *KCPB* primary pancreatic tumor cells was determined by a transwell cell invasion assay after 48h. Invaded cells were visualized by crystal violet staining. Means ± SD (*n*=3 representative tumor cells per genotype). **P*<0.05.

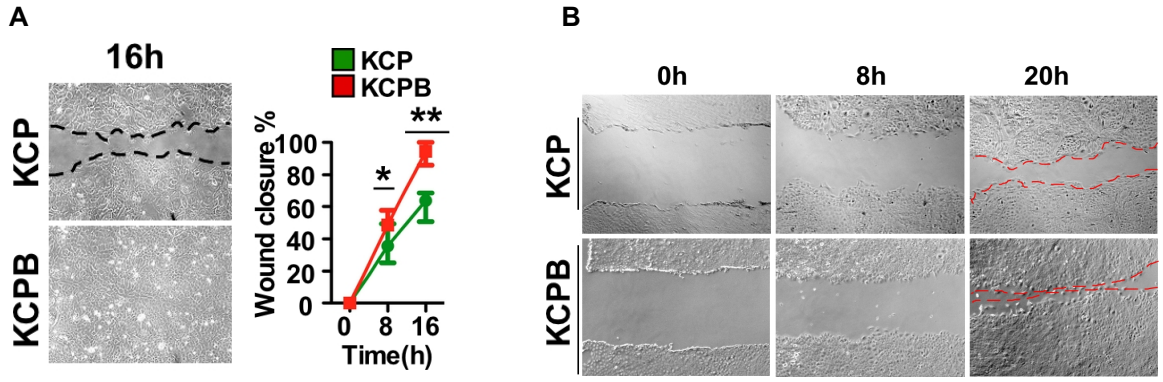

Figure 3-16: Loss of Bcl-3 promotes migration *in vitro*. (**A**) Migration assay of *KCP* vs. *KCPB* primary pancreatic tumor cells; wound closure was calculated after 8h and 16h. Means ± SD (*n*=4-6 representative tumor cells per genotype). **P*<0.05, ***P*<0.01. (**B**) Wound healing assay of *KCP* vs. *KCPB* primary representative pancreatic tumor cells.

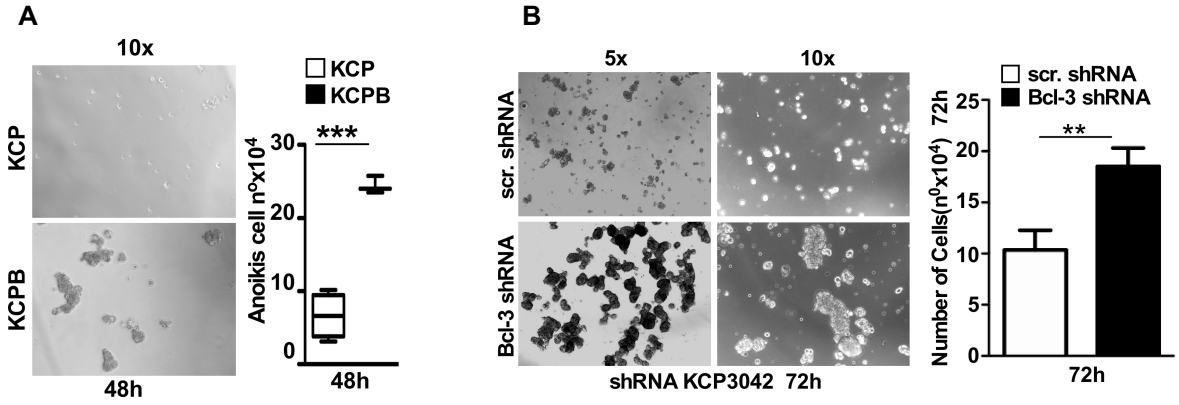

Figure 3-17: Loss of Bcl-3 promotes cell survival *in intro*. (**A**) Anoikis assay of *KCP* vs. *KCPB* primary pancreatic tumor cells; number of cells undergoing anoikis at 48h were quantified. Means ± SD (*n*=3-4 representative tumor cell lines per genotype). ****P*<0.001. (**B**) Anoikis assay of *KCP* cell lines with stable lentiviral Bcl-3 shRNA knockdown was determined by anoikis assay after 72h; number of cells undergoing anoikis at 72h were quantified. Means ± SD (*n*=3-4 representative tumor cell lines per genotype). ***P*<0.01.

Moreover, a direct contribution of Bcl-3 deficiency on the cellular invasive capacity of KCP-derived tumor cells with stable Bcl-3 mRNA knockdown was also observed (Figure 3-18).

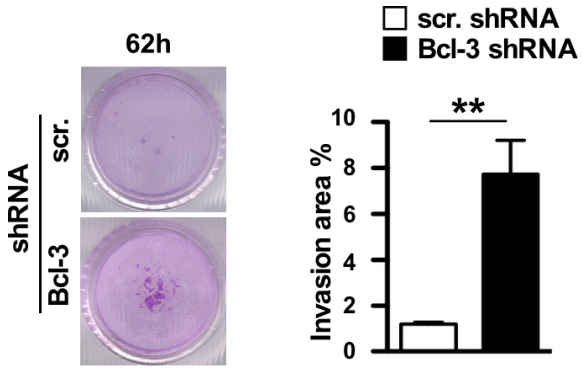

Figure 3-18: Knockdown of Bcl-3 promotes invasion capacity of cells. Cell invasion of *KCP* cell lines with stable lentiviral Bcl-3 shRNA knockdown was determined by a transwell cell invasion assay after 62h. Invaded cells were visualized by crystal violet staining. Summary of the percentage of invaded area. Means ± SD (*n*=3). ***P*<0.01.

To further validate a cell autonomous Bcl-3-driven metastatic promoting phenotype, we performed *in vivo* syngeneic metastases studies by injecting primary PDAC cells isolated from either Bcl-3 deficient (KCPB) or Bcl-3 competent KCP mice into background-matched mice, and monitored lung metastasis development over the course of 25 days. While mice injected with Bcl-3 deficient KCPB tumor cells suffered from severe metastatic burden, mice injected with Bcl-3 competent KCP tumor cells remained metastasis free (Figure 3-19 A-C).

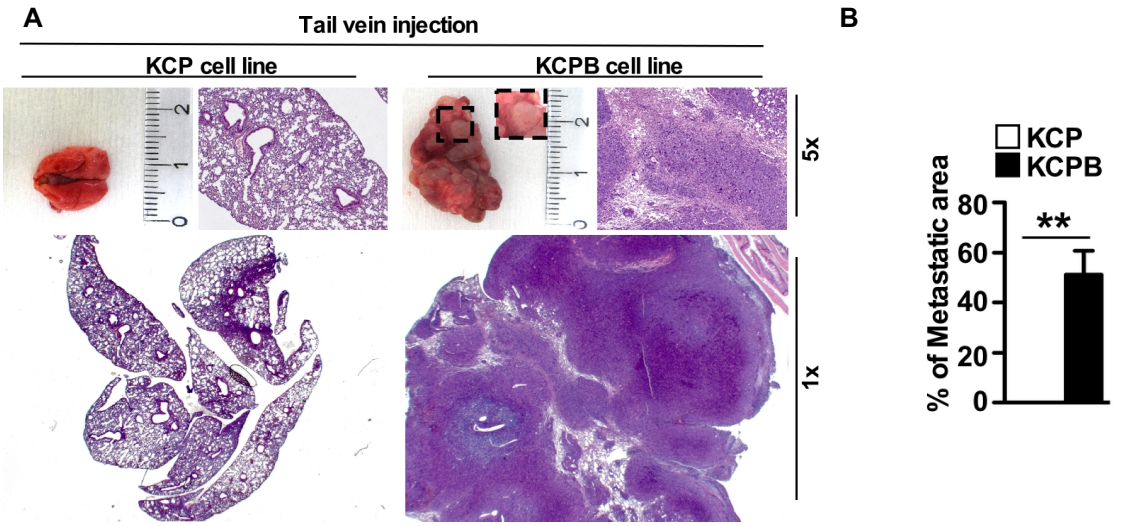

C

n=22	MET	No MET	
KCP	0	8	p=0.00014
KCPB	12	2	

Figure 3-19: Experimental metastasis assay. (**A**) H&E staining of the lung of tail vein injected syngeneic mice. (**B**) *KCP* and *KCPB* representative primary pancreatic tumor cells were injected into the tail vein of syngeneic mice. Metastatic area in the lung was determined. Three H&E slides of 1x magnification 20 μm apart were analyzed per group. Means ± SD (*n*=4-7 tail vein injected syngeneic mice; n=3, three different representative *KCP* or *KCPB* primary pancreatic tumor cells were used). ***P*<0.01. (**C**) Syngeneic mice were divided into two groups according to the presence of metastasis (MET) (*n*=22; ****P*=0.00014 using Fisher's exact test).

Importantly, similar to the primary tumor an EMT-like phenotype, characterized by Vimentin and Twist expression and E-cadherin and β-catenin downregulation, was observed in the lung metastasis developed from Bcl-3 deficient tumor cells (Figure 3-20).

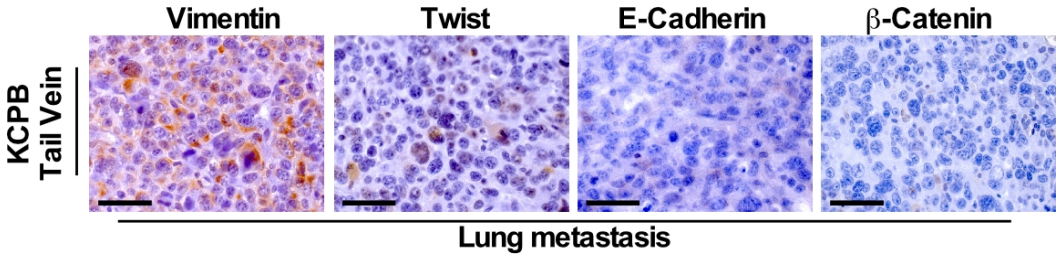

Figure 3-20: Immunohistochemical analysis of EMT. IHC for vimentin, twist, E-cadherin, β-catenin in lung metastasis of syngeneic tail vein injected mice (*KCPB* representative primary pancreatic tumor cells) Scale bars = 50µm.

Bioluminescence imaging of tail vein injected NSG mice with either luciferase-labeled Bcl-3 deficient (KCPB) or Bcl-3 competent (KCP) tumor cells revealed similar findings (Figure 3-21 A and B).

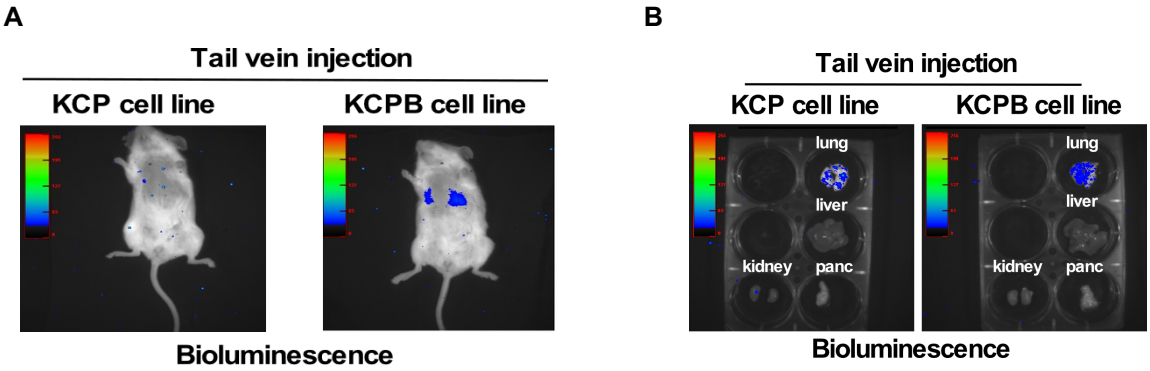

Figure 3-21: Luciferase assay for metastasis. (**A**) Luciferase-labeled *KCP* or *KCPB* primary pancreatic tumor cells were injected into the tail vein of NSG mice. Metastasis growth was monitored using non-invasive bioluminescence imaging. (**B**) Bioluminescence imaging of lung, liver, pancreas and kidney obtained from NSG mice after tail vein injection of luciferase-labeled *KCP* or *KCPB* representative primary pancreatic tumor cells.

Thus, unlike previously published Bcl-3/EMT associations, our findings demonstrate that Bcl-3 deficiency rather than overexpression drives PDAC metastatic burden *in vivo* in a cell autonomous and direct manner.

3.4 Bcl-3 deficient tumor cells harbor features compatible with oxidative metabolism

Accumulating evidence implicate metabolic alterations as important for controlling tumor progression and metastatic burden. Consequently, analysis of functional mitochondria, TCA cycle intermediates, and amino acids such as glutamine and glutamate are currently emerging as key players in the metastatic process[146]. Although the role of Bcl-3 in metabolic processes is largely undefined, it was

previously shown that Bcl-3 activates genes involved in cellular energy metabolism and interacts with PGC-1α to orchestrate the cellular energy metabolism response in a yeast two-hybrid screen [147]. To unravel the potential metabolic role of Bcl-3 in PDAC we performed a significant analysis of microarray (SAM) on Bcl-3 deficient (KCPB) vs. Bcl-3 competent (KCP)-derived primary tumor cells. Of all KEGG pathway gene sets enriched in the absence of Bcl-3, metabolic process was the most significantly enriched (with >25% of at least 2-fold enriched genes involved), indicating a significant impact of Bcl-3 loss in the metabolic process of PDAC cells. Consistent with the EMT phenotypes observed in KPCB tumors and derived cell lines, genes linked to cell adhesion were decreased in the Bcl-3 deficient subset (Figure 3-22).

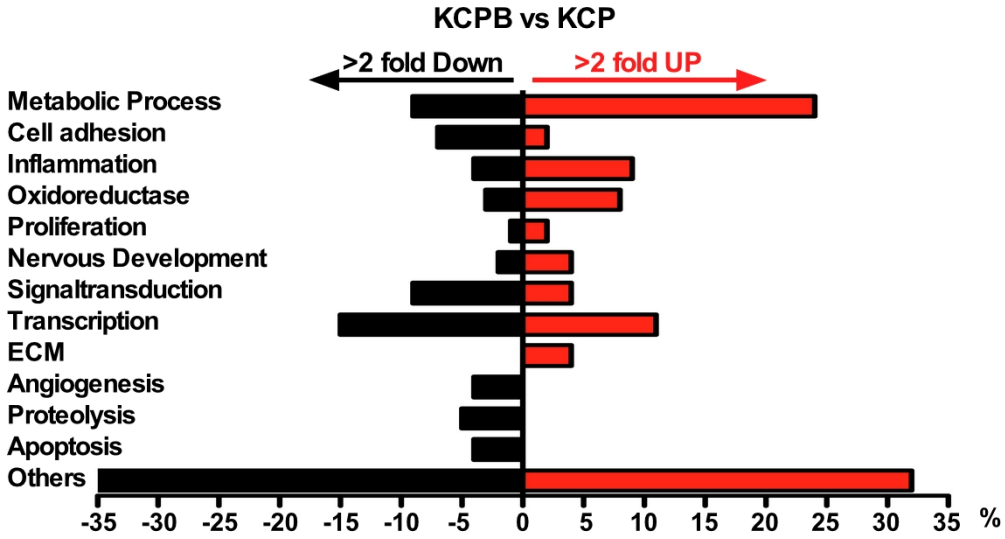

Figure 3-22: Microarray analysis for KCP and KCPB primary tumor cells. Microarray based SAM analysis of *KCP* and *KCPB* primary tumor cells revealed 12 KEGG pathway gene sets to be either >two-fold up- or down-regulated in *KCPB* compared with *KCP* primary tumor cells (Delta = 0.46, n=3).

To define the metabolic role of Bcl-3 we performed targeted metabolomics. In addition to metabolites involved in amino acid metabolism/GSH cycle such as glutamate, glutamine, γ-glutamyl amino, alanine, and 5'oxoproline, TCA cycle/oxidative phosphorylation-derived intermediates such as succinate, malate, and NADH were significantly increased in the absence of Bcl-3 (Figure 3-23 A and B), suggesting metabolic features compatible with oxidative mitochondrial respiration/metabolism.

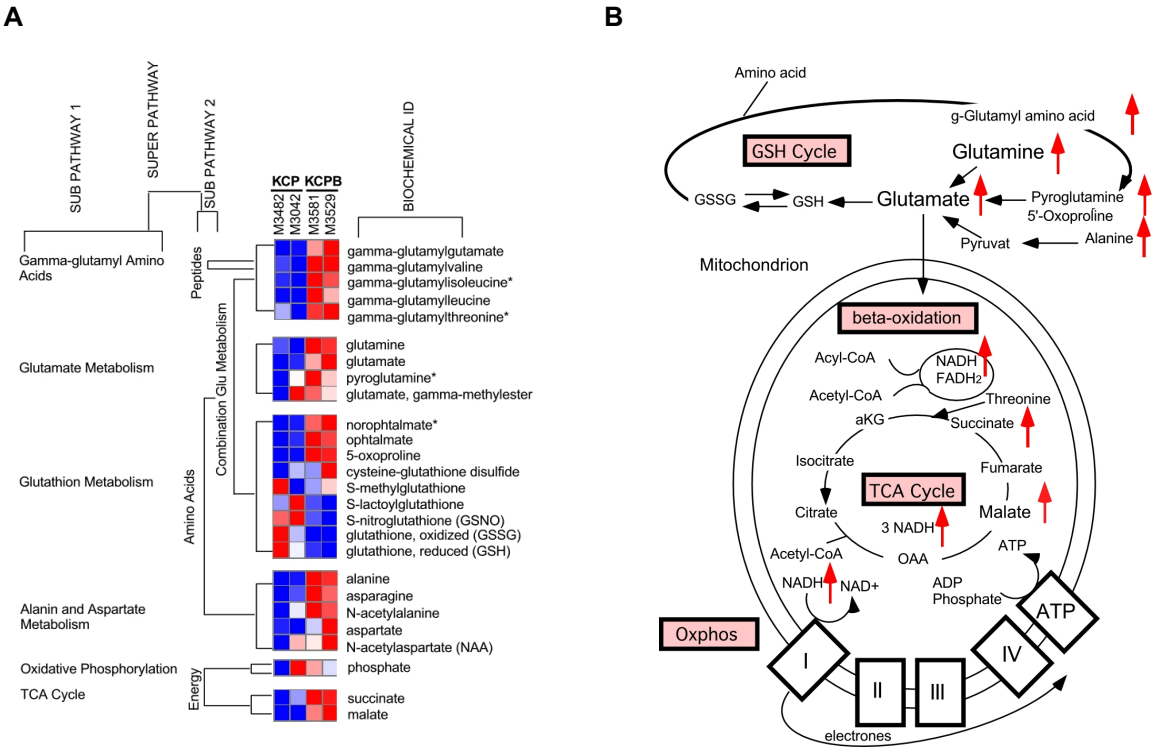

Figure 3-23: Loss of Bcl-3 leads to features compatible with oxidative metabolism. (A) Heat map with metabolic pathway clustering of highly regulated metabolites in *KCPB* vs. *KCP* primary pancreatic tumor cells as identified by non-targeted metabolomics. **(B)** Metabolites up-regulated in *KCPB* vs. *KCP* primary pancreatic tumor cells as identified by non-targeted metabolomics (*n*=2-3); significantly up-regulated metabolites are marked with a red arrow. CoA, Co-enzyme A; GSH, glutathione; GSSG, glutathione oxidized; FAD, flavin adenine dinucleotide; FADH, flavin adenine dinucleotide reduced; NAD nicotinamide adenine dinucleotide; NADH, nicotinamide adenine dinucleotide reduced; TCA, tricarboxylic acid; Oxphos, oxidative phosphorylation. **P* < 0.05 for succinate, malate, NADH, glutamate, g-glutamyl amino acid; ***P* < 0.01 for glutamine, alanine; ****P* < 0.001 for 5'oxoproline.

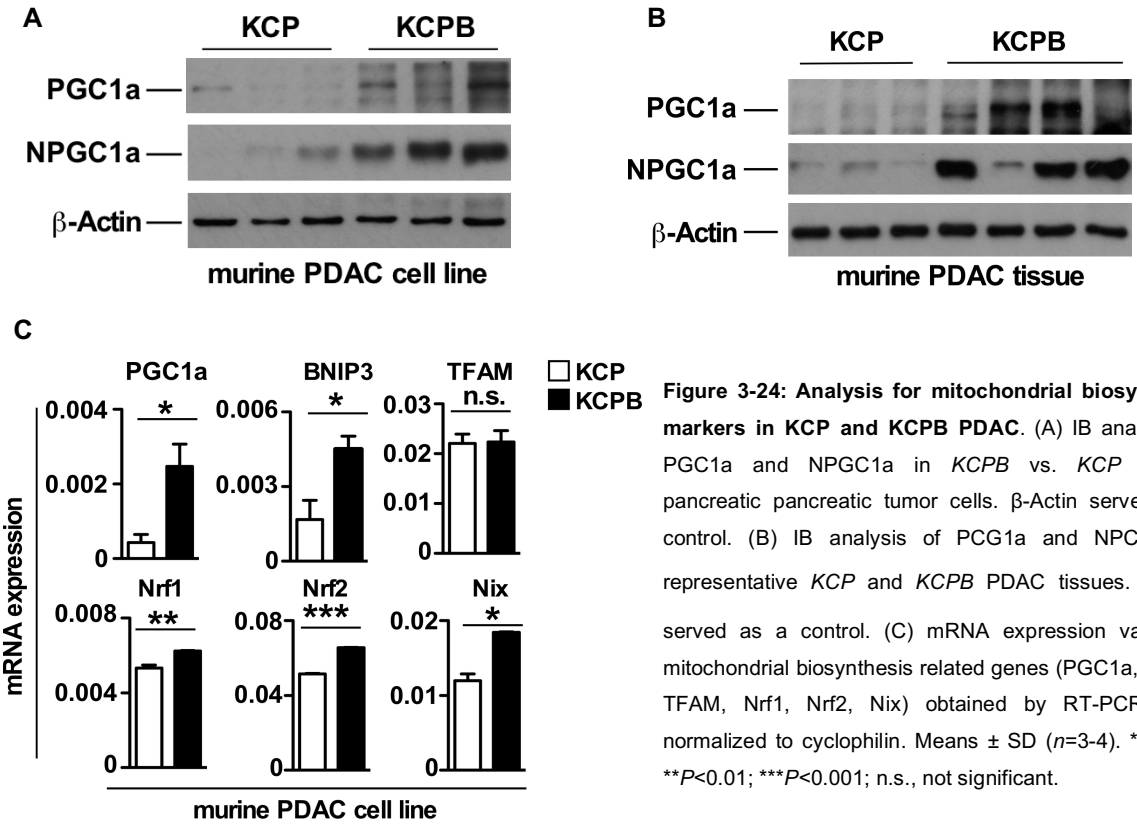

Figure 3-24: Analysis for mitochondrial biosynthesis markers in KCP and KCPB PDAC. (A) IB analysis for PGC1a and NPGC1a in *KCPB* vs. *KCP* primary pancreatic pancreatic tumor cells. β-Actin served as a control. (B) IB analysis of PCG1a and NPCG1a in representative *KCP* and *KCPB* PDAC tissues. β-Actin served as a control. (C) mRNA expression values of mitochondrial biosynthesis related genes (PGC1a, BNIP3, TFAM, Nrf1, Nrf2, Nix) obtained by RT-PCR. Data normalized to cyclophilin. Means ± SD (*n*=3-4). **P*<0.05; ***P*<0.01; ****P*<0.001; n.s., not significant.

In addition, IB analysis revealed an up-regulation of PGC1α in tumor tissue and primary pancreatic tumor cells isolated from Bcl-3 deficient (KCPB) vs. control (KCP) tumor mice (Figure 3-24 A and B). Furthermore, mRNA expression levels of several mitochondrial biosynthesis markers including PGC1α, BNIP3, Nrf1, Nrf2, and Nix were significantly increased in Bcl-3 deficient (KCPB) vs. control (KCP) tumor cells (Figure 3-24 C).

Consistently, the mitochondrial/nuclear DNA ratio was significantly increased in Bcl-3 deficient (KCPB) vs. control (KCP) tumor cells (Figure 3-25 A). Mito Tracker (M7512, Invitrogen) for immunofluorescence (IF) in KCP and KCPB cells also showed the increased mitochondria biogenesis in KCPB vs. KCP (Figure 3-25 B).

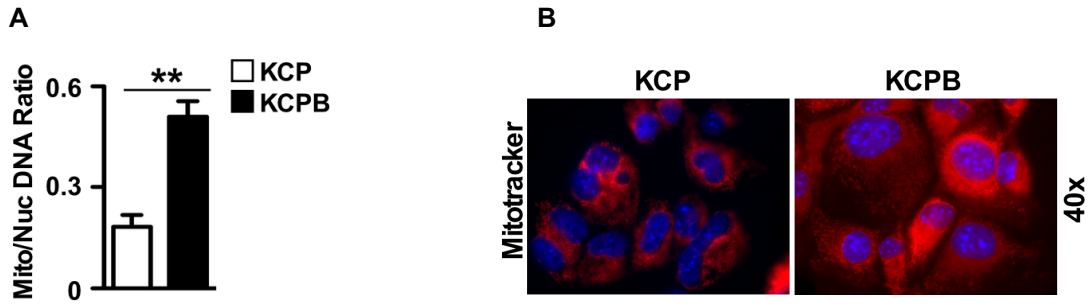

Figure 3-25: Loss of Bcl-3 increases mitochondria biogenesis. (A) Ratio of mitochondrial/nuclear DNA content in *KCPB* and *KCP* primary pancreatic tumor cells. Means ± SD (n=3-4). **P<0.01. **(B)** Image showing immunofluorescence of Mitotracker in *KCP* and *KCPB* cells. Magnification: 40x.

While taken together these data argued in favor of Bcl-3 deficient cells increasing mitochondrial biosynthesis and using OXPHOS as a means of meeting their energy requirements, we functionally validated this hypothesis by measuring oxygen consumption rates (OCR) in the presence or absence of distinct mitochondrial inhibitors. Baseline OCR, ATP production and maximum OCR were significantly increased in Bcl-3 deficient (KCPB) vs. Bcl-3 competent (KCP) control tumor cells (Figure 3-26 A and B).

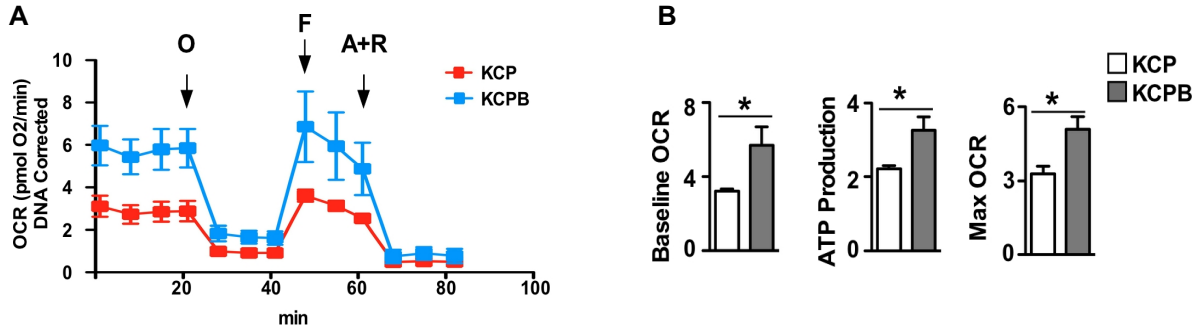

Figure 3-26: Seahorse assay. (A) Oxygen consumption rate (OCR) of *KCP* and *KCPB* primary pancreatic tumor cells was measured using the XF Extracellular Flux Analyzer. Tumor cell cultures were subsequently treated by injection of oligomycin (O), FCCP (F), and antimycin plus rotenone (A+R) into the culture medium (*n*=3). **(B)** Summary of baseline oxygen consumption rate (OCR; DNA corrected), ATP production (DNA corrected) and maximum OCR (non-mitochondrial respiration and DNA corrected) in *KCP* and *KCPB* primary pancreatic tumor cells determined by the XF Extracellular Flux Analyzer. Means ± SD (*n*=3). **P*<0.05.

These data as a whole suggested that Bcl-3 deficiency promotes metabolic features compatible with oxidative metabolism, characterized by an increase in TCA and oxidative phosphorylation enzymes as well as an increase in mitochondria DNA content, mitochondrial biosynthesis related gene expression and OCR.

3.5 Bcl-3 deficiency contributes to cancer stem cell-ness and CSC-enriched tumor formation in PDACs

Since Sancho et al. recently reported that pancreatic cancer stem cells (CSCs) have increased levels of PGC1α and meet their energy requirements via OXPHOS due to suppression of c-MYC [140], we next asked whether Bcl-3 might indirectly participate in this process and/or act as an important PDAC CSC modulator. Strikingly, microarray analyses revealed a significant decrease of MYC target gene sets in Bcl-3 deficient (KCPB) vs. Bcl-3 competent (KCP) tumor cells (Figure 3-27).

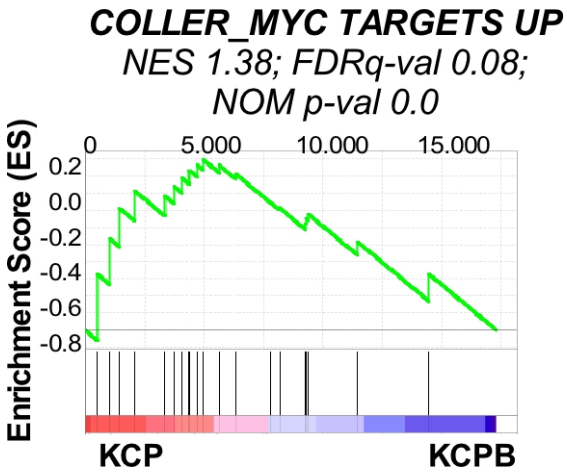

Figure 3-27: Microarray analysis for MYC in PDAC cells. GSEA microarray data analysis of *KCP vs. KCPB* primary pancreatic tumor cells (NES 1.38; FDR *q*-value 0.08; NOM ****P*-value 0.000) *n*=3, pancreatic tumor cells per genotype.

Furthermore, a direct Bcl-3 deficiency-dependent down-regulation of c-Myc was demonstrated by IB analysis of KCP tumor cells with either transient or stable knock down of Bcl-3 mRNA using Bcl-3 siRNAs or shRNAs, respectively (Figure 3-28 A). In addition, a cell autonomous Bcl-3 deficiency-dependent suppression of c-Myc was confirmed performing an IB analysis on Bcl-3 deficient (KCPB) vs. Bcl-3 competent (KCP) tumor cells (Figure 3-28 B). Since these data paralleled previously published studies showing a link between c-Myc downregulation and “stemness” [140], we performed additional CSC *in vitro* and *in vivo* characterization experiments.

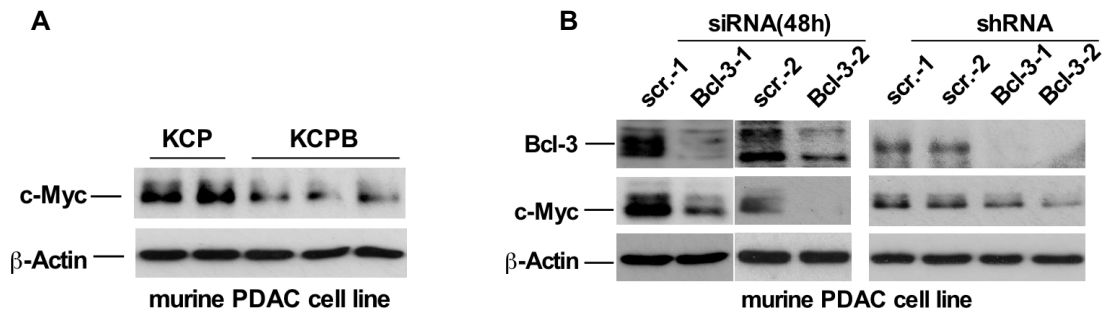

Figure 3-28: IB analysis for c-Myc. (A) IB analysis for Bcl-3 and c-Myc expression in *KCP* primary pancreatic tumor cells with either a transient (Bcl-3 siRNA) or stable (lentiviral Bcl3-shRNA) knockdown of Bcl-3. β-Actin served as a control. **(B)** IB analysis of c-Myc in *KCP* and *KCPB* primary pancreatic tumor cells. β-Actin served as a control.

To test self-renewal, we generated anchorage-independent sphere cultures from Bcl-3 deficient (KCPB) and Bcl-3 competent (KCP) tumor-derived cells, and observed a significant increase in sphere formation capacity in the absence of Bcl-3 (Figure 3-29 A), suggesting that Bcl-3 deficiency impacts CSC self-renewal. Moreover, Bcl-3 deficient tumor-derived cells (KCPB) showed increased expression of pluripotency-associated and EMT gene transcripts (i.e. HES1, OCT3/4, Sox2, Snail, and Zeb1) compared to control Bcl-3 competent (KCP) tumor cells (Figure 3-29 B).

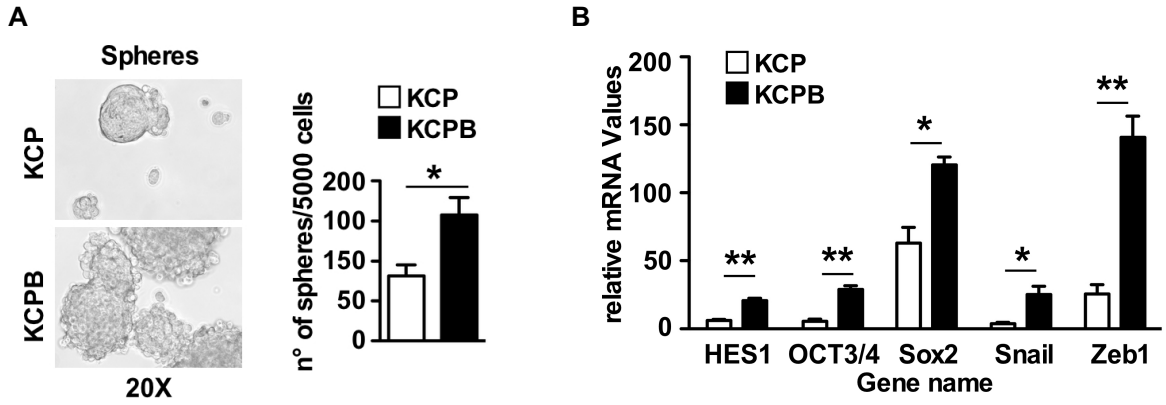

Figure 3-29: Sphere formation assay and mRNA expression of stem cell markers. (A) Spheres formation assay in *KCP* and *KCPB* primary pancreatic tumor cells. Summary of the number of spheres/ml formed from 5000 input tumor cells. Means ± SD (*n*=3-4). **P*<0.05. **(B)** *HES, OCT3/4, SOX2, SNAIL* and *ZEB1* mRNA expression levels were measured in *KCP* and *KCPB* primary tumor cells and normalized to HPRT. Means ± SD (*n*=2;6). **P*<0.05; ***P*<0.01.

Even more profound, loss of Bcl-3 enriched for CD133+ or CD44+ CSCs in FFPE PDAC tumors and in freshly digested Bcl-3 deficient PDAC tissues compared to control PDAC tissues using flow cytometry to detect CSC, defined either as CD44+, CD133+ or CXCR4+ expressing cells (Figures 3-30 A and B).

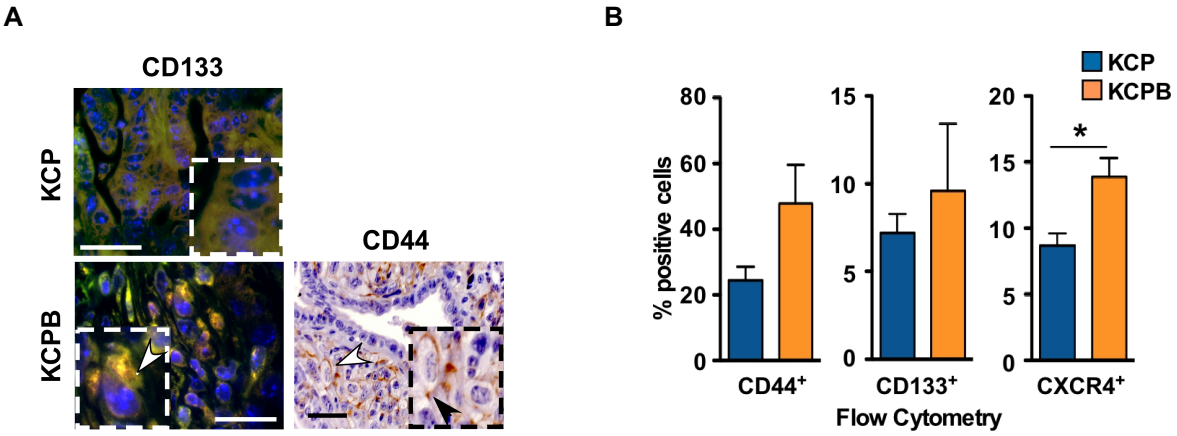

Figure 3-30: Analysis for cancer stem cell markers in KCP and KCPB PDAC. (**A**) IHC for CD44 and IF staining for CD133 (APC) and DAPI in *KCP* and *KCPB* PDACs. (**B**) The percentage of CD44, CD133, CXCR4 positive tumor cells were determined in digested pancreatic tumors of *KCP* and *KCPB* mice using flow cytometry. Means ± SD (*n*=3-4). **P*<0.05; n.s. not significant. Scale bars =50µm.

In summary, these results argue that Bcl-3 deficiency is indeed an important regulator of cancer stem cell-ness in PDAC, by suppressing in a cell autonomous and direct manner c-Myc expression, which leads to both enhanced stem-ness features in pancreatic cancer cells and an enrichment of the CSC compartment.

3.6 Bcl-3 deficiency favors a CSC compartment expansion resulting in enhanced tumorigenesis.

Accumulating evidence has linked CSCs to tumor aggressiveness, treatment resistance, and tumor recurrence as well as to metastatic spread in PDAC [148] [149]. CSCs display inherent self-renewal capacity and bear exclusive long-term *in vivo* tumorigenicity [150]. In response to specific stimuli CSCs can also acquire enhanced mobility and activate an EMT, both of which can facilitate the dissemination of CSCs to distant organs to initiate metastatic secondary lesions [70]. The apparent expansion of CSCs in the experiments detailed above led us to test the tumorigenic potential of Bcl-3 deficient (KCPB) vs. Bcl-3 competent (KCP) tumor cells *in vivo* in an extreme limiting dilution assay. Bcl-3 deficient cells revealed consistently increased tumor take, enhanced tumorigenicity, greater tumor volumes and a higher CSC frequency compared to Bcl-3 competent (KCP) tumor cells. Notably, this effect was particularly evident when low cell numbers (5 and 50 cells) were injected (Figure 3-31 A-D). Applying the extreme limiting dilution analysis algorithm (http://bioinf.wehi.edu.au/software/elda/index.html) (right, 95% CI) CSC frequencies were determined to be significantly higher in Bcl-3 deficient (KCPB) cells (1 in 16) compared to control (KCP) tumor cells (1 in 149). Thus, our results demonstrate that Bcl-3 deficient tumor cells contain a higher CSC frequency, enhancing overall tumorigenesis *in vivo* (Figure 3-31 D).

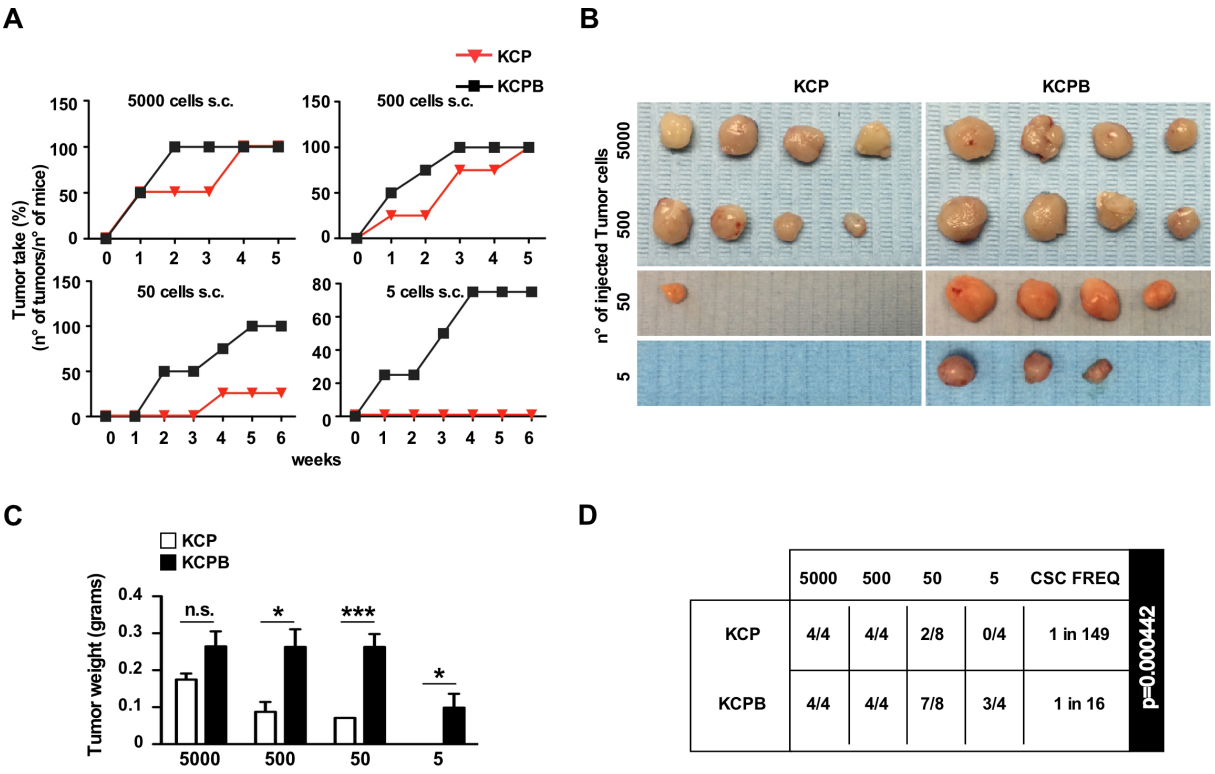

Figure 3-31: Loss of Bcl3 favors an expansion of the CSC compartment resulting in increased tumorigenesis. Mice were subcutaneously injected with the indicated number of *KCP* and *KCPB* cells resuspended in Matrigel (n=4-8 mice/dilution/group). (**A**) Summary of in vivo tumor take and growth over the course of 6 weeks. (**B-D**) Five or six weeks post injection, tumors were resected and analyzed. (**B**) Images of resected tumors, (**C**) tumor weights and (**D**) number of tumors formed per injection and CSC frequencies determined using the extreme limiting dilution analysis algorithm (http://bioinf.wehi.edu.au/software/elda/index. html) (right, 95% CI). (**P*<0.05, ****P*<0.001, n.s.: not significant).

Moreover, analysis of $CD133^+/CXCR4^+$ expressing cells in excised tumors revealed increased expression of this highly metastatic double positive population [27] in tumors derived from Bcl-3 deficient cells compared to control tumor cells (Figure 3-32).

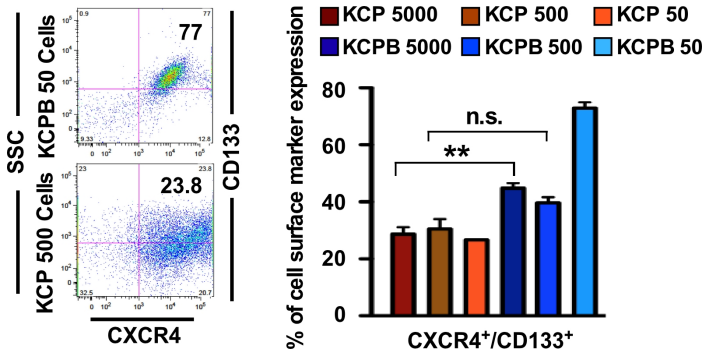

Figure 3-32: Cancer stem cell markers detected by flow cytometry in tumor excised from xenograft mice. Tumors were digested and the percentage of CD133 and CXCR4 positive cells was determined by flow cytometry. Summary of CD133/CXCR4 cell surface expression in cells isolated from all tumors as indicated (***P*<0.01, n.s., not significant).

Importantly and consistent with our previous findings, the tumors that developed from Bcl-3 deficient tumor cells displayed an undifferentiated/anaplastic phenotype (with almost no desmoplastic stroma response) (Figure 3-33 A and B). Together, these results corroborate our hypothesis that Bcl-3 deficiency induces a cancer stem cell-like phenotype and more importantly, drives PDAC tumorigenesis and tumor aggressiveness.

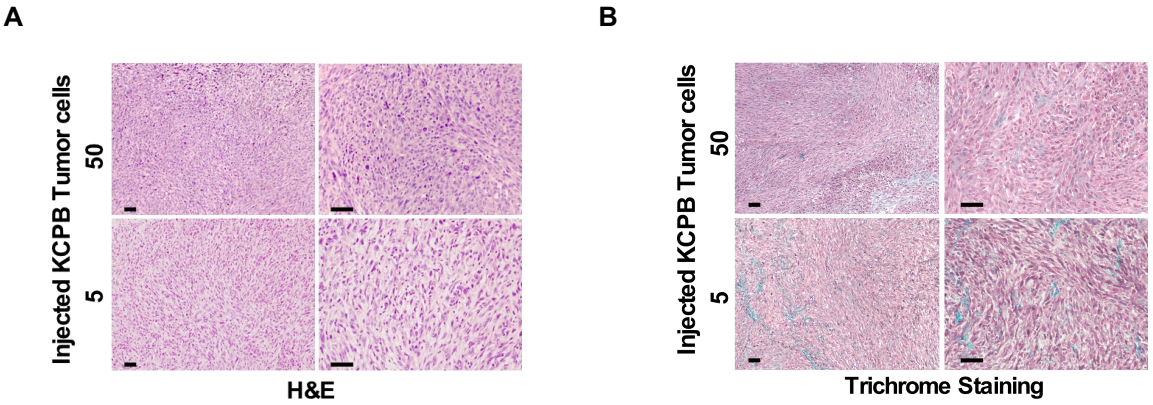

Figure 3-33: HE and Trichrome staining in xenograft tumor. (**A**) H&E staining from tumors obtained after injecting 5 and 50 *KCPB* tumor cells into nude mice. (**B**) Masson's Trichrome staining from tumors obtained after injecting 5 and 50 *KCPB* tumor cells into nude mice. Scale bars = 50μm.

3.7 Bcl-3 determines tumor burden and metastatic disease in human PDAC patients.

The fact that Bcl-3 deficiency drives CSC-ness-mediated tumorigenesis and metastatic tumor burden in the *Kras*^{G12D} mouse model of pancreatic cancer suggests a putative function for Bcl-3 in human PDAC. To demonstrate a link across species we investigated the role of Bcl-3 in terms of cancer stem cell-ness, tumor burden and metastatic capacity in a panel of human PDAC tumors. While Bcl-3 was detectable in 71% of human PDACs investigated, almost 30% of tumors were Bcl3-negative, suggesting that Bcl-3 deficiency may also have an important role in human disease (Figures 3-34 A and B). We next classified our panel of human PDAC samples into two groups according to their Bcl-3 expression (a Bcl-3 positive and Bcl-3 negative group) and found a significant increase in lymph node metastasis in the Bcl-3 negative group (Figure 3-34 C). However, since the human PDAC collection was limited to patients at an early resectable stage (AJCC-UICC stages I and II) only a tendency towards distant metastatic capacity driven by Bcl-3 deficiency was found (Figure 3-34 D, Table 2-14 of clinical human data).

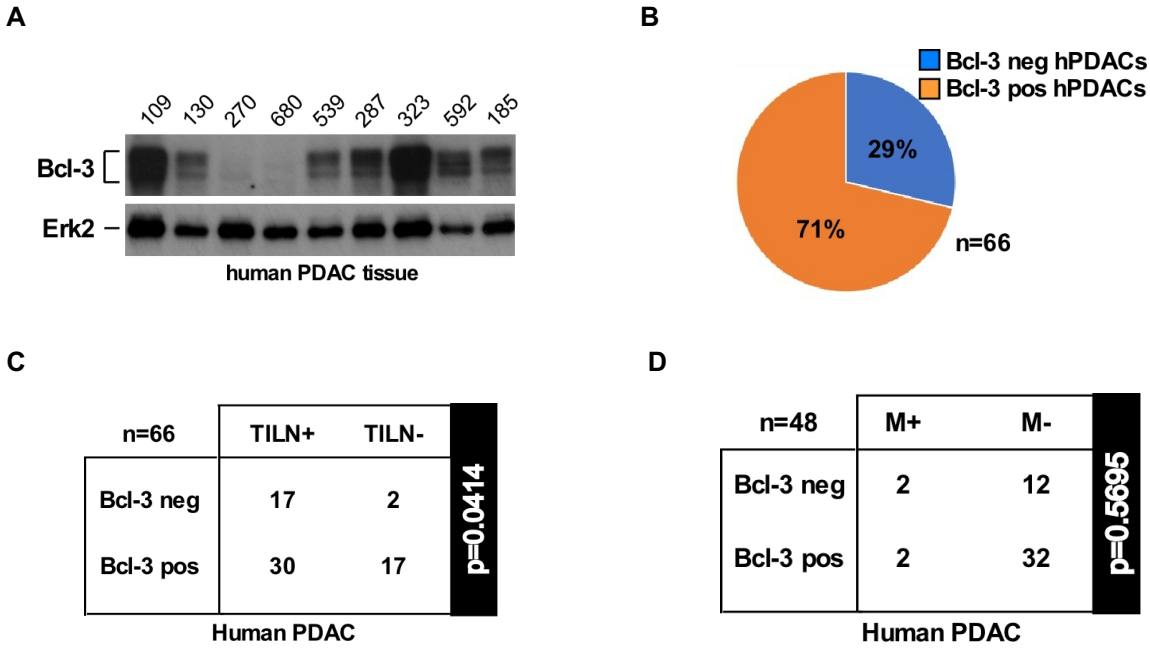

Figure 3-34: Bcl-3 determines tumor burden and metastatic disease in human PDAC patients. (**A**) Immunoblot of Bcl-3 in representative human PDAC tissues. ERK2 served as a control. (**B**) 66 human PDACs were screened by IB analysis for Bcl-3 expression. 29% (*n*=19) failed to express Bcl-3; 71% (*n*=47) revealed strong Bcl-3 expression. (**C**) 17 out of 19 hPDACs patients bearing Bcl-3 negative PDACs suffered from tumor infiltrated lymphnodes (TILN). 30 out of 47 patients with Bcl-3 positive PDACs were diagnosed with TILN. (*n*=66; **P*=0.0414, using Fisher's exact test). (**D**) 66 human PDAC patients were screened for Bcl-3 expression by IB analysis. 2 out of 14 hPDACs patients bearing Bcl-3 negative PDACs suffered from a metastatic disease. 2 out of 34 patients with Bcl-3 positive PDACs were diagnosed with metastatic disease (*n*=48; *P*=0.5695 using Fisher's exact test).

Nonetheless, together these results suggested that Bcl-3 deficiency may indeed increase the metastatic capacity of PDACs in humans similar to what we had observed in mice. To further elucidate whether Bcl-3 deficiency favors a cancer cell stem-like phenotype in human PDAC, we compared Bcl-3 mRNA expression levels in primary human PDAC cultures enriched in CSCs (sphere cultures) compared to non-CSC-enriched cultures (adherent monolayers)(Figure 3-35), as previously described [140].

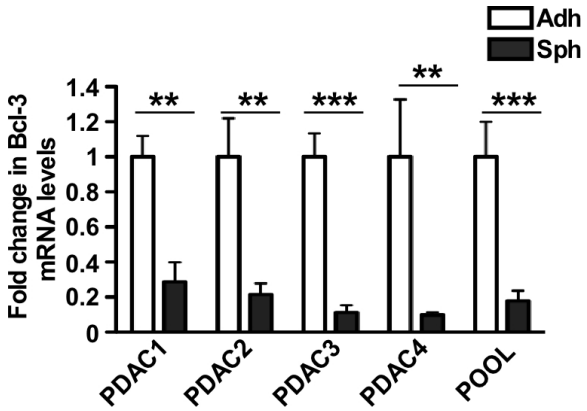

Figure 3-35: Bcl-3 expression in adherent and sphere cultures of human PDAC cells. Bcl-3 relative mRNA levels were determined by RT-PCR in adherent and spheres cultures of human PDAC cells. Data normalized to β-actin. Fold changes were determined relative to adherent cultures. Means ± SD (*n*=6). ***P*<0.01; ****P*<0.001.

Indeed, CSC-enriched sphere cultures showed significantly lower Bcl-3 expression compared to non-CSC-enriched adherent cultures. In line with a functional role for Bcl-3 loss in CSC biology, Bcl-3 overexpression in human PDAC cells markedly reduced overall sphere size and sphere forming capacity (Figure 3-36 A), indicating that high Bcl-3 levels antagonize certain stem-like properties of PDAC CSCs. In line with this conclusion, we also observed a decrease in the percentage of sphere-derived cells expressing the classic CSC markers CD133 and CXCR4 when Bcl-3 was overexpressed while no change in EpCAM staining was observed, as expected (Figure 3-36 B). In addition, using CMXRos to measure mitochondrial membrane potential, we observed decreased membrane potential in sphere-derived cells over-expressing Bcl-3, whereas no difference in mitochondrial mass was found (Figures 3-36 C and D). These findings would suggest that Bcl3 over expression in human PDAC cells affects CSC features such as sphere formation, CSC cell surface marker expression and mitochondrial membrane potential, demonstrating that Bcl-3 deficiency drives metastatic capacities as well as cancer stem cell-ness features across species.

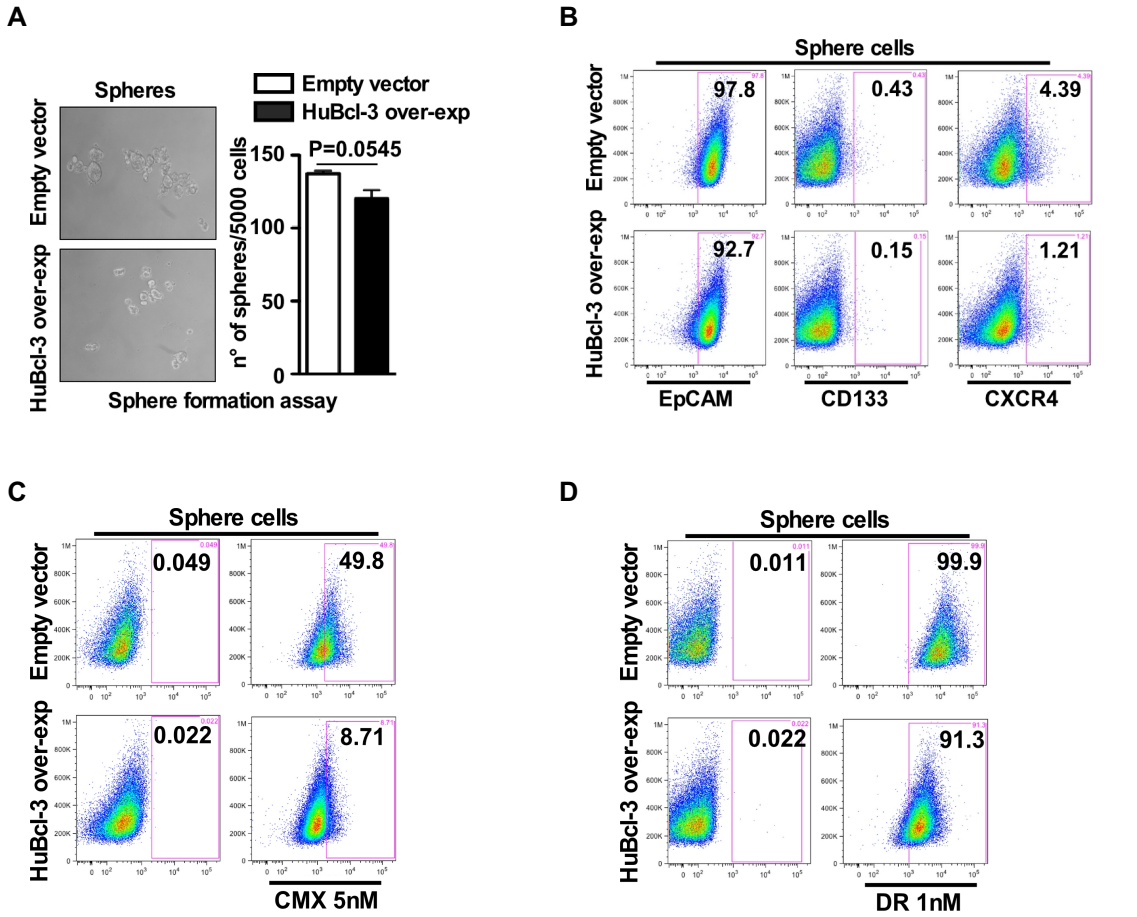

Figure 3-36: Sphere formation assay and flow cytometry for cancer stem cell markers. (**A**) Spheres formation of hPDAC cells transfected with the HuBcl-3 overexpressing vector compared to empty vector controls. Summary of the number of spheres/ml formed from 5000 input cells. Means ± SD (*n*=4). n.s., not significant. (**B**) Cytometry plots of EpCAM, CD133 and CXCR4 positive cells in Bcl-3 overexpressing spheres determined by flow cytometry. (**C**) Cytometer plots of mitochondrial membrane potential using CMXRos 5nM in spheres originating from Bcl-3 overexpressing and control human PDAC cells. (**D**) Mitochondrial mass was determined by flow cytometry using DR 1nM in spheres originating from Bcl-3 overexpressing and control human PDAC cells.

Thus, our results illustrate for the first time the implication of Bcl-3 in PDAC and highlight several new aspects of Bcl-3 in PDAC tumor and cancer stem cell biology.

4 Discussion

This study determines for the first time the role of Bcl-3 in pancreatic cancer. We demonstrate overexpression of Bcl-3 in human and murine PDAC *in vivo* and *in vitro*, and using various genetic tools a central tumor suppressor role for Bcl-3 in metastasis of pancreatic tumor cells through regulation of epithelial-mesenchymal translation (EMT) was revealed. In addition, deletion of Bcl-3 in tumor cells resulted in metabolic alterations promoting oxidative metabolism and expansion of the tumor CSC compartment. Central findings were replicated in human PDAC cell lines and tissues. As a whole, our results illustrate a previously unknown tumor suppressor role for Bcl-3 in PDAC and highlight several new biologic aspects of Bcl-3 in this disease.

4.1 The role of Bcl-3 in solid tumors

While the role of Bcl-3 in hematological malignancies is well established such as Bcl-3 as an oncogene in B-cell chronic lymphocytic leukemias, its involvement and function in solid tumors remains less understood. Recently some publications show that Bcl-3 expression increases in certain solid cancers. For example, Massoumi et al. report that nuclear accumulation of Bcl-3 controls proliferation and tumor growth in skin tumor [98]. Choi et al. show Bcl-3 is critical for the inhibition of apoptosis and tumor progression by stabilization of CtBP1 in breast cancer [118]. Based on the ErbB-positive mouse model, Bcl-3 promotes metastatic tumor burden in the lungs [129]. In addition, Bcl-3 knockdown suppresses colorectal tumor cell growth *in vitro* [116]. Although these data suggest an oncogenic role for Bcl-3 in the context of solid tumor entities, Bcl-3 might have a more complex and versatile function beyond that of acting solely as a proto-oncogene. For example, more recently Tang et al. reveal a tumor suppressive role of Bcl-3 in the inflammation associated mouse model for colorectal tumorigenesis in epithelial cells [123]. Likewise, in hepatocarcinogenesis mouse model with hepatocyte-specific overexpression of Bcl-3, Bcl-3 overexpression reduced hepatocarcinogenesis due to decreased survival of diethylnitrosamine (DEN) and phenobarbital (PB) related to damaged premalignant cells [124]. All these reports suggest a distinct tumorigenic potential depending on the cell type and microenvironment. Here, we show for the first time that Bcl-3 is highly expressed in a majority of human PDACs and during all stages of tumorigenesis in a $KRAS^{G12D}$-driven mouse model of pancreatic cancer, suggesting *a priori* an important pro-tumor role for Bcl-3 in the pancreatic tumorigenesis. Surprisingly, and opposed to general consensus, we found that Bcl-3 in PDAC instead exerts tumor suppressive functions and curtails survival in tumor prone mice. Compared to mice that express normal levels of Bcl-3, excessive tumor growth with an anaplastic/sarcomatoid/ undifferentiated phenotype was consistently seen in Bcl-3 deficient mice as well as increased metastatic burden was observed. Similarly, at the cellular level tumor cells derived from Bcl-3-deficient mice showed increased proliferation and dedifferentiation as well as the survival capacity. SiRNA and Lentiviral delivery of shRNA for Bcl-3 in tumor cells from control mice illustrated the same results. Taken together, these data highlight that Bcl-3 does not function as a pro-oncogenic factor in PDAC,

but rather as a tumor suppressor.

Bcl-3 is not only regulated by its expression levels, but also by a multitude of post-translational modifications that can affect its nuclear entry, stability and/or transcriptional activity for example via phosphorylation and ubiquitination [151] [152]. According to previous evidence, Bcl-3 is constitutively hyper-phosphorylated at its C-terminal end via a GSK3-mediated mechanism [97] [142] [128], which has been shown to modulate its function and activity [97] [142]. While the relevance of the hyper-phosphorylated state of Bcl-3 remains unclear, studies suggest that Bcl-3 phosphorylation by GSK3 regulates Bcl-3 turnover and transcriptional activity. In PDAC we found Bcl-3 in a hyper-phosphorylated state and highly expressed in both the cytoplasm and nucleus in murine and human PDAC cells. Whether the phosphorylation of Bcl3, its turnover rate or its location determines it pro- or anti-tumor role in PDAC is still uncertain and is currently under investigation. Bcl-3 is also a modulator of NF-κB activity and a regulator of NF-κB target gene expression [153]. However, levels of NF-κB activation were not affected by Bcl-3 abrogation in murine PDAC cell lines, suggesting a NF-κB-independent function of Bcl-3 in pancreatic tumor development. The protein levels of members of IκB family including IκB-α, IκB-β were not different in control and in Bcl-3 deficient murine PDAC tissues and cell lines. Furthermore, RAS activity and related pathways could be excluded as being directly regulated by Bcl-3.

4.2 The loss of Bcl-3 drives an epithelial-mesenchymal transition (EMT)-like phenotype

Accumulating evidence links EMT to metastatic tumor burden in a variety of cancers. EMT contributes to tumor invasion, migration and metastatic outgrowth [154]. While Bcl-3 has been shown to be a critical promoter of metastasis in several tumor entities such as breast cancer and colorectal cancer [130] [38] [129], its contribution to metastatic disease in PDAC remains poorly understood. Prior evidence indicates that NF-κB and Bcl-3 cooperate to induce and maintain EMT in Ras-transformed epithelial cells. However, we show herein that Bcl-3 negatively regulates EMT in a cell autonomous and direct manner in murine and human PDACs. Specifically, we found a significant enhanced metastatic burden in Bcl-3 deficient tumor mice, with a clear mesenchymal over epithelial marker expression profile observed in both Bcl-3 deficient murine tumors and in low Bcl-3-expressing human PDACs, strongly confirming that Bcl-3 ablates rather than favors an EMT-like phenotype in PDAC. Consistent with these findings, *in vitro* pancreatic cancer cell lines devoid of Bcl-3 showed decreased anoikis, increased invasive and migratory capacities. Knockdown of Bcl-3 promoted the expression of mesenchymal marker and decreased the expression of epithelial marker in siRNA assay and shRNA assay. In addition, when injected into mice, Bcl-3 deficient cells (KCPB) efficiently metastasized to the lungs. Thus, in contrary to current paradigm that describes Bcl-3 as a crucial promoter of metastasis, our data demonstrate that the loss of Bcl-3 increases metastatic potential and burden in PDAC mice.

4.3 Bcl-3 deficiency promotes metabolic processes in PDAC

Metabolic alterations have become of major interest with respect to their role in tumor progression and metastatic burden. Accumulating evidence proposes functional mitochondria and TCA cycle intermediates as focal components in the metastatic process. Mitochondria could play as bioenergetics sensors promoting migratory, invasive and EMT progression to cancer cells survived in distant microenvironmental conditions. TCA cycle is also increasing production in metastatic tumor cells. Summary these, mitochondrial could drive cancer metastasis in special condition [155]. Bcl-3 has previously been demonstrated to activate genes regulating cellular energy metabolism and to interact with PGC-1α, a master regulator of mitochondrial biogenesis, to juggle the cellular energetic and metabolic response [147]. Invasive and metastatic cancer cells could enhance mitochondrial biogenesis, mitochondrial respiration and increase ATP production by using PGC-1α to promote invasive and metastatic potential [156]. Again, contrary to published reports in other systems, in PDAC Bcl-3 deficiency substantially promoted metabolic processes compatible with oxidative metabolism, and thus metabolites involved in amino acid metabolism/GSH cycle and TCA cycle/oxidative phosphorylation were significantly increased. In addition, genes involved in mitochondrial biogenesis (e.g. PGC-1α), mitochondria DNA fraction and mitochondrial respiration (OCR) strongly and consistently increased in the absence of Bcl-3, suggesting that Bcl-3 is a negative regulator of mitochondrial biosynthesis and respiration in PDAC. Mechanistically we observed that loss of Bcl-3 suppressed, in a direct and cell autonomous manner, MYC expression in murine PDAC cell lines, thereby allowing PGC1α expression levels to increase, resulting in enhanced mitochondrial biogenesis, mitochondrial respiration and metabolic alterations consistent with oxidative metabolism. This observation is in line with work by Sancho et al. showing a direct inhibitory effect of MYC on PGC1α at the transcriptional level in PDAC. The authors also showed low MYC expression in human CSCs conferred high PGC-1α expression levels which enhanced mitochondrial biogenesis and activity [140]. Moreover, Bcl-3 has been reported to stabilize Myc and to promote colorectal cancer development by regulating ERK or AKT signaling. Increased expression of Bcl-3 resulted in increased expression of Myc via ERK-regulated phosphorylation of Myc [116] [117]. Thus, the loss of Myc expression in Bcl-3 deficient cells and the subsequent activation of PGC-1α is consistent with the aforementioned previously published studies.

4.4 The deletion of Bcl-3 favors a cancer stem cell-like phenotype

The increase in mitochondrial biosynthesis and respiration in Bcl-3 deficient cells was reminiscent of the previous work in CSCs, where a similar decrease in Myc levels promoted a metabolic phenotype consistent with OXPHOS specifically in CSCs [140]. In this study, loss of Bcl-3 unexpectedly enhanced stem-ness features in pancreatic cancer cells from Bcl-3 deficiency (KCPB*)* mice, such as increased self-renewal capacity, overexpression of CSC markers, activation of genes associated with pluripotency, promoted invasion and EMT, and enhanced *in vivo* tumorigenicity as well as metastasis, all of which are defining hallmarks of CSCs [157] [70] [150]. Thus, Bcl-3 deficiency favors a cancer stem cell-like phenotype resulting in a CSC compartment expansion, enhanced tumor

burden/aggressiveness, and accelerated tumorigenesis as well as metastatic potential in mice. It is important to highlight that analysis of CSCs versus non-CSCs from primary human PDAC tumor cultures showed a significant decrease in Bcl-3 expression, and overexpression of Bcl-3 antagonized certain CSC properties such as sphere formation, CSC cell surface marker expression (e.g. $CD133^+$ and $CXCR4^+$), and mitochondrial membrane potential. Thus, these data support the notion that Bcl-3 is a negative regulator of stem-ness and loss of Bcl-3 promotes cancer stem cell (CSC) expansion; however, how Bcl-3 loss promotes CSC-like properties is still unknown. Finally, consistent with our findings in the $Kras^{G12D}$ mouse model, a notable link between low Bcl-3 protein expression and tumor burden/metastatic capacity (i.e. lymph node metastasis) was observed in a large set of human PDAC samples, highlighting the role of Bcl-3 as a tumor suppressor across species.

Altogether Bcl-3 seems to exhibit tumor suppressive functions in murine and human PDAC. The loss of Bcl-3 drives not only an EMT-like phenotype, accompanied by enhanced tumor burden and metastatic disease, but it also switches the metabolism of cells, promoting oxidative phosphorylation (OXPHOS) over glycolysis. While we cannot rule out that other players are involved, our data strongly support a Bcl-3 driven cell autonomous and direct suppression of MYC with a subsequent abolished inhibitory effect on PGC1α resulting in a cancer stem cell expansion. Gain of cancer stem cell-like features cumulate in CSC enriched tumor formation and enhanced tumor burden and metastatic diseases in PDAC across species.

5 Abstract

The focus of this study was to analyze the role of B-cell CLL/lymphoma 3 (Bcl-3) in pancreatic ductal adenocarcinoma (PDAC). PDAC is a highly lethal solid tumor and is aimed to become the second most frequent cause of cancer-related deaths by 2030. PDAC is usually detected at the metastatic stage, which is associated with poor prognosis and lack of effective treatment. Pancreatic cancer is characterized by the rapid progression to metastatic disease. However, the mechanisms regulating metastatic capacities are not fully understood.

Bcl-3, an atypical member of the Inhibitor of kappa-B (IkappaB) family of proteins, is an established oncogene in hematologic malignancies. Moreover, emerging evidence indicates that Bcl-3 is also important in solid tumor formation and growth. To elucidate the role of Bcl-3 in PDAC, various genetic tools *in vivo* and *in vitro* were used.

Here, we demonstrate the overexpression of Bcl-3 in human and murine PDAC both *in vivo* and *in vitro* for the first time. Loss of Bcl-3 in $Kras^{G12D}$ mouse model with the pancreas-specific inactivation of p53 significantly impacted tumor burden by accelerating tumorigenesis, proliferation and curtailing overall survival. A remarkably high incidence of undifferentiated/anaplastic/sarcomatoid pancreatic tumors was found in Bcl-3 deficient mice. Our analyses confirmed a Bcl-3 deficiency-driven direct and cell autonomous effect on epithelial to mesenchymal transition (EMT) in murine PDAC tissue and cells. Moreover, in humans, an inverse correlation of Bcl-3 mRNA expression levels with EMT genes could be identified, suggesting the same mechanism across species. Deletion of Bcl-3 in tumor cells resulted in metabolic alterations promoting oxidative metabolism and a cancer stem cell-like phenotype, giving rise to highly metastatic tumors.

These data indicate an important role of Bcl-3 in pancreatic tumor progression and highlight several new aspects of Bcl-3 in this disease. These findings could be useful to open a new path for the targeted therapy of pancreatic ductal adenocarcinoma and metastasis.

6 References

[1] A. Jemal, R. Siegel, E. Ward, Y. Hao, J. Xu, T. Murray, and M. J. Thun, “Cancer Statistics, 2008,” *CA. Cancer J. Clin.*, vol. 58, no. 2, pp. 71–96, Jan. 2008.

[2] J. Kleeff, M. Korc, M. Apte, C. La Vecchia, C. D. Johnson, A. V. Biankin, R. E. Neale, M. Tempero, D. A. Tuveson, R. H. Hruban, and J. P. Neoptolemos, “Pancreatic cancer,” *Nat. Rev. Dis. Prim.*, vol. 2, p. 16022, Apr. 2016.

[3] L. Rahib, B. D. Smith, R. Aizenberg, A. B. Rosenzweig, J. M. Fleshman, and L. M. Matrisian, “Projecting Cancer Incidence and Deaths to 2030: The Unexpected Burden of Thyroid, Liver, and Pancreas Cancers in the United States,” *Cancer Res.*, vol. 74, no. 11, pp. 2913–2921, Jun. 2014.

[4] J. Kleeff, C. Reiser, U. Hinz, J. Bachmann, J. Debus, D. Jaeger, H. Friess, and M. W. Büchler, “Surgery for recurrent pancreatic ductal adenocarcinoma.,” *Ann. Surg.*, vol. 245, no. 4, pp. 566–72, Apr. 2007.

[5] H. G. Smeenk, T. C. K. Tran, J. Erdmann, C. H. J. van Eijck, and J. Jeekel, “Survival after surgical management of pancreatic adenocarcinoma: does curative and radical surgery truly exist?,” *Langenbeck’s Arch. Surg.*, vol. 390, no. 2, pp. 94–103, Apr. 2005.

[6] D. Li, K. Xie, R. Wolff, and J. L. Abbruzzese, “Pancreatic cancer,” *Lancet*, vol. 363, no. 9414, pp. 1049–1057, Mar. 2004.

[7] A. Chan, E. P. Diamandis, and I. M. Blasutig, “Strategies for discovering novel pancreatic cancer biomarkers.,” *J. Proteomics*, vol. 81, pp. 126–34, Apr. 2013.

[8] C. J. Halbrook and C. A. Lyssiotis, “Employing Metabolism to Improve the Diagnosis and Treatment of Pancreatic Cancer,” *Cancer Cell*, vol. 31, no. 1, pp. 5–19, Jan. 2017.

[9] J. Guo, K. Xie, and S. Zheng, “Molecular Biomarkers of Pancreatic Intraepithelial Neoplasia and Their Implications in Early Diagnosis and Therapeutic Intervention of Pancreatic Cancer,” *Int. J. Biol. Sci.*, vol. 12, no. 3, pp. 292–301, 2016.

[10] C. Guerra and M. Barbacid, “Genetically engineered mouse models of pancreatic adenocarcinoma,” *Mol. Oncol.*, vol. 7, no. 2, pp. 232–247, Apr. 2013.

[11] C. Guerra, M. Collado, C. Navas, A. J. Schuhmacher, I. Hernández-Porras, M. Cañamero, M. Rodriguez-Justo, M. Serrano, and M. Barbacid, “Pancreatitis-induced inflammation contributes to pancreatic cancer by inhibiting oncogene-induced senescence.,” *Cancer Cell*, vol. 19, no. 6, pp. 728–39, Jun. 2011.

[12] M. Lesina, M. U. Kurkowski, K. Ludes, S. Rose-John, M. Treiber, G. Klöppel, A. Yoshimura, W. Reindl, B. Sipos, S. Akira, R. M. Schmid, and H. Algül, “Stat3/Socs3 activation by IL-6 transsignaling promotes progression of pancreatic intraepithelial neoplasia and development of pancreatic cancer.,” *Cancer Cell*, vol. 19, no. 4, pp. 456–69, Apr. 2011.

[13] F. McAllister, J. M. Bailey, J. Alsina, C. J. Nirschl, R. Sharma, H. Fan, Y. Rattigan, J. C. Roeser, R. H. Lankapalli, H. Zhang, E. M. Jaffee, C. G. Drake, F. Housseau, A. Maitra, J. K. Kolls, C. L. Sears, D. M. Pardoll, and S. D. Leach, “Oncogenic Kras Activates a Hematopoietic-to-Epithelial

IL-17 Signaling Axis in Preinvasive Pancreatic Neoplasia," *Cancer Cell*, vol. 25, no. 5, pp. 621–637, May 2014.

[14] S. M. Wörmann and H. Algül, "Risk factors and therapeutic targets in pancreatic cancer.," *Front. Oncol.*, vol. 3, p. 282, Nov. 2013.

[15] J. C. Walrath, J. J. Hawes, T. Van Dyke, and K. M. Reilly, "Genetically Engineered Mouse Models in Cancer Research," in *Advances in cancer research*, vol. 106, 2010, pp. 113–164.

[16] P. K. Mazur and J. T. Siveke, "Genetically engineered mouse models of pancreatic cancer: unravelling tumour biology and progressing translational oncology," *Gut*, vol. 61, no. 10, pp. 1488–1500, Oct. 2012.

[17] S. R. Hingorani, E. F. Petricoin, A. Maitra, V. Rajapakse, C. King, M. A. Jacobetz, S. Ross, T. P. Conrads, T. D. Veenstra, B. A. Hitt, Y. Kawaguchi, D. Johann, L. A. Liotta, H. C. Crawford, M. E. Putt, T. Jacks, C. V. E. E. Wright, R. H. Hruban, A. M. Lowy, and D. A. Tuveson, "Preinvasive and invasive ductal pancreatic cancer and its early detection in the mouse.," *Cancer Cell*, vol. 4, no. 6, pp. 437–450, Dec. 2003.

[18] I. J. Fidler, "Timeline: The pathogenesis of cancer metastasis: the 'seed and soil' hypothesis revisited," *Nat. Rev. Cancer*, vol. 3, no. 6, pp. 453–458, Jun. 2003.

[19] C. L. Chaffer and R. A. Weinberg, "A Perspective on Cancer Cell Metastasis," *Science (80-.)*., vol. 331, no. 6024, pp. 1559–1564, Mar. 2011.

[20] J. Ferlay, I. Soerjomataram, R. Dikshit, S. Eser, C. Mathers, M. Rebelo, D. M. Parkin, D. Forman, and F. Bray, "Cancer incidence and mortality worldwide: Sources, methods and major patterns in GLOBOCAN 2012," *Int. J. Cancer*, vol. 136, no. 5, pp. E359–E386, Mar. 2015.

[21] D. X. Nguyen, P. D. Bos, and J. Massagué, "Metastasis: from dissemination to organ-specific colonization," *Nat. Rev. Cancer*, vol. 9, no. 4, pp. 274–284, Apr. 2009.

[22] J. Liu, L. Gao, H. Zhang, D. Wang, M. Wang, J. Zhu, C. Pang, and C. Wang, "Succinate dehydrogenase 5 (SDH5) regulates glycogen synthase kinase 3β-β-catenin-mediated lung cancer metastasis.," *J. Biol. Chem.*, vol. 288, no. 41, pp. 29965–73, Oct. 2013.

[23] A. F. Chambers, A. C. Groom, and I. C. MacDonald, "Metastasis: Dissemination and growth of cancer cells in metastatic sites," *Nat. Rev. Cancer*, vol. 2, no. 8, pp. 563–572, Aug. 2002.

[24] G. P. Gupta and J. Massagué, "Cancer Metastasis: Building a Framework," *Cell*, vol. 127, no. 4, pp. 679–695, Nov. 2006.

[25] H. Haeno, M. Gonen, M. B. Davis, J. M. Herman, C. A. Iacobuzio-Donahue, and F. Michor, "Computational Modeling of Pancreatic Cancer Reveals Kinetics of Metastasis Suggesting Optimum Treatment Strategies," *Cell*, vol. 148, no. 1–2, pp. 362–375, Jan. 2012.

[26] S. Baranwal and S. K. Alahari, "miRNA control of tumor cell invasion and metastasis," *Int. J. Cancer*, vol. 126, no. 6, p. NA-NA, Mar. 2010.

[27] P. C. Hermann, S. L. Huber, T. Herrler, A. Aicher, J. W. Ellwart, M. Guba, C. J. Bruns, and C. Heeschen, "Distinct populations of cancer stem cells determine tumor growth and metastatic activity in human pancreatic cancer.," *Cell Stem Cell*, vol. 1, no. 3, pp. 313–23, Sep. 2007.

[28] E. Giovannetti, C. L. van der Borden, A. E. Frampton, A. Ali, O. Firuzi, and G. J. Peters, "Never let it go: Stopping key mechanisms underlying metastasis to fight pancreatic cancer," *Semin. Cancer Biol.*, vol. 44, pp. 43–59, Jun. 2017.

[29] B. Costa-Silva, N. M. Aiello, A. J. Ocean, S. Singh, H. Zhang, B. K. Thakur, A. Becker, A. Hoshino, M. T. Mark, H. Molina, J. Xiang, T. Zhang, T.-M. Theilen, G. García-Santos, C. Williams, Y. Ararso, Y. Huang, G. Rodrigues, T.-L. Shen, K. J. Labori, I. M. B. Lothe, E. H. Kure, J. Hernandez, A. Doussot, S. H. Ebbesen, P. M. Grandgenett, M. A. Hollingsworth, M. Jain, K. Mallya, S. K. Batra, W. R. Jarnagin, R. E. Schwartz, I. Matei, H. Peinado, B. Z. Stanger, J. Bromberg, and D. Lyden, "Pancreatic cancer exosomes initiate pre-metastatic niche formation in the liver.," *Nat. Cell Biol.*, vol. 17, no. 6, pp. 816–26, Jun. 2015.

[30] S. Yachida, S. Jones, I. Bozic, T. Antal, R. Leary, B. Fu, M. Kamiyama, R. H. Hruban, J. R. Eshleman, M. A. Nowak, V. E. Velculescu, K. W. Kinzler, B. Vogelstein, and C. A. Iacobuzio-Donahue, "Distant metastasis occurs late during the genetic evolution of pancreatic cancer," *Nature*, vol. 467, no. 7319, pp. 1114–1117, Oct. 2010.

[31] R. Kalluri and R. A. Weinberg, "The basics of epithelial-mesenchymal transition.," *J. Clin. Invest.*, vol. 119, no. 6, pp. 1420–8, Jun. 2009.

[32] J. Caramel and et al., "A switch in the expression of embryonic EMT-inducers drives the development of malignant melanoma," *Cancer Cell*, vol. 24, no. 11, pp. 466–480, 2013.

[33] N. Tiwari, A. Gheldof, M. Tatari, and G. Christofori, "EMT as the ultimate survival mechanism of cancer cells," *Semin. Cancer Biol.*, vol. 22, no. 3, pp. 194–207, Jun. 2012.

[34] T. Brabletz, "To differentiate or not — routes towards metastasis," *Nat. Rev. Cancer*, vol. 12, no. 6, pp. 425–436, May 2012.

[35] M. Guarino, "Epithelial–mesenchymal transition and tumour invasion," *Int. J. Biochem. Cell Biol.*, vol. 39, no. 12, pp. 2153–2160, 2007.

[36] L. D. Roy, M. Sahraei, D. B. Subramani, D. Besmer, S. Nath, T. L. Tinder, E. Bajaj, K. Shanmugam, Y. Y. Lee, S. I. L. Hwang, S. J. Gendler, and P. Mukherjee, "MUC1 enhances invasiveness of pancreatic cancer cells by inducing epithelial to mesenchymal transition," *Oncogene*, vol. 30, no. 12, pp. 1449–1459, Mar. 2011.

[37] M. P. Ponnusamy, I. Lakshmanan, M. Jain, S. Das, S. Chakraborty, P. Dey, and S. K. Batra, "MUC4 mucin-induced epithelial to mesenchymal transition: a novel mechanism for metastasis of human ovarian cancer cells," *Oncogene*, vol. 29, no. 42, pp. 5741–5754, Oct. 2010.

[38] S. D. Puvvada, W. K. Funkhouser, K. Greene, A. Deal, H. Chu, A. S. Baldwin, J. E. Tepper, and B. H. O'Neil, "NF-kB and Bcl-3 activation are prognostic in metastatic colorectal cancer.," *Oncology*, vol. 78, no. 3–4, pp. 181–8, 2010.

[39] J. Miyoshi and Y. Takai, "Structural and functional associations of apical junctions with cytoskeleton," *Biochim. Biophys. Acta - Biomembr.*, vol. 1778, no. 3, pp. 670–691, Mar. 2008.

[40] A. Natalwala, R. Spychal, and C. Tselepis, "Epithelial-mesenchymal transition mediated tumourigenesis in the gastrointestinal tract.," *World J. Gastroenterol.*, vol. 14, no. 24, pp. 3792–7, Jun. 2008.

[41] A. M. Lowy, J. Knight, and J. Groden, "Restoration of E-cadherin/beta-catenin expression in pancreatic cancer cells inhibits growth by induction of apoptosis.," *Surgery*, vol. 132, no. 2, pp. 141–8, Aug. 2002.

[42] C. S. Scanlon, E. A. Van Tubergen, R. C. Inglehart, and N. J. D'Silva, "Biomarkers of epithelial-mesenchymal transition in squamous cell carcinoma.," *J. Dent. Res.*, vol. 92, no. 2, pp. 114–21,

Feb. 2013.

[43] J. H. Tsai and J. Yang, “Epithelial-mesenchymal plasticity in carcinoma metastasis.,” *Genes Dev.*, vol. 27, no. 20, pp. 2192–206, Oct. 2013.

[44] F. H. Brembeck, M. Rosário, and W. Birchmeier, “Balancing cell adhesion and Wnt signaling, the key role of β-catenin,” *Curr. Opin. Genet. Dev.*, vol. 16, no. 1, pp. 51–59, Feb. 2006.

[45] Y. Tomizawa, T. T. Wu, and K. K. Wang, “Epithelial mesenchymal transition and cancer stem cells in esophageal adenocarcinoma originating from barrett’s esophagus,” vol. 3, no. 5, pp. 1059–1063, May 2012.

[46] M. A. Khan, H. Chen, D. Zhang, and J. Fu, “Twist: a molecular target in cancer therapeutics,” *Tumor Biol.*, vol. 34, no. 5, pp. 2497–2506, Oct. 2013.

[47] Y. Wang, J. Liu, X. Ying, P. C. Lin, and B. P. Zhou, “Twist-mediated Epithelial-mesenchymal Transition Promotes Breast Tumor Cell Invasion via Inhibition of Hippo Pathway,” *Sci. Rep.*, vol. 6, no. 1, p. 24606, Jul. 2016.

[48] J. Yang, S. A. Mani, J. L. Donaher, S. Ramaswamy, R. A. Itzykson, C. Come, P. Savagner, I. Gitelman, A. Richardson, and R. A. Weinberg, “Twist, a Master Regulator of Morphogenesis, Plays an Essential Role in Tumor Metastasis,” *Cell*, vol. 117, no. 7, pp. 927–939, Jun. 2004.

[49] F. Vesuna, P. van Diest, J. H. Chen, and V. Raman, “Twist is a transcriptional repressor of E-cadherin gene expression in breast cancer,” *Biochem. Biophys. Res. Commun.*, vol. 367, no. 2, pp. 235–241, Mar. 2008.

[50] R. F. Niu, L. Zhang, G. M. Xi, X. Y. Wei, Y. Yang, Y. R. Shi, and X. S. Hao, “Up-regulation of Twist induces angiogenesis and correlates with metastasis in hepatocellular carcinoma.,” *J. Exp. Clin. Cancer Res.*, vol. 26, no. 3, pp. 385–94, Sep. 2007.

[51] M. M. Javle, J. F. Gibbs, K. K. Iwata, Y. Pak, P. Rutledge, J. Yu, J. D. Black, D. Tan, and T. Khoury, “Epithelial-Mesenchymal Transition (EMT) and Activated Extracellular Signal-regulated Kinase (p-Erk) in Surgically Resected Pancreatic Cancer,” *Ann. Surg. Oncol.*, vol. 14, no. 12, pp. 3527–3533, Nov. 2007.

[52] B. Hotz, M. Arndt, S. Dullat, S. Bhargava, H.-J. Buhr, and H. G. Hotz, “Epithelial to Mesenchymal Transition: Expression of the Regulators Snail, Slug, and Twist in Pancreatic Cancer,” *Clin. Cancer Res.*, vol. 13, no. 16, pp. 4769–4776, Aug. 2007.

[53] T. Arumugam, V. Ramachandran, K. F. Fournier, H. Wang, L. Marquis, J. L. Abbruzzese, G. E. Gallick, C. D. Logsdon, D. J. McConkey, and W. Choi, “Epithelial to Mesenchymal Transition Contributes to Drug Resistance in Pancreatic Cancer,” *Cancer Res.*, vol. 69, no. 14, pp. 5820–5828, Jul. 2009.

[54] J. von Burstin, S. Eser, M. C. Paul, B. Seidler, M. Brandl, M. Messer, A. von Werder, A. Schmidt, J. Mages, P. Pagel, A. Schnieke, R. M. Schmid, G. Schneider, and D. Saur, “E-Cadherin Regulates Metastasis of Pancreatic Cancer In Vivo and Is Suppressed by a SNAIL/HDAC1/HDAC2 Repressor Complex,” *Gastroenterology*, vol. 137, no. 1, p. 361–371.e5, Jul. 2009.

[55] J. Comijn, G. Berx, P. Vermassen, K. Verschueren, L. van Grunsven, E. Bruyneel, M. Mareel, D. Huylebroeck, and F. van Roy, “The two-handed E box binding zinc finger protein SIP1 downregulates E-cadherin and induces invasion.,” *Mol. Cell*, vol. 7, no. 6, pp. 1267–78, Jun.

2001.

[56] H. Peinado, M. Quintanilla, and A. Cano, “Transforming Growth Factor β-1 Induces Snail Transcription Factor in Epithelial Cell Lines,” *J. Biol. Chem.*, vol. 278, no. 23, pp. 21113–21123, Jun. 2003.

[57] R. Hiraga, M. Kato, S. Miyagawa, and T. Kamata, “Nox4-derived ROS signaling contributes to TGF-β-induced epithelial-mesenchymal transition in pancreatic cancer cells.,” *Anticancer Res.*, vol. 33, no. 10, pp. 4431–8, Oct. 2013.

[58] F. Sato, F. Sato, T. Yamada, U. K. Bhawal, T. Kawamoto, K. Fujimoto, M. Noshiro, H. Seino, S. Morohashi, K. Hakamada, Y. Abiko, Y. Kato, and H. Kijima, “The BHLH transcription factor DEC1 plays an important role in the epithelial-mesenchymal transition of pancreatic cancer,” *Int. J. Oncol.*, vol. 41, no. 4, pp. 1337–46, Jul. 2012.

[59] A. D. Yang, E. R. Camp, F. Fan, L. Shen, M. J. Gray, W. Liu, R. Somcio, T. W. Bauer, Y. Wu, D. J. Hicklin, and L. M. Ellis, “Vascular Endothelial Growth Factor Receptor-1 Activation Mediates Epithelial to Mesenchymal Transition in Human Pancreatic Carcinoma Cells,” *Cancer Res.*, vol. 66, no. 1, pp. 46–51, Jan. 2006.

[60] S. Hamada, K. Satoh, M. Hirota, K. Kimura, A. Kanno, A. Masamune, and T. Shimosegawa, “Bone morphogenetic protein 4 induces epithelial-mesenchymal transition through MSX2 induction on pancreatic cancer cell line,” *J. Cell. Physiol.*, vol. 213, no. 3, pp. 768–774, Dec. 2007.

[61] J. Unno, K. Satoh, M. Hirota, A. Kanno, S. Hamada, H. Ito, A. Masamune, N. Tsukamoto, F. Motoi, S. Egawa, M. Unno, A. Horii, and T. Shimosegawa, *International journal of oncology.*, vol. 35, no. 4. University of Crete, Faculty of Medicine, Laboratory of Clinical Virology, 2009.

[62] H. Taniguchi, C. Moriya, H. Igarashi, A. Saitoh, H. Yamamoto, Y. Adachi, and K. Imai, “Cancer stem cells in human gastrointestinal cancer.,” *Cancer Sci.*, vol. 107, no. 11, pp. 1556–1562, Nov. 2016.

[63] K. Ishizawa, Z. A. Rasheed, R. Karisch, Q. Wang, J. Kowalski, E. Susky, K. Pereira, C. Karamboulas, N. Moghal, N. V. Rajeshkumar, M. Hidalgo, M. Tsao, L. Ailles, T. K. Waddell, A. Maitra, B. G. Neel, and W. Matsui, “Tumor-Initiating Cells Are Rare in Many Human Tumors,” *Cell Stem Cell*, vol. 7, no. 3, pp. 279–282, Sep. 2010.

[64] T. Reya, S. J. Morrison, M. F. Clarke, and I. L. Weissman, “Stem cells, cancer, and cancer stem cells.,” *Nature*, vol. 414, no. 6859, pp. 105–111, Nov. 2001.

[65] L. Vermeulen, M. R. Sprick, K. Kemper, G. Stassi, and J. P. Medema, “Cancer stem cells – old concepts, new insights,” *Cell Death Differ.*, vol. 15, no. 6, pp. 947–958, Jun. 2008.

[66] A. Jimeno, G. Feldmann, A. Suárez-Gauthier, Z. Rasheed, A. Solomon, G.-M. Zou, B. Rubio-Viqueira, E. García-García, F. López-Ríos, W. Matsui, A. Maitra, and M. Hidalgo, “A direct pancreatic cancer xenograft model as a platform for cancer stem cell therapeutic development.,” *Mol. Cancer Ther.*, vol. 8, no. 2, pp. 310–4, Feb. 2009.

[67] L. V. Nguyen, R. Vanner, P. Dirks, and C. J. Eaves, “Cancer stem cells: an evolving concept,” *Nat. Rev. Cancer*, vol. 12, no. 2, pp. 133–43, Jan. 2012.

[68] B. K. Garvalov and T. Acker, “Cancer stem cells: a new framework for the design of tumor therapies,” *J. Mol. Med.*, vol. 89, no. 2, pp. 95–107, Feb. 2011.

[69] Y. Shiozawa, B. Nie, K. J. Pienta, T. M. Morgan, and R. S. Taichman, “Cancer stem cells and their role in metastasis.,” *Pharmacol. Ther.*, vol. 138, no. 2, pp. 285–93, May 2013.

[70] I. Malanchi, A. Santamaria-Martínez, E. Susanto, H. Peng, H.-A. Lehr, J.-F. Delaloye, and J. Huelsken, “Interactions between cancer stem cells and their niche govern metastatic colonization,” *Nature*, vol. 481, no. 7379, pp. 85–89, Dec. 2011.

[71] M. Shipitsin, L. L. Campbell, P. Argani, S. Weremowicz, N. Bloushtain-Qimron, J. Yao, T. Nikolskaya, T. Serebryiskaya, R. Beroukhim, M. Hu, M. K. Halushka, S. Sukumar, L. M. Parker, K. S. Anderson, L. N. Harris, J. E. Garber, A. L. Richardson, S. J. Schnitt, Y. Nikolsky, R. S. Gelman, and K. Polyak, “Molecular Definition of Breast Tumor Heterogeneity,” *Cancer Cell*, vol. 11, no. 3, pp. 259–273, Mar. 2007.

[72] B. Giebel, D. Corbeil, J. Beckmann, J. Höhn, D. Freund, K. Giesen, J. Fischer, G. Kögler, and P. Wernet, “Segregation of lipid raft markers including CD133 in polarized human hematopoietic stem and progenitor cells,” *Blood*, vol. 104, no. 8, 2004.

[73] T. Moriyama, K. Ohuchida, K. Mizumoto, L. Cui, N. Ikenaga, N. Sato, and M. Tanaka, “Enhanced cell migration and invasion of CD133+ pancreatic cancer cells cocultured with pancreatic stromal cells,” *Cancer*, vol. 116, no. 14, pp. 3357–3368, Apr. 2010.

[74] L. Vermeulen, M. Todaro, F. de Sousa Mello, M. R. Sprick, K. Kemper, M. Perez Alea, D. J. Richel, G. Stassi, J. P. Medema, M. Mori, A. Chadburn, A. Murphy, D. Valenzuela, N. Gale, G. Thurston, G. Yancopoulos, M. D’Angelica, N. Kemeny, D. Lyden, and S. Rafii, “Single-cell cloning of colon cancer stem cells reveals a multi-lineage differentiation capacity,” *Proc. Natl. Acad. Sci.*, vol. 105, no. 36, pp. 13427–13432, Sep. 2008.

[75] Q. Wang, Z.-G. Chen, C.-Z. Du, H.-W. Wang, L. Yan, and J. Gu, “Cancer stem cell marker CD133+ tumour cells and clinical outcome in rectal cancer,” *Histopathology*, vol. 55, no. 3, pp. 284–293, Sep. 2009.

[76] K. Shien, S. Toyooka, K. Ichimura, J. Soh, M. Furukawa, Y. Maki, T. Muraoka, N. Tanaka, T. Ueno, H. Asano, K. Tsukuda, M. Yamane, T. Oto, K. Kiura, and S. Miyoshi, “Prognostic impact of cancer stem cell-related markers in non-small cell lung cancer patients treated with induction chemoradiotherapy,” *Lung Cancer*, vol. 77, no. 1, pp. 162–167, Jul. 2012.

[77] S. A. Mani, W. Guo, M.-J. Liao, E. N. Eaton, A. Ayyanan, A. Y. Zhou, M. Brooks, F. Reinhard, C. C. Zhang, M. Shipitsin, L. L. Campbell, K. Polyak, C. Brisken, J. Yang, and R. A. Weinberg, “The Epithelial-Mesenchymal Transition Generates Cells with Properties of Stem Cells,” *Cell*, vol. 133, no. 4, pp. 704–715, May 2008.

[78] K. Polyak and R. A. Weinberg, “Transitions between epithelial and mesenchymal states: acquisition of malignant and stem cell traits,” *Nat. Rev. Cancer*, vol. 9, no. 4, pp. 265–273, Apr. 2009.

[79] C. Scheel and R. A. Weinberg, “Cancer stem cells and epithelial–mesenchymal transition: Concepts and molecular links,” *Semin. Cancer Biol.*, vol. 22, no. 5–6, pp. 396–403, Oct. 2012.

[80] W. Hwang, M. Yang, M. Tsai, H. Lan, S. Su, S. Chang, H. Teng, S. Yang, Y. Lan, S. Chiou, and H. Wang, “SNAIL Regulates Interleukin-8 Expression, Stem Cell–Like Activity, and Tumorigenicity of Human Colorectal Carcinoma Cells,” *Gastroenterology*, vol. 141, no. 1, p. 279–291.e5, Jul. 2011.

[81] U. Wellner, J. Schubert, U. C. Burk, O. Schmalhofer, F. Zhu, A. Sonntag, B. Waldvogel, C. Vannier, D. Darling, A. zur Hausen, V. G. Brunton, J. Morton, O. Sansom, J. Schüler, M. P. Stemmler, C. Herzberger, U. Hopt, T. Keck, S. Brabletz, and T. Brabletz, "The EMT-activator ZEB1 promotes tumorigenicity by repressing stemness-inhibiting microRNAs," *Nat. Cell Biol.*, vol. 11, no. 12, pp. 1487–1495, Dec. 2009.

[82] M.-H. Yang, D. S.-S. Hsu, H.-W. Wang, H.-J. Wang, H.-Y. Lan, W.-H. Yang, C.-H. Huang, S.-Y. Kao, C.-H. Tzeng, S.-K. Tai, S.-Y. Chang, O. K.-S. Lee, and K.-J. Wu, "Bmi1 is essential in Twist1-induced epithelial–mesenchymal transition," *Nat. Cell Biol.*, vol. 12, no. 10, pp. 982–992, Oct. 2010.

[83] A. Puisieux, T. Brabletz, and J. Caramel, "Oncogenic roles of EMT-inducing transcription factors," *Nat. Cell Biol.*, vol. 16, no. 6, pp. 488–494, May 2014.

[84] T. Brabletz, A. Jung, S. Spaderna, F. Hlubek, and T. Kirchner, "Opinion: Migrating cancer stem cells — an integrated concept of malignant tumour progression," *Nat. Rev. Cancer*, vol. 5, no. 9, pp. 744–749, Sep. 2005.

[85] J. P. Thiery, H. Acloque, R. Y. J. Huang, and M. A. Nieto, "Epithelial-Mesenchymal Transitions in Development and Disease," *Cell*, vol. 139, no. 5, pp. 871–890, Nov. 2009.

[86] G. Pirozzi, V. Tirino, R. Camerlingo, R. Franco, A. La Rocca, E. Liguori, N. Martucci, F. Paino, N. Normanno, and G. Rocco, "Epithelial to Mesenchymal Transition by TGFβ-1 Induction Increases Stemness Characteristics in Primary Non Small Cell Lung Cancer Cell Line," *PLoS One*, vol. 6, no. 6, p. e21548, Jun. 2011.

[87] S.-J. Park, J.-G. Kim, N. D. Kim, K. Yang, J. W. Shim, and K. Heo, "Estradiol, TGF-β1 and hypoxia promote breast cancer stemness and EMT-mediated breast cancer migration.," *Oncol. Lett.*, vol. 11, no. 3, pp. 1895–1902, Mar. 2016.

[88] E. V. Abel and D. M. Simeone, "Biology and Clinical Applications of Pancreatic Cancer Stem Cells," *Gastroenterology*, vol. 144, no. 6, pp. 1241–1248, May 2013.

[89] C. Li, D. G. Heidt, P. Dalerba, C. F. Burant, L. Zhang, V. Adsay, M. Wicha, M. F. Clarke, and D. M. Simeone, "Identification of Pancreatic Cancer Stem Cells," *Cancer Res.*, vol. 67, no. 3, pp. 1030–1037, Feb. 2007.

[90] C. Li, J.-J. Wu, M. Hynes, J. Dosch, B. Sarkar, T. H. Welling, M. Pasca di Magliano, and D. M. Simeone, "c-Met is a marker of pancreatic cancer stem cells and therapeutic target.," *Gastroenterology*, vol. 141, no. 6, p. 2218–2227.e5, Dec. 2011.

[91] E. V. Abel, E. J. Kim, J. Wu, M. Hynes, F. Bednar, E. Proctor, L. Wang, M. L. Dziubinski, and D. M. Simeone, "The Notch Pathway Is Important in Maintaining the Cancer Stem Cell Population in Pancreatic Cancer," *PLoS One*, vol. 9, no. 3, p. e91983, Mar. 2014.

[92] F.-T. Huang, Y.-X. ZHUAN-SUN, Y.-Y. Zhuang, S.-L. Wei, J. Tang, W.-B. Chen, and S.-N. Zhang, "Inhibition of hedgehog signaling depresses self-renewal of pancreatic cancer stem cells and reverses chemoresistance," *Int. J. Oncol.*, vol. 41, no. 5, pp. 1707–1714, Nov. 2012.

[93] S. M. Sureban, R. May, S. A. Lightfoot, A. B. Hoskins, M. Lerner, D. J. Brackett, R. G. Postier, R. Ramanujam, A. Mohammed, C. V. Rao, J. H. Wyche, S. Anant, and C. W. Houchen, "DCAMKL-1 Regulates Epithelial-Mesenchymal Transition in Human Pancreatic Cells through a miR-200a-Dependent Mechanism," *Cancer Res.*, vol. 71, no. 6, pp. 2328–2338, Mar. 2011.

[94] H. Ohno, G. Takimoto, and T. W. McKeithan, “The candidate proto-oncogene bcl-3 is related to genes implicated in cell lineage determination and cell cycle control.,” *Cell*, vol. 60, no. 6, pp. 991–7, 1990.

[95] V. Bours, G. Franzoso, V. Azarenko, S. Park, T. Kanno, K. Brown, and U. Siebenlist, “The oncoprotein Bcl-3 directly transactivates through kappa B motifs via association with DNA-binding p50B homodimers.,” *Cell*, vol. 72, no. 5, pp. 729–39, Mar. 1993.

[96] G. Franzoso, V. Bours, V. Azarenko, S. Park, M. Tomita-Yamaguchi, T. Kanno, K. Brown, and U. Siebenlist, “The oncoprotein Bcl-3 can facilitate NF-kappa B-mediated transactivation by removing inhibiting p50 homodimers from select kappa B sites.,” *EMBO J.*, vol. 12, no. 10, pp. 3893–3901, 1993.

[97] D. L. Bundy and T. W. McKeithan, “Diverse Effects of BCL3 Phosphorylation on Its Modulation of NF- B p52 Homodimer Binding to DNA,” *J. Biol. Chem.*, vol. 272, no. 52, pp. 33132–33139, Dec. 1997.

[98] R. Massoumi, K. Chmielarska, K. Hennecke, A. Pfeifer, and R. Fässler, “Cyld inhibits tumor cell proliferation by blocking Bcl-3-dependent NF-kappaB signaling.,” *Cell*, vol. 125, no. 4, pp. 665–77, 2006.

[99] V. Maldonado and J. Melendez-Zajgla, “Role of Bcl-3 in solid tumors.,” *Mol. Cancer*, vol. 10, p. 152, Dec. 2011.

[100] S. D. Westerheide, M. W. Mayo, V. Anest, J. L. Hanson, and A. S. Baldwin, “The putative oncoprotein Bcl-3 induces cyclin D1 to stimulate G(1) transition.,” *Mol. Cell. Biol.*, vol. 21, no. 24, pp. 8428–36, 2001.

[101] S. Rocha, A. M. Martin, D. W. Meek, and N. D. Perkins, “p53 represses cyclin D1 transcription through down regulation of Bcl-3 and inducing increased association of the p52 NF-kappaB subunit with histone deacetylase 1.,” *Mol. Cell. Biol.*, vol. 23, no. 13, pp. 4713–27, Jul. 2003.

[102] J. Wessells, M. Baer, H. A. Young, E. Claudio, K. Brown, U. Siebenlist, and P. F. Johnson, “BCL-3 and NF-κB p50 Attenuate Lipopolysaccharide-induced Inflammatory Responses in Macrophages,” *J. Biol. Chem.*, vol. 279, no. 48, pp. 49995–50003, Nov. 2004.

[103] R. J. Carmody, Q. Ruan, S. Palmer, B. Hilliard, and Y. H. Chen, “Negative Regulation of Toll-Like Receptor Signaling by NF- B p50 Ubiquitination Blockade,” *Science (80-.).*, vol. 317, no. 5838, pp. 675–678, Aug. 2007.

[104] V. Y.-F. Wang, W. Huang, M. Asagiri, N. Spann, A. Hoffmann, C. Glass, and G. Ghosh, “The Transcriptional Specificity of NF-κB Dimers Is Coded within the κB DNA Response Elements,” *Cell Rep.*, vol. 2, no. 4, pp. 824–839, Oct. 2012.

[105] M. S. Hayden and S. Ghosh, “Shared Principles in NF-κB Signaling,” *Cell*, vol. 132, no. 3, pp. 344–362, Feb. 2008.

[106] U. Siebenlist, K. Brown, and E. Claudio, “Control of lymphocyte development by nuclear factor-κB,” *Nat. Rev. Immunol.*, vol. 5, no. 6, pp. 435–445, Jun. 2005.

[107] M. Nishikori, Y. Maesako, C. Ueda, M. Kurata, T. Uchiyama, and H. Ohno, “High-level expression of BCL3 differentiates t(2;5)(p23;q35)-positive anaplastic large cell lymphoma from Hodgkin disease,” *Blood*, vol. 101, no. 7, pp. 2789–2796, Apr. 2003.

[108] H. Ohno, M. Nishikori, Y. Maesako, and H. Haga, “Reappraisal of BCL3 as a molecular marker

of anaplastic large cell lymphoma.," *Int. J. Hematol.*, vol. 82, no. 5, pp. 397–405, Dec. 2005.

[109] G. Z. Rassidakis, M. P. Oyarzo, and L. J. Medeiros, "BCL-3 overexpression in anaplastic lymphoma kinase-positive anaplastic large cell lymphoma," *Blood*, vol. 102, no. 3, pp. 1146–1147, Apr. 2003.

[110] H. A. H. Ibrahim, F. Amen, A. G. Reid, and K. N. Naresh, "BCL3 rearrangement, amplification and expression in diffuse large B-cell lymphoma," *Eur. J. Haematol.*, vol. 87, no. 6, pp. 480–485, Dec. 2011.

[111] W. Y. Au, D. E. Horsman, H. Ohno, R. J. Klasa, and R. D. Gascoyne, "Bcl-3/IgH translocation (14;19)(q32;q13) in Non-Hodgkin's Lymphomas," *Leuk. Lymphoma*, vol. 43, no. 4, pp. 813–816, Jan. 2002.

[112] O. Canoz, G. Z. Rassidakis, J. H. Admirand, and L. J. Medeiros, "Immunohistochemical detection of BCL-3 in lymphoid neoplasms: a survey of 353 cases," *Mod. Pathol.*, vol. 17, no. 8, pp. 911–917, Aug. 2004.

[113] E. Schlette, G. Z. Rassidakis, O. Canoz, and L. J. Medeiros, "Expression of bcl-3 in Chronic Lymphocytic Leukemia Correlates With Trisomy 12 and Abnormalities of Chromosome 19," *Am. J. Clin. Pathol.*, vol. 123, no. 3, pp. 465–471, Mar. 2005.

[114] M. F. J. Bassetti, J. White, J. W. Kappler, and P. Marrack, "Transgenic Bcl-3 slows T cell proliferation," *Int. Immunol.*, vol. 21, no. 4, pp. 339–348, Apr. 2009.

[115] K. Brocke-Heidrich, B. Ge, H. Cvijic, G. Pfeifer, D. Löffler, C. Henze, T. W. McKeithan, and F. Horn, "BCL3 is induced by IL-6 via Stat3 binding to intronic enhancer HS4 and represses its own transcription," *Oncogene*, vol. 25, no. 55, pp. 7297–7304, Nov. 2006.

[116] Z. Liu, Y. Jiang, Y. Hou, Y. Hu, X. Cao, Y. Tao, C. Xu, S. Liu, S. Wang, L. Wang, Y. Shi, U. Siebenlist, and X. Zhang, "The I B family member Bcl-3 stabilizes c-Myc in colorectal cancer," *J. Mol. Cell Biol.*, vol. 5, no. 4, pp. 280–282, Aug. 2013.

[117] B. C. Urban, T. J. Collard, C. J. Eagle, S. L. Southern, A. Greenhough, M. Hamdollah-Zadeh, A. Ghosh, R. Poulsom, C. Paraskeva, A. Silver, and A. C. Williams, "BCL-3 expression promotes colorectal tumorigenesis through activation of AKT signalling.," *Gut*, vol. 65, no. 7, p. 1151, Jun. 2015.

[118] H. J. Choi, J. M. Lee, H. Kim, H. J. Nam, H.-J. R. Shin, D. Kim, E. Ko, D.-Y. Noh, K. Il Kim, J. H. Kim, and S. H. Baek, "Bcl3-dependent stabilization of CtBP1 is crucial for the inhibition of apoptosis and tumor progression in breast cancer," *Biochem. Biophys. Res. Commun.*, vol. 400, no. 3, pp. 396–402, Sep. 2010.

[119] B. H. O'Neil, P. Bůzková, H. Farrah, D. Kashatus, H. Sanoff, R. M. Goldberg, A. S. Baldwin, and W. K. Funkhouser, "Expression of nuclear factor-kappaB family proteins in hepatocellular carcinomas.," *Oncology*, vol. 72, no. 1–2, pp. 97–104, 2007.

[120] K. Tu, Z. Liu, B. Yao, Y. Xue, M. Xu, C. Dou, G. Yin, and J. Wang, "BCL-3 promotes the tumor growth of hepatocellular carcinoma by regulating cell proliferation and the cell cycle through cyclin D1.," *Oncol. Rep.*, Feb. 2016.

[121] J. Pallares, J. L. Martínez-Guitarte, X. Dolcet, D. Llobet, M. Rue, J. Palacios, J. Prat, and X. Matias-Guiu, "Abnormalities in the NF-κB family and related proteins in endometrial carcinoma," *J. Pathol.*, vol. 204, no. 5, pp. 569–577, Dec. 2004.

[122] N. J. Thornburg, R. Pathmanathan, and N. Raab-Traub, “Activation of nuclear factor-kappaB p50 homodimer/Bcl-3 complexes in nasopharyngeal carcinoma.,” *Cancer Res.*, vol. 63, no. 23, pp. 8293–301, Dec. 2003.

[123] W. Tang, H. Wang, H. L. Ha, I. Tassi, R. Bhardwaj, E. Claudio, and U. Siebenlist, “The B-cell tumor promoter Bcl-3 suppresses inflammation-associated colon tumorigenesis in epithelial cells,” *Oncogene*, May 2016.

[124] N. Gehrke, M. A. Wörns, A. Mann, Y. Huber, N. Hoevelmeyer, T. Longerich, A. Waisman, P. R. Galle, and J. M. Schattenberg, “Hepatic B cell leukemia-3 suppresses chemically-induced hepatocarcinogenesis in mice through altered MAPK and NF-κB activation,” *Oncotarget*, Nov. 2016.

[125] N. Hövelmeyer, F. T. Wunderlich, R. Massoumi, C. G. Jakobsen, J. Song, M. A. Wörns, C. Merkwirth, A. Kovalenko, M. Aumailley, D. Strand, J. C. Brüning, P. R. Galle, D. Wallach, R. Fässler, and A. Waisman, “Regulation of B cell homeostasis and activation by the tumor suppressor gene CYLD.,” *J. Exp. Med.*, vol. 204, no. 11, pp. 2615–27, Oct. 2007.

[126] A. Keutgens, K. Shostak, P. Close, X. Zhang, B. Hennuy, M. Aussems, J.-P. Chapelle, P. Viatour, A. Gothot, M. Fillet, and A. Chariot, “The repressing function of the oncoprotein BCL-3 requires CtBP, while its polyubiquitination and degradation involve the E3 ligase TBLR1.,” *Mol. Cell. Biol.*, vol. 30, no. 16, pp. 4006–4021, 2010.

[127] A. Keutgens, X. Zhang, K. Shostak, I. Robert, S. Olivier, A. Vanderplasschen, J.-P. Chapelle, P. Viatour, M.-P. Merville, F. Bex, A. Gothot, and A. Chariot, “BCL-3 Degradation Involves Its Polyubiquitination through a FBW7-independent Pathway and Its Binding to the Proteasome Subunit PSMB1,” *J. Biol. Chem.*, vol. 285, no. 33, pp. 25831–25840, Aug. 2010.

[128] P. Viatour, E. Dejardin, M. Warnier, F. Lair, E. Claudio, F. Bureau, J.-C. C. Marine, M.-P. P. Merville, U. Maurer, D. Green, J. Piette, U. Siebenlist, V. Bours, and A. Chariot, “GSK3-Mediated BCL-3 Phosphorylation Modulates Its Degradation and Its Oncogenicity,” *Mol. Cell*, vol. 16, no. 1, pp. 35–45, 2004.

[129] A. Wakefield, J. Soukupova, A. Montagne, J. Ranger, R. French, W. J. Muller, and R. W. E. Clarkson, “Bcl3 selectively promotes metastasis of ERBB2-driven mammary tumors.,” *Cancer Res.*, vol. 73, no. 2, pp. 745–55, Jan. 2013.

[130] X. Chen, X. Cao, X. Sun, R. Lei, P. Chen, Y. Zhao, Y. Jiang, J. Yin, R. Chen, D. Ye, Q. Wang, Z. Liu, S. Liu, C. Cheng, J. Mao, Y. Hou, M. Wang, U. Siebenlist, Y. Eugene Chin, Y. Wang, L. Cao, G. Hu, and X. Zhang, “Bcl-3 regulates TGFβ signaling by stabilizing Smad3 during breast cancer pulmonary metastasis,” *Cell Death Dis.*, vol. 7, no. 12, p. e2508, Dec. 2016.

[131] E. L. Jackson, N. Willis, K. Mercer, R. T. Bronson, D. Crowley, R. Montoya, T. Jacks, and D. A. Tuveson, “Analysis of lung tumor initiation and progression using conditional expression of oncogenic K-ras.,” *Genes Dev.*, vol. 15, no. 24, pp. 3243–3248, Dec. 2001.

[132] H. Nakhai, S. Sel, J. Favor, L. Mendoza-Torres, F. Paulsen, G. I. W. Duncker, and R. M. Schmid, “Ptf1a is essential for the differentiation of GABAergic and glycinergic amacrine cells and horizontal cells in the mouse retina,” *Development*, vol. 134, no. 6, 2007.

[133] J. Jonkers, R. Meuwissen, H. van der Gulden, H. Peterse, M. van der Valk, and A. Berns, “Synergistic tumor suppressor activity of BRCA2 and p53 in a conditional mouse model for

breast cancer.," *Nat. Genet.*, vol. 29, no. 4, pp. 418–425, Dec. 2001.

[134] M. Riemann, R. Endres, S. Liptay, K. Pfeffer, and R. M. Schmid, "The IkappaB protein Bcl-3 negatively regulates transcription of the IL-10 gene in macrophages.," *J. Immunol.*, vol. 175, no. 6, pp. 3560–8, Sep. 2005.

[135] S. M. Wörmann, L. Song, J. Ai, K. N. Diakopoulos, M. U. Kurkowski, K. Görgülü, D. Ruess, A. Campbell, C. Doglioni, D. Jodrell, A. Neesse, I. E. Demir, A.-P. Karpathaki, M. Barenboim, T. Hagemann, S. Rose-John, O. Sansom, R. M. Schmid, M. P. Protti, M. Lesina, and H. Algül, "Loss of P53 Function Activates JAK2–STAT3 Signaling to Promote Pancreatic Tumor Growth, Stroma Modification, and Gemcitabine Resistance in Mice and Is Associated With Patient Survival," *Gastroenterology*, vol. 151, no. 1, p. 180–193.e12, Jul. 2016.

[136] R. H. Hruban, N. V. Adsay, J. Albores-Saavedra, M. R. Anver, A. V. Biankin, G. P. Boivin, E. E. Furth, T. Furukawa, A. Klein, D. S. Klimstra, G. Klőppel, G. Y. Lauwers, D. S. Longnecker, J. Lűttges, A. Maitra, G. J. A. Offerhaus, L. Pérez-Gallego, M. Redston, and D. A. Tuveson, "Pathology of Genetically Engineered Mouse Models of Pancreatic Exocrine Cancer: Consensus Report and Recommendations," *Cancer Res.*, vol. 66, no. 1, 2006.

[137] P. Neuhöfer, S. Liang, H. Einwächter, C. Schwerdtfeger, T. Wartmann, M. Treiber, H. Zhang, H. Schulz, K. Dlubatz, M. Lesina, K. N. Diakopoulos, S. Wörmann, W. Halangk, H. Witt, R. M. Schmid, and H. Algül, "Deletion of IκBα Activates RelA to Reduce Acute Pancreatitis in Mice Through Up-regulation of Spi2A," *Gastroenterology*, vol. 144, no. 1, pp. 192–201, 2013.

[138] K. N. Diakopoulos, M. Lesina, S. Wörmann, L. Song, M. Aichler, L. Schild, A. Artati, W. Römisch-Margl, T. Wartmann, R. Fischer, Y. Kabiri, H. Zischka, W. Halangk, I. E. Demir, C. Pilsak, A. Walch, C. S. Mantzoros, J. M. Steiner, M. Erkan, R. M. Schmid, H. Witt, J. Adamski, and H. Algül, "Impaired Autophagy Induces Chronic Atrophic Pancreatitis in Mice via Sex- and Nutrition-Dependent Processes," *Gastroenterology*, vol. 148, no. 3, p. 626–638.e17, Mar. 2015.

[139] P. Viatour, M.-P. P. Merville, V. Bours, and A. Chariot, "Protein phosphorylation as a key mechanism for the regulation of BCL-3 activity," *Cell cycle*, vol. 3, no. 12, pp. 1498–1501, Dec. 2004.

[140] P. Sancho, E. Burgos-Ramos, A. Tavera, T. Bou Kheir, P. Jagust, M. Schoenhals, D. Barneda, K. Sellers, R. Campos-Olivas, O. Graña, C. R. Viera, M. Yuneva, B. Sainz, and C. Heeschen, "MYC/PGC-1α balance determines the metabolic phenotype and plasticity of pancreatic cancer stem cells," *Cell Metab.*, 2015.

[141] M. S. Hayden and S. Ghosh, "Signaling to NF- B," *Genes Dev.*, vol. 18, no. 18, pp. 2195–2224, Sep. 2004.

[142] G. P. Nolan, T. Fujita, K. Bhatia, C. Huppi, H. C. Liou, M. L. Scott, and D. Baltimore, "The bcl-3 proto-oncogene encodes a nuclear I kappa B-like molecule that preferentially interacts with NF-kappa B p50 and p52 in a phosphorylation-dependent manner.," *Mol. Cell. Biol.*, vol. 13, no. 6, pp. 3557–3566, Jun. 1993.

[143] L. A. Donehower, M. Harvey, B. L. Slagle, M. J. McArthur, C. A. Montgomery, J. S. Butel, and A. Bradley, "Mice deficient for p53 are developmentally normal but susceptible to spontaneous tumours," *Nature*, vol. 356, no. 6366, pp. 215–221, Mar. 1992.

[144] N. Jonckheere, R. Vasseur, and I. Van Seuningen, "The cornerstone K-RAS mutation in

pancreatic adenocarcinoma: From cell signaling network, target genes, biological processes to therapeutic targeting," *Crit. Rev. Oncol. Hematol.*, vol. 111, pp. 7–19, Mar. 2017.

[145] M. B. Salt, S. Bandyopadhyay, and F. McCormick, "Epithelial-to-Mesenchymal Transition Rewires the Molecular Path to PI3K-Dependent Proliferation," *Cancer Discov.*, vol. 4, no. 2, pp. 186–199, Feb. 2014.

[146] V. L. Payen, P. E. Porporato, B. Baselet, and P. Sonveaux, "Metabolic changes associated with tumor metastasis, part 1: tumor pH, glycolysis and the pentose phosphate pathway," *Cell. Mol. Life Sci.*, vol. 73, no. 7, pp. 1333–1348, 2016.

[147] J. Yang, R. S. Williams, and D. P. Kelly, "Bcl3 interacts cooperatively with peroxisome proliferator-activated receptor gamma (PPARgamma) coactivator 1alpha to coactivate nuclear receptors estrogen-related receptor alpha and PPARalpha," *Mol. Cell. Biol.*, vol. 29, no. 15, pp. 4091–4102, 2009.

[148] F. H. Sarkar, Y. Li, Z. Wang, and D. Kong, "Pancreatic cancer stem cells and EMT in drug resistance and metastasis.," *Minerva Chir.*, vol. 64, no. 5, pp. 489–500, Oct. 2009.

[149] Z. Yu, T. G. Pestell, M. P. Lisanti, and R. G. Pestell, "Cancer stem cells.," *Int. J. Biochem. Cell Biol.*, vol. 44, no. 12, pp. 2144–51, Dec. 2012.

[150] B. Sainz Jr., S. Alcala, E. Garcia, Y. Sanchez-Ripoll, M. M. Azevedo, M. Cioffi, M. Tatari, I. Miranda-Lorenzo, M. Hidalgo, G. Gomez-Lopez, M. Canamero, M. Erkan, J. Kleeff, S. Garcia-Silva, P. Sancho, P. C. Hermann, and C. Heeschen, "Microenvironmental hCAP-18/LL-37 promotes pancreatic ductal adenocarcinoma by activating its cancer stem cell compartment," *Gut*, vol. 64, no. 12, pp. 1921–1935, 2015.

[151] S. Palmer and Y. H. Chen, "Bcl-3, a multifaceted modulator of NF-kappaB-mediated gene transcription," *Immunol. Res.*, vol. 42, no. 1–3, pp. 210–218, 2008.

[152] M. Schuster, M. Annemann, C. Plaza-Sirvent, and I. Schmitz, "Atypical IkappaB proteins - nuclear modulators of NF-kappaB signaling," *Cell Commun. Signal.*, vol. 11, no. 1, p. 23, 2013.

[153] I. Tassi, N. Rikhi, E. Claudio, H. Wang, W. Tang, H. L. Ha, S. Saret, D. H. Kaplan, and U. Siebenlist, "The NF-kappaB regulator Bcl-3 modulates inflammation during contact hypersensitivity reactions in radioresistant cells," *Eur. J. Immunol.*, vol. 45, no. 4, pp. 1059–1068, 2015.

[154] K. T. Yeung and J. Yang, "Epithelial-mesenchymal transition in tumor metastasis," *Mol. Oncol.*, vol. 11, no. 1, pp. 28–39, 2017.

[155] P. E. Porporato, V. L. Payen, B. Baselet, and P. Sonveaux, "Metabolic changes associated with tumor metastasis, part 2: Mitochondria, lipid and amino acid metabolism," *Cell. Mol. Life Sci.*, vol. 73, no. 7, pp. 1349–1363, Apr. 2016.

[156] V. S. LeBleu, J. T. O'Connell, K. N. Gonzalez Herrera, H. Wikman, K. Pantel, M. C. Haigis, F. M. de Carvalho, A. Damascena, L. T. Domingos Chinen, R. M. Rocha, J. M. Asara, and R. Kalluri, "PGC-1α mediates mitochondrial biogenesis and oxidative phosphorylation in cancer cells to promote metastasis," *Nat. Cell Biol.*, vol. 16, no. 10, pp. 992–1003, Sep. 2014.

[157] Y. Yu, G. Ramena, and R. C. Elble, "The role of cancer stem cells in relapse of solid tumors," *Front. Biosci.*, vol. 4, pp. 1528–1541, 2012.

Book:

[158] F. T. Bosman, F. Carneiro, R. Hruban, N. D. Theise (Eds). WHO Classification of Tumours of the Digestive System. Chapter 12-Tumours of the Pancreas (Lyon, France: IARC Press), Chapter 12.

7 Abbreviations

ABC	avidin-biotin complex
APS	Ammonium persulfate(NH4)2S2O8
Bcl-3	B cell leukemia 3
BSA	Bovine Serum Albumin
CSC	Cancer stem cell
DAB	3,3'-diaminobenzidine
DMSO	Dimethyl sulfoxide
DNA	eoxyribonucleic acid
DTT	Dithiothreitol
DAPI	4',6-diamidino-2-phenylindole
EDTA	Ethylenediaminetetraacetic acid
EMT	Epithelial mesenchymal transition
et al.	And others
FACS	Fluorescence-activated cell sorting
FCS	Fetal bovine serum
G-418	Geneticin
HCL	Hydrochloric acid
IκB	Inhibitor of NF-κB
IKK	IκB kinase
kDa	kilodalton
Kras	Kirsten rat sarcoma viral oncogene homolog
mM	Millimolar
MLB	Mg^{2+} Lysis/wash Buffer
NF-κB	Nuclear factor κB
NEAA	Non-Essential Amino Acid
PanIN	Pancreatic intraepithelial neoplasia

PCR	Polymerase chain reaction
PFA	Paraformaldehyde
PBS	Phosphate buffered saline
PMSF	phenylmethane sulfonyl fluoride
PVDF	Polyvinylidene fluoride
P/S	Penicilline and Steptomycine
Poly-HEMA	Poly(2-hydroxyethylmethacrylate)
PDAC	Pancreatic ductal adenocarcinoma
RT-PCR	Quantitative real-time polymerase chain reaction
RHD	Rel homology domain
RNA	Ribonucleic acid
rpm	revolutions per minute
RBC lysis buffer	Red Blood Cell Lysis Buffer
SDS	Sodium dodecyl sulfate
TEMED	Tetramethylethylenediamine
TP53	Tumor protein 53
WT	Wild type
μl	microliter
μM	micromolar

8 Acknowledgements

First of all, I would like to deeply thank Prof. Dr. med. Hana Algül for accepting me as a graduate student and giving me the chance to do research about cancer which is highly related with human disease and big problem in the clinical treatment. I express my great gratitude for the opportunity to study and work in one of the most famous hospitals of Munich. Prof. Dr. Algül provided me with excellent supervision, continuous support, helpful discussions, kind assistance and good scientific environment. Since 2003 I started to study medicine and since 2008 I started to study and work on oncology in laboratory of oncology and in clinical oncology department of hospital. It is my biggest luck that I can join the AG Prof. Med. Algül since 2012. It is a very high-level condition of laboratory and full of new ideas and good technologies. I think I have got a lot of progress in this great laboratory and good environment. Prof. Algül have provided a lot of supports in my project of PDAC which is exciting to me because of its characters of tumor project and it will be very useful for my future clinical work as well as future research of tumor. Except this, he also gives a lot of care to me to solve the life problems which is very difficult for me in the beginning when I come as a foreigner. Because of his help, I can stand and make progress step by step. Moreover, I thank my committee meeting members Prof. Dr. Heiko Witt, Prof. Dr. med. Roland M. Schmid, who along with Prof. Dr. Algül opened the doors for my doctoral studies at the TUM.

Secondly, I want to express my gratitude to my homeland and the China Scholarship Council(CSC). CSC financially support students who are diligent and wishing to study abroad. I thank CSC for giving me the chance to develop my education and to know the world.

Continuing, I would like to express my gratitude to all the members of my laboratory including Dr. Marina Lesina (Laboratory Manager), who is very kind-hearted to greatly help me a lot including correcting my dissertation, Nina, Angelika, Kivanc, Dietrich, Matthias, Derya, Chantal, Viktoria, Alex, Marlena, Katrin, Ezgi and especial Liang Song, who has given me huge amounts of help in research and life with his kind and patient heart. Another big help is from my mentor Sonja who teaches me a lot of knowledge and experiment and help me to solve the language and system problems. I thank you for the friendly, creative environment, the helpful discussions, and the great support. Additionally, I want to express my gratitude to Dr. Bruno Sainz for providing the assistance in cancer stem cell assay.

Finally, I want to thank my family and friends. I am especially grateful to my beloved parents and kind girlfriend who have always been helping me out of difficulties, supporting without a word of complaint, and giving me great confidence all these years. Thank you for enriching my background and creating an environment where new ideas can always be fostered and realized.

A wholehearted thank to all of you.